December
2024
Vol. 19 – N. 2

SOCIETAS HERPETOLOGICA ITALICA

Acta Herpetologica

ISSN 1827-9635

FIRENZE UNIVERSITY PRESS

Acta Herpetologica

Acta Herpetologica è la rivista ufficiale della *Societas Herpetologica Italica* (S.H.I.), un'associazione scientifica che promuove la ricerca erpetologica di base e applicata, la divulgazione delle conoscenze e la protezione degli Anfibi e Rettili e dei loro habitat.

Acta Herpetologica is the official journal of the *Societas Herpetologica Italica* (S.H.I.), a scientific association that promotes basic, applied, and conservation researches on Amphibians and Reptiles.

Sito ufficiale S.H.I. (Official S.H.I. website): http://www-9.unipv.it/webshi

Modalità di associazione
Le nuove domande di associazione sono esaminate periodicamente dal Consiglio Direttivo; solo successivamente i nuovi soci riceveranno la comunicazione di accettazione con le modalità per regolarizzare l'iscrizione (ulteriori informazioni sul sito: http://www.unipv.it/webshi). La quota annuale di iscrizione alla S.H.I. è di € 35,00. I soci sono invitati a versare la quota di iscrizione sul conto corrente postale n. 62198205 intestato a: SHI *Societas Herpetologica Italica*. In alternativa è possibile effettuare un bonifico bancario sul Conto Corrente Postale: n. conto 62198205 intestatario: SHI *Societas Herpetologica Italica* IBAN: IT-54-K-07601-03200-000062198205.

Membership
The S.H.I. Council will examine periodically new applications to S.H.I.: if accepted, new Members will receive confirmation and payment information (for more information contact the official website: http://www.unipv.it/webshi). Annual membership fee is € 35.00 (Euro). Payments are made on the postal account of SHI *Societas Herpetologica Italica* no. 62198205, or by bank transfer on postal account no. 62198205 IBAN: IT-54-K-07601-03200-000062198205 to SHI *Societas Herpetologica Italica.*

Versione on-line: http://www.fupress.com/ah

SOCIETAS
HERPETOLOGICA
ITALICA

Acta Herpetologica

Vol. 19, n. 2 - December 2024

Firenze University Press

Referee list. In alphabetical order the scientists that have accepted to act as editorial board members of Acta Herpetologica vol. 19 (2024).

Elenco dei revisori. In ordine alfabetico gli studiosi che hanno fatto parte del comitato editoriale di Acta Herpetologica vol. 19 (2024).

Brett Butler, Carlos Taboada, Daniele Salvi, Daniele Marini, David Blackburn, Dino Biancolini, Diogo Borges Provete, Federico Storniolo, Giacomo Rosa, Giovanni Scillitani, Guohua Ding, Hugues-Alexandre Blain, Jelka Crnobrnja-Isailović, Krister T. Smith, Liming Chang, Marcello Mezzasalma, Marco Mangiacotti, Marco A.L. Zuffi, Marcus Thadeu T. Santos, Marion Segall, Martin Ivanov, Mattia Falaschi, Megan J. Folwell, Meihua Zhang, Pablo Grenat, Raquel Vasconcelos, Roberto Sacchi, Simone Giachello, Siti Othman, Stefano Scali, Valentina Zaffaroni-Caorsi.

Acta Herpetologica 19(2): 81-95, 2024
DOI: 10.36253/a_h-15928

Interpopulation and seasonal variations in habitat and microhabitat use of *Vipera ammodytes*

Angel V. Dyugmedzhiev[1,*], Borislav Y. Naumov[1], Nikolay D. Tzankov[2,†]

[1] *Institute of Biodiversity and Ecosystem Research, Bulgarian Academy of Sciences, 2 Gagarin Street, 1113 Sofia, Bulgaria*
[2] *National Museum of Natural History, Bulgarian Academy of Sciences, 1 Tsar Osvoboditel Blvd., 1000 Sofia, Bulgaria*
[*]*Corresponding author.* Email: angeldiugmedjiev@gmail.com

Submitted on: 2023, 14th March; revised on: 2024, 12th July; accepted on: 2024, 13th September
Editor: Mattia Falaschi

Abstract. Despite the abundant data on habitat use of *Vipera ammodytes*, most studies are purely descriptive, merely listing the habitats in which the species is most often found. More complete studies evaluating the habitat preference of the species are lacking. The intraspecific variation (i.e., interpopulation or seasonal) in habitat and microhabitat utilization of the species also remains a poorly studied topic. In the current study, we assessed the general patterns of habitat and microhabitat use of *V. ammodytes* and their interpopulation and seasonal variations, based on habitat/microhabitat availability. To achieve that, we studied five different populations along a latitudinal gradient in western Bulgaria. In all of the studied areas, *V. ammodytes* showed a clear preference for various stony and rocky habitats and microhabitats, overgrown with herbaceous and shrub vegetation, while it avoided bare habitats, dark deciduous forests as well as cultivated agricultural lands. There were clear interpopulation and seasonal variations in habitat and microhabitat preference and spatial niche utilization. Our results suggest that habitat and microhabitat use of *V. ammodytes* depend on a combination of many factors such as season, locally specific characteristics like habitat structure and availability, population dynamics, food availability, physical and microclimatic conditions, and possibly on the extent of the interspecific competition.

Keywords. Reptilia, spatial niche, viperidae, snakes, nose-horned viper.

INTRODUCTION

A species' habitat is defined as the biotic and abiotic conditions that allow the survival and reproduction of this species (Hall et al., 1997; Morrison, 2009). A microhabitat is a smaller-scale subset of a habitat, which represents a specific place or a physical requirement of the species in a given habitat (Connell, 1961; Lugo et al., 1999; Petren, 2001; Bailey, 2009; Keith et al., 2020). A habitat can include several microhabitats, which may differ in their structure or conditions (i.e., vegetation, light exposure, humidity, temperature, air circulation) (Connell, 1961; Lugo et al., 1999; Petren, 2001; Bailey, 2009; Keith et al., 2020). Therefore, when researching the spatial niche of a particular species, it is important to assess both its habitat and microhabitat requirements to better understand its utilisation of the environment. Such assessments are crucial for properly and effectively delivering conservation actions on a target species.

Many snakes are generally sedentary animals with low dispersal abilities so their distribution usually depends on both the climatic and habitat characteristics of the environment. The microclimatic and microhabitat conditions play a major role in snakes' habitat selection (Vitt and Caldwell, 2014). For instance, the presence of stony microhabitats often plays a major role in the hierarchical selection of habitats as they provide snakes with favorable thermal conditions for thermoregulation and

ISSN 1827-9635 (print)
ISSN 1827-9643 (online)

easy access to shelter from extreme environmental conditions or predators (Reinert, 1993; Kurek et al., 2018). Habitat use may vary across seasons, age groups, and populations of the same species, or depending on the reproductive status of individuals (Reinert, 1984, 1993; Sweet, 1985; Shine, 1986; Seigel, 1986; Burger and Zappalorti, 1989; Luiselli et al., 1994; Charland and Gregory, 1995; Webb and Shine, 1998). Habitat use variability can be due to different factors, such as habitat and microhabitat availability, presence and location of suitable areas for hibernation and/or thermoregulation, or differences in food abundance between habitats (Reinert and Kodrich, 1982; Huey et al., 1989; Madsen and Shine, 1996). Moreover, variability is also common in microhabitat use (Neumeyer, 1987; Brito, 2003; Martínez-Freiría et al., 2010; Strugariu et al., 2011).

European vipers usually adhere to a certain small to medium-sized home range territory throughout most of their lives (Neumeyer, 1987; Naulleau et al., 1996; Saint Girons, 1997; Brito, 2003; Weinmann et al., 2004; Graitson, 2008; Plasinger et al., 2014; Dyugmedzhiev et al., 2020). When hibernating sites, sites for thermoregulation, shelters from unfavorable climatic conditions or predators, and a sufficient food base are all available within a given small territory, vipers can inhabit it throughout the entire activity period (Saint Girons, 1952, 1980; Neumeyer, 1987; Naulleau et al., 1998; Thomas, 2004; Wollesen and Schwartze, 2004). However, places suitable for hibernation, those with high food availability or with suitable summer' microclimatic conditions, often do not coincide. In such places, vipers conduct seasonal migrations from the hibernating areas to the summer habitats, and in autumn, they return to the hibernating areas (Duguy, 1963; Viitanen, 1967; Prestt, 1971; Saint Girons, 1980; Naulleau et al., 1998; Anderson, 2003; Wollesen and Schwartze, 2004; Graitson, 2008). The scales of these migrations depend on individual locality, with the biggest documented migrations being for *Vipera berus* (Linnaeus, 1758), from England and Finland, where some individuals may travel up to 1.5-2 km from the hibernating areas to the summer habitats (Viitanen, 1967; Prestt, 1971).

The nose-horned viper, *Vipera ammodytes* (Linnaeus, 1758), is distributed from the western foothills of the Alps across the entire Balkan Peninsula and many Aegean islands to north-western and northern Asia Minor and the Lesser Caucasus (Speybroeck et al., 2016). Throughout its range, it inhabits a wide variety of habitats. However, the species is most frequently found in different types of open and sunny stony or rocky habitats with shrubs and grasses, also in different types of open deciduous forests (Tuleshkov, 1959; Bruno, 1967; Beshkov, 1993; Ioannidis and Bousbouras, 1997; Stumpel and Hahn, 2001; Heckes et al., 2005; Crnobrnja-Isailović et al., 2007; Plasinger et al., 2014; Mebert et al., 2015; Ghira, 2016). Within this wide variety of habitats, however, nose-horned vipers usually adhere to stony and rocky microhabitats (Beshkov, 1993, Mebert et al., 2015; Ghira, 2016). The microhabitat type is considered one of the main determinants for population density of the species because optimal microhabitats provide more access to shelter and a richer food base for the vipers (Ghira, 2016).

Despite the abundant data on the habitat use of *Vipera ammodytes*, most studies only describe the variety of habitats in which the species is found. More complete studies, taking into consideration habitat availability, in order to evaluate the habitat preference of the species, are lacking. To date, the intraspecific variation (i.e., interpopulation or seasonal) in habitat and microhabitat use of the nose-horned viper also remains a poorly studied topic, with data mainly on the seasonal variations in habitat and microhabitat use. In Serbia, Montenegro, and Northern Macedonia, males are usually detected in spring, exploiting open deciduous forests with southwest exposure; females are most often detected in summer, in rocky habitats with east and south exposure (Crnobrnja-Isailović et al., 2007). In Bulgaria, in early spring and late autumn, nose-horned vipers mainly inhabit rocky and stony sunny terrains with scarce vegetation (Beshkov, 1993). From the late spring until the beginning of autumn, vipers conduct short migrations to adjacent habitats, such as herbaceous vegetation, shrublands, and forests, often close to water sources (Beshkov, 1993). To date, there are no studies comparing habitat and microhabitat use among different populations of the nose-horned viper.

In Bulgaria, *V. ammodytes* is widespread throughout the country, except in the high mountains and urbanized or intensively cultivated agricultural lands (Stojanov et al., 2011). The current study aims to assess the general patterns of habitat and microhabitat use of *V. ammodytes*, based on habitat/microhabitat availability. In light of the available literature on vipers' habitat and microhabitat use, and under the assumption that nose-horned viper habitat and microhabitat use can vary among populations, the following hypotheses were tested: 1) *V. ammodytes* prefers various stony and rocky habitats and microhabitats, overgrown with shrubs and herbaceous vegetation; 2) habitat and microhabitat preference are highly dependent on their respective availability; 3) habitat and microhabitat preferences vary among different populations of *V. ammodytes*; 4) habitat and microhabitat use vary between the different seasons of the activity period.

MATERIALS AND METHODS

Study sites

Five sites along the latitudinal gradient in western Bulgaria were studied: 1) near Karlukovo Village, north-western Bulgaria (43°10'N, 24°3'E; 111-250 m a.s.l.); 2) near Gara Lakatnik Village, north-western Bulgaria (43°5'N; 23°23'E; 352-733 m a.s.l.); 3) near Balsha Village, the central parts of western Bulgaria (42°51'N; 23°15'E; 652-853 m a.s.l.); 4) near Bosnek Village, the central parts of western Bulgaria (42°29'N, 23°11'E; 942-1332 m a.s.l.); 5) the "Gabrovitsa" area in the Kresna Gorge, south-western Bulgaria (41°46'N, 23°9'E; 165-488 m a.s.l.; presented as "Kresna" in the tables and figures). Both sites 1 and 2 are karst valleys along the Iskar River, with steep rock cliffs, and patches of deciduous forests. Site 3 is an abandoned quarry, surrounded by fields, bare hills, and deciduous forests. Site 4 is a middle-mountain karst valley along the upper reaches of the Struma River, with rocky slopes, vegetated with shrubs and thin deciduous forests. Site 5 is a plain area along the middle reaches of the Struma River, vegetated with grass, scattered shrubs, and abandoned vineyards and surrounded by steep stony slopes overgrown with forest vegetation. Map and photographs of the sites are presented in Dyugmedzhiev et al. (2020). All sites fall in the temperate-continental climate zone except site 5, which lies in the continental-Mediterranean zone (Kopralev, 2002).

Fieldwork

Fieldwork was conducted mainly between April and September from 2014 to 2017, and each site was visited regularly once per month in 2014 and twice per month from 2015 onwards. Visits were also made between January–March and October–December, however, they were not evenly distributed among sites. Each visit lasted one day. All visits were made on days with daily temperatures above 15 °C, on which vipers' activity could be expected (Dyugmedzhiev et al., 2021). Searches started when morning temperatures reached at least 15-16 °C: usually around 12:00 in winter, at 11:00 in March, October, and November, at 9:00 in April, May, and September and at 8:00 during the summer. From October to March, searches continued until ambient temperatures dropped below 13-14 °C, which was usually in the afternoon. From April to September, searches continued until dusk (i.e., around 30 minutes before dark), however, during some days vipers were also searched throughout parts of the night, usually until 23:00-24:00. Search efforts covered the entire vicinity of the study sites, with the exception of some physically inaccessible areas (e.g., too thick patches of shrubs, very steep rock cliffs). The same route scheme was followed in each visit, which covered parts of each of the different habitat types in a site. However, due to the different size areas of the different habitat types, the search effort was not equal across habitats. Vipers were located by sight as well as by inspection of potential shelters such as under stones and logs or inside rock crevices. Geographic position (Garmin eTrex 20; precision: 5 m), habitat and microhabitat characteristics of the location were recorded for each viper or viper's molt found. Habitat types were categorized visually, based on a list of habitat categories generated from the mobile application Smart-Birds Pro (Popgeorgiev et al., 2015). A total of 24 habitat type categories were derived (see Table 1). Microhabitat characteristics of the location were categorized according to the percentage of trees/shrubs, grasses, stones/rocks, water surfaces, and roads within a radius of 2.5 m from the snake's location (Martínez-Freiría et al., 2010; Mebert et al., 2015; Dyugmedzhiev et al., 2019). Based on the period of observation, seasons were categorized as spring (beginning of March-end of May), summer (beginning of June-end of August), and autumn (beginning of September-end of November). Captured vipers were measured (snout to vent [SVL] and tail length [TL]; precision 0.5 cm), weighted (precision: 0.01 g), color marked, and photographed for individual identification (Dyugmedzhiev et al., 2018) and then released on the site of capture, usually within 15-30 min following the capture.

Statistical analyses

Individuals found more than once throughout the day were included in the analyses only with the data from the first observation since the capture and measuring procedures can cause changes in vipers' natural activity patterns. Pre-shedding vipers (2-3 days before the shedding) usually avoided conducting long movements until they shed their skin and mostly basked or hid in shelters within a very small area, until shedding their skin. Therefore, found molts were considered a reliable source of habitat and microhabitat selection of pre-shedding vipers. To avoid collecting data for the same molt in two different field visits (pseudoreplication), each found molt was torn apart and removed from the site. Dead animals were excluded from the analyses, as it was impossible to objectively assess whether they died while passing through the habitat on their way to a neighboring, more suitable one, or whether they actually stayed in this particular habitat prior to their death.

Habitat preference was analyzed with Ivlev's index. The index is calculated with the formula:

Table 1. Description of the characteristics of the different habitat types in which vipers were searched for and the microhabitat characteristics, presented by the percentage of trees/shrubs, grasses, and stones/rocks in the places where vipers were observed in each habitat. Values are expressed as "means ± SD (Min-Max)" when n > 1, "[absolute value]" when n = 1, or "–" when n = 0.

Habitat type	Microhabitat characteristics		
	Trees/Shrubs	Grass	Stones/Rocks
H1: Rocks / screes (natural) with scattered shrubs and trees growing on them	23.45 ± 8.57 (10 – 50)	18.97 ± 8.17 (0 – 40)	57.59 ± 8.72 (30 – 70)
H2: Abandoned quarries overgrown with a mixture of grasses, shrubs and scattered trees	26.38 ± 12.26 (0 – 50)	18.07 ± 13.73 (0 – 70)	55.71 ± 14.47 (20 – 90)
H3: Abandoned old buildings and ruins	13.33 ± 5.77 (10 – 20)	43.33 ± 25.17 (20 – 70)	43.33 ± 25.17 (20 – 70)
H4: Stone piles / stone walls (man-made) overgrown with grass, and with only scattered shrubs present	17.5 ± 13.88 (0 – 30)	41.25 ± 18.85 (20 – 70)	40 ± 10.69 (20 – 50)
H5: Stone piles / stone walls (man-made) entirely or almost entirely overgrown with shrubs	30 ± 9.29 (10 – 50)	33.65 ± 12.05 (10 – 70)	36.15 ± 8.44 (20 – 60)
H6: Stone piles / stone walls (man-made) entirely or almost entirely overgrown with a mixture of trees and shrubs	40.5 ± 8.87 (20 – 50)	21.5 ± 14.61 (0 – 50)	38 ± 19.56 (10 – 60)
H7: Rocky / stony areas (natural), overgrown with a mixture of grass and shrubs	24.02 ± 14.57 (0 – 70)	32.61 ± 14.66 (0 – 80)	43.01 ± 13.73 (0 – 80)
H8: Rocky / stony road scarps (man-made) overgrown with a mixture of grass and shrubs	22.67 ± 10.81 (0 – 40)	23 ± 12.64 (0 – 50)	32.33 ± 9.35 (20 – 60)
H9: Light highly sparse deciduous forests with shrub undergrowth, growing on rocky / stony areas	30 ± 11.55 (20 – 40)	32.5 ± 9.57 (20 – 40)	42.5 ± 5 (40 – 50)
H10: Rivers and streams	[10]	[0]	[30]
H11: Rocky / stony areas (natural) entirely or almost entirely overgrown with trees and shrubs	23.75 ± 15.98 (0 – 40)	25 ± 13.09 (10 – 40)	47.5 ± 19.82 (20 – 80)
H12: Light mediumly sparse deciduous forests with shrub undergrowth, growing on rocky / stony areas	37.35 ± 14.42 (10 – 80)	18.09 ± 12.73 (0 – 60)	44.56 ± 15.3 (10 – 80)
H13: Bare or almost bare rocks / screes with a very sparse grass vegetation growing on them	20 ± 15.19 (0 – 40)	23.57 ± 10.08 (10 – 50)	57.86 ± 17.62 (30 – 90)
H14: Dirt roads	10 ± 14.14 (0 – 20)	15 ± 7.07 (10 – 20)	20 ± 0 (20 – 20)
H15: Ecotone – bordering area between a forest and an open habitat, overgrown with mixture of trees, shrubs and grasses	40 ± 13.09 (10 – 50)	48.75 ± 14.58 (30 – 80)	11.25 ± 8.35 (0 – 30)
H16: Shrubbery area without or with very few stones /rocks	35 ± 21.21 (20 – 50)	30 ± 14.14 (20 – 40)	35 ± 7.07 (30 – 40)
H17: Meadows / pastures with scattered shrubs and no or very few stones /rocks on them	30.71 ± 13.28 (10 – 60)	45 ± 14.54 (30 – 70)	24.29 ± 11.58 (0 – 40)
H18: Asphalt roads	–	–	–
H19: Abandoned bare or almost bare quarries with a very scarce vegetation	–	–	–
H20: Dry ravines in thick and dark deciduous forests with shrub undergrowth	–	–	–
H21: Grassy road scarps (man-made) without or with very few rocks / stones	–	–	–
H22: Mud / dirt / muck areas without vegetation	–	–	–
H23: Bare sand screes without vegetation	–	–	–
H24: Abandoned old gardens / vineyards / pastures, which are not cultivated or planted anymore	–	–	–

$$\frac{U - A}{U + A} \quad (1)$$

where U is the number of observed individuals in habitat i / number of observed individuals in all habitats, and A is the size area of habitat i / total size area of all habitats (Kenward, 1992). Positive values of this index indicate that the habitat is used more often than expected, based on its availability, and negative values indicate that it is less used. Values of -1 of this index indicate that the habitat is not used at all. The area of each habitat type was drawn out via satellite pictures, obtained from

Google Earth Pro, and its size was calculated with ArcGIS v. 10.4.1. (ESRI, Redlands, CA, USA). Ivlev's index was calculated for each available habitat type, both for the combined data from all populations and for each separate population. In order to assess the local variation in habitat preference, two types of habitat preference were derived, general and local. The estimated values of each habitat type's Ivlev's index based on the combined data from all populations were used as reference values to assess the general species' habitat preference. The estimated index values for each separate population were then used to assess the local preference of habitat types, which were then compared to the general preference for evaluating the interpopulation variations in habitat preference. For this purpose, habitat types were divided into four categories, based on the values of the Ivlev's index: preferred, PR – habitat types with values between 0.5 and 1; often used, OU – habitat types with values between 0.5 and 0; rarely used, RU – habitat types with values between 0 and -0.5; avoided, AV – habitat types with values between -0.5 and -1. Therefore, if a certain habitat type is placed within different categories based on the values for general and local preference, this was considered as an indication of local variation in preference of this habitat type.

To analyze the breadth of each population's spatial niche, Levins' index (B) was used. This index was calculated by the formula:

$$B = \frac{1}{\sum p_i^2} \quad (2)$$

where p_i is the relative proportion of individuals found in habitat i compared to the number of individuals in all habitats (Krebs, 1999). The index was standardized via the formula:

$$B_{st} = \frac{B-1}{n-1} \quad (3)$$

where B is the Levins' index, and n is the number of habitats, thus, the index vary from zero to one, with a value of zero indicating maximum specialization (all individuals are found in only one of the habitats), a value of one – absence of specialization (equal number of individuals in all habitats) (Cooper-Bohannon et al., 2016). A cluster analysis (by the commonly used UPGMA algorithm) based on the Morisita's similarity index was used to compare the different populations in regard to habitat use and to assess potential latitude-based patterns in habitat use. This index was estimated using a frequency matrix representing the number of observations of vipers in each habitat type for each separate population. This similarity index was chosen, as it is the most robust and independent of sample size when the number of individuals is used for its calculation (Wolda, 1981). The combined data for both a live individuals and found molts were used for the calculation of each of the three indices, used to assess general and interpopulation patterns of habitat use.

A correspondence analysis was used to evaluate the general seasonal variations in habitat use based on the combined data from all five populations. This analysis was used to clarify which habitat types are associated with each separate season (Rohlf, 1988). A frequency matrix representing the number of observations of live individuals in each habitat type for each of the seasons was used for this analysis. Habitat types in which vipers were never observed were excluded from this frequency matrix. When sample size allowed it, the differences within a separate population between the number of observations of vipers in a particular habitat type during the different seasons were analyzed with a χ^2 test. Information provided by the found molts were excluded from all analyses on seasonal variation of habitat and microhabitat use because often was not possible to assess in which season a particular moult was shed. Due to the smaller and uneven sample sizes for sites 4 and 5, in which most of the vipers were found in spring (Table S1), the seasonal patterns of habitat and microhabitat use of those populations were not analyzed.

Since a normal distribution of the data could not be achieved (Kolmogorov-Smirnov & Liliefors, $P < 0.05$), a Kruskal-Wallis H test was used to analyze the microhabitat use of the species. Due to the low percentage of water surfaces and roads, only the data for trees/shrubs, grasses, and stones/rocks were used as groups in the analyses. The use of each of these three groups was compared between different populations with the combined data for all seasons, as well as between different seasons for each separate population with sufficient sample size (i.e., sites 1, 2, and 3).

Kruskal-Wallis H test, χ^2 test, and correspondence analysis were processed with Statistica 10.0 (StatSoft, Inc. 2011). Morisita's similarity index was calculated using Past 3.25 (Hammer et al., 2001). Statistical significance was accepted at $P < 0.05$.

RESULTS

General habitat preference

A total of 708 records of *Vipera ammodytes* (651 a live individuals and 57 molts) from the five study sites were used to analyze the species' habitat preference: 244 from Karlukovo (223 a live and 21 molts), 168 from Lakatnik

(160 a live and 8 molts), 163 from Balsha (149 a live and 14 molts), 65 from Bosnek (58 a live and 7 molts) and 68 from Kresna Gorge (61 a live and 7 molts) (Table S1). Vipers were found in 17 of all 24 available habitat types. The analyses of the combined data for all populations revealed that, based on the values of the Ivlev's index, five habitat types are preferred (PR: H1-H5), four are often used (OU: H6-H9), four are rarely used (RU: H10-H13) and 11 are avoided (AV: H14-H24) (Fig. 1A).

Interpopulation variations in habitat use

In site 1 (Karlukovo), vipers were found in six of all 12 available habitat types: one habitat type classified as OU, two as RU, and three as AV (Fig. 1B). The habitat types with the largest areas were the ones classified as OU, followed by the AV and the RU categories (Fig. 2). The PR category was the one with the smallest area (Fig. 2; Table S1). The local preference of four habitat types differed from the general habitat preference – H2, H3, H10, and H13 (Figs. 1A and B). In site 2 (Lakatnik), vipers were found in seven of all nine available habitat types: two PR, one OU, and four RU (Fig. 1C). The most available habitat types were the OU and the RU, while the AV and the PR habitat types were with much smaller size (Fig. 2; Table S1). The local preference of three habitat types differed from the general habitat preference – H6, H7, and H9 (Figs. 1A and C). In site 3 (Balsha), vipers were found in eight of all 15 available habitat types: three PR, two OU, and three RU (Fig. 1D). The most available habitat types were the AV, followed by the RU, while the PR and the OU were with much smaller size (Fig. 2; Table S1). The local preference of three habitat types differed from the general habitat preference: H4, H6, and H12 (Figs. 1A and D). In site 4 (Bosnek), vipers were found in six of all 12 available habitat types: four OU, one RU, and one AV (Fig. 1E). The most available habitat types were the OU, followed by the RU and the AV, while the PR covered a negligible size (Fig. 2; Table S1). The local preference of five habitat types differed from the general habitat preference: H1, H6, H10, H11, and H13 (Figs. 1A and E). In site 5 (Kresna Gorge), vipers were found in seven of all 11 available habitat types: three PR, one OU, one RU, and two AV (Fig. 1F). The AV clearly dominated in abundance, while the PR, the OU, and the RU were with much smaller size (Fig. 2; Table S1). The local preference of three habitat types differed from the general habitat preference: H1, H6, and H15 (Figs. 1A and F).

In each of the five sites, *V. ammodyes* had very narrow niche breadth and the species used the available habitat types very unevenly. The values of the Levins' index were close to 0 for all sites. They were the lowest in site 1 (B_{st} = 0.03), followed by sites 3 and 4 (B_{st} = 0.06 and 0.07, respectively), and were the highest in sites 5 and 2 (B_{st} = 0.13 and 0.19, respectively). The cluster analysis showed no grouping pattern based on latitude. Site 4 and site 1 were grouped together, followed by site 2. Site 3 was grouped as an outside group from the latter three, and site 5 – as an outside group of the combined cluster of sites 1-4 (Fig. 3).

Seasonal variations in habitat use

The analysis of the combined data from all five populations revealed a clear seasonal variation in habitat use. The first two dimensions of the correspondence analysis explained 100% of the variance (Fig. 4). Separation based on the first dimension was weak. The second dimension, however, clearly separated summer from both spring and autumn. Three habitat types were grouped closer to summer than to spring and autumn – H1, H6, and H7. Four habitat types were grouped between spring and autumn (H2, H8, H11, and H12), and four were closer to spring (H4, H5, H15, and H17). The rest of the habitat types did not group close to any of the seasons.

In site 1, there was a statistically significant difference between the number of observations of vipers in the different seasons for each of the two habitat types with sufficient sample size for the χ^2 test – H7 and H12 (Table 2). H7 was more used in summer than in the other two seasons, while in H12, the opposite trend was present (Table S1). In site 2, four habitat types had a sufficient sample size for the χ^2 test – H1, H7, H8, and H12. A statistically significant difference was present only for H1 and H7 (Table 2), with both being more used in summer than in the other two seasons (Table S1). In site 3, two habitat types had sufficient sample sizes for the χ^2 test, H2, and H5, with statistically significant differences present only for H2 (Table 2). This habitat type was much more used in spring and autumn, while in summer vipers were found rarely in it (Table S1).

Interpopulation variations in microhabitat use

In the studied populations of *V. ammodytes* from the northern and central parts of western Bulgaria (Sites 1, 2, 3, and 4), vipers were found mostly in stony-rocky microhabitats with less presence of grasses and trees/shrubs. Moving south to site 5 there was a gradual decrease in the amount of stones/rocks at the expense of an increase in grasses and trees/shrubs in the microhabitats occupied by the species, with the latter two components having equal presence to that of the stones/rocks (Fig. 5A). Statistically

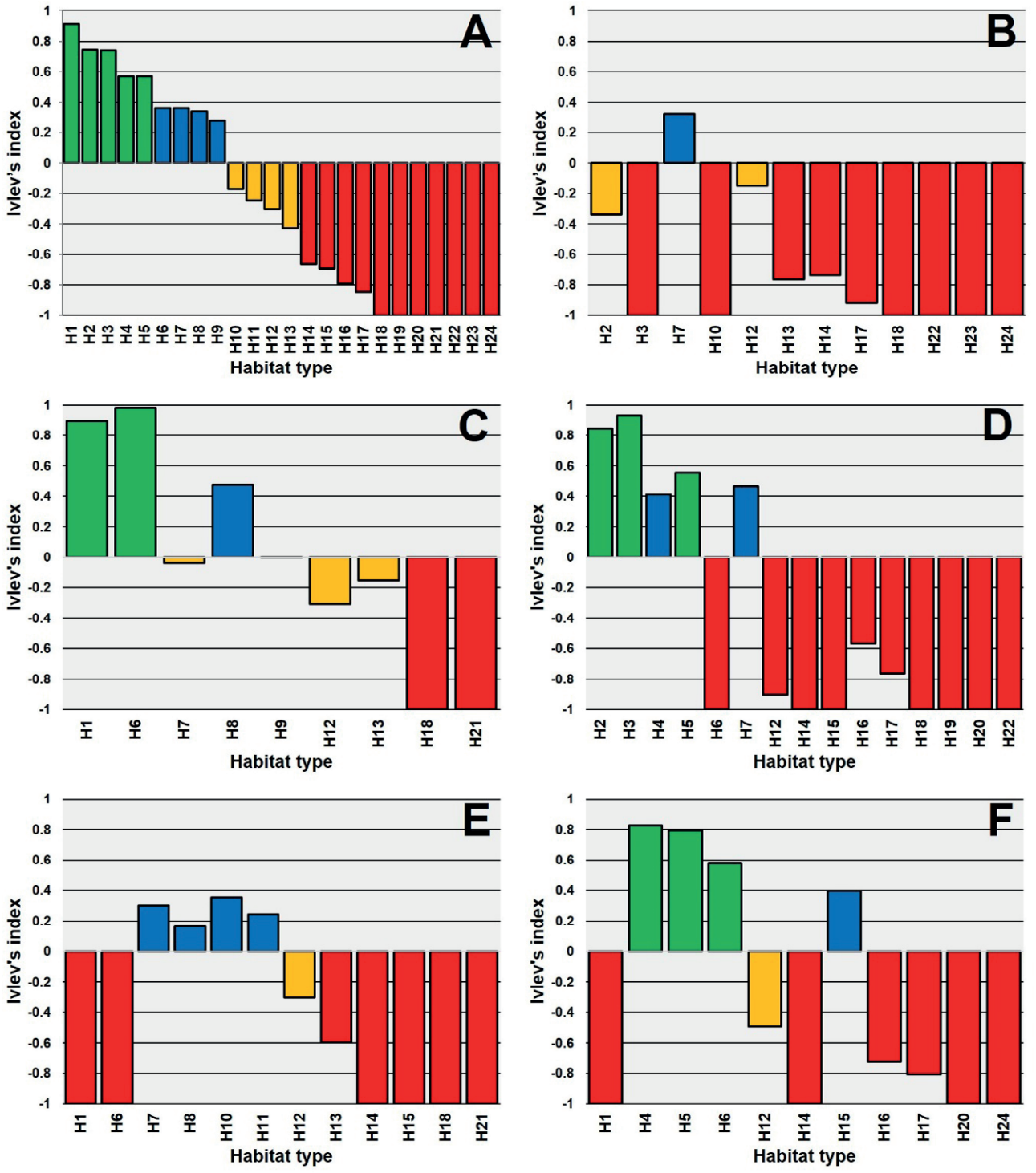

Fig. 1. General and local habitat preference of *V. ammodytes* based on the values of the Ivlev's index. A) Categorization of the different habitat types, based on the values for general preference of the Ivlev's index, calculated with the combined data from all five populations; categorization of the different habitat types, based on the values for local preference of the Ivlev's index, calculated for Karlukovo (B), Lakatnik (C), Balsha (D), Bosnek (E) and Kresna Gorge (F). Different preference categories are presented with different colors: green bars – preferred habitat types, PR; blue bars – often used habitat types, OU; orange bars – rarely used habitat types, RU; red bars – avoided habitat types, AV. For abbreviations of the habitat types, see Table 1.

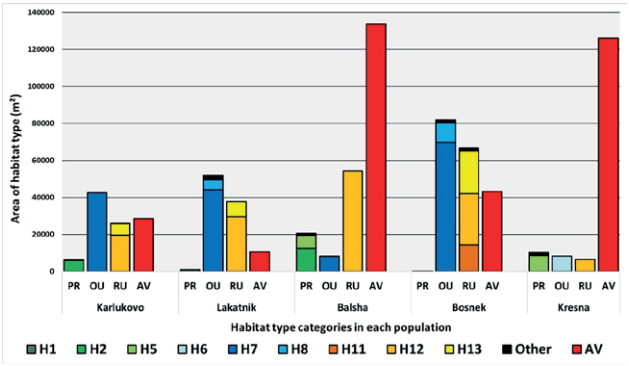

Fig. 2. Area of the different habitat type categories in the different study sites, based on the values for the general habitat preference of the Ivlev's index, calculated with the combined data from all five populations. The most abundant habitat types from each preference category are presented within the bar, except those from the AV category, which are presented combined. Habitat types with very small areas are presented combined as "Other". For abbreviations and exact size of the habitat types, see Table 1 and S1, respectively.

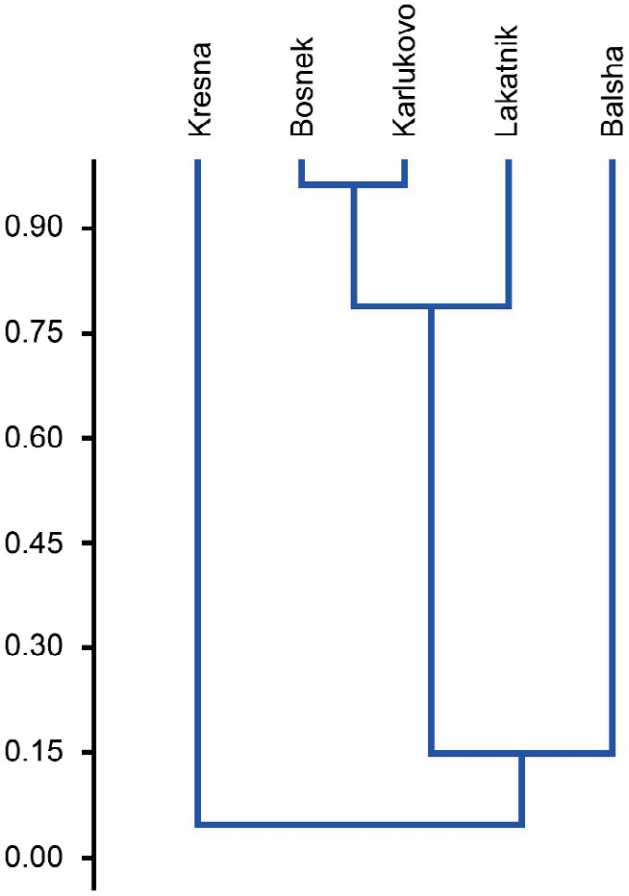

Fig. 3. Similarity in habitat use of *V. ammodytes* between the five studied populations, based on the Morisita index.

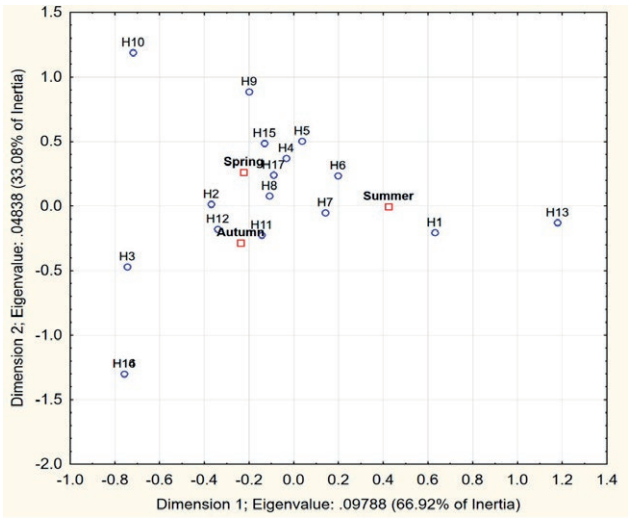

Fig. 4. Grouping between habitat types used by *V. ammodytes* and seasons, based on the results from the first two dimensions of the correspondence analysis. For abbreviations of the habitat types, see Table 1.

Table 2. Results from the χ2 test between the number of observations of vipers during the different seasons in habitat types with sufficient sample size for each of the five populations. For abbreviations of the habitat types, see Table 1.

Population	Habitat type	χ2	df	P
Karlukovo	H7	10.78	2	0.005
	H12	11.51	2	0.003
Lakatnik	H1	14.33	2	0.0008
	H7	8.38	2	0.02
	H8	3.91	2	0.14
	H12	1.91	2	0.39
Balsha	H2	14.87	2	0.0006
	H7	1.99	2	0.37

significant differences were found between some of the populations. Regarding the presence of trees/shrubs, statistically significant differences were found between the population from site 5 and those from both sites 1 and 2 (Table 3). Site 5 had the highest values for trees/shrubs presence, compared to all five populations, while site 2 had the lowest values (Fig. 5A). In regards to the presence of grasses, both the populations from sites 3 and 5 differed significantly from each of the other populations (Table 3). The presence of grasses was the lowest in site 3 and was the highest in site 5 (Fig. 5A). In regards to the presence of stones/rocks, again the population in site 3 differed significantly from the other populations. The population from site 5 was significantly different from the other populations, with the exception of site 4, where the result was

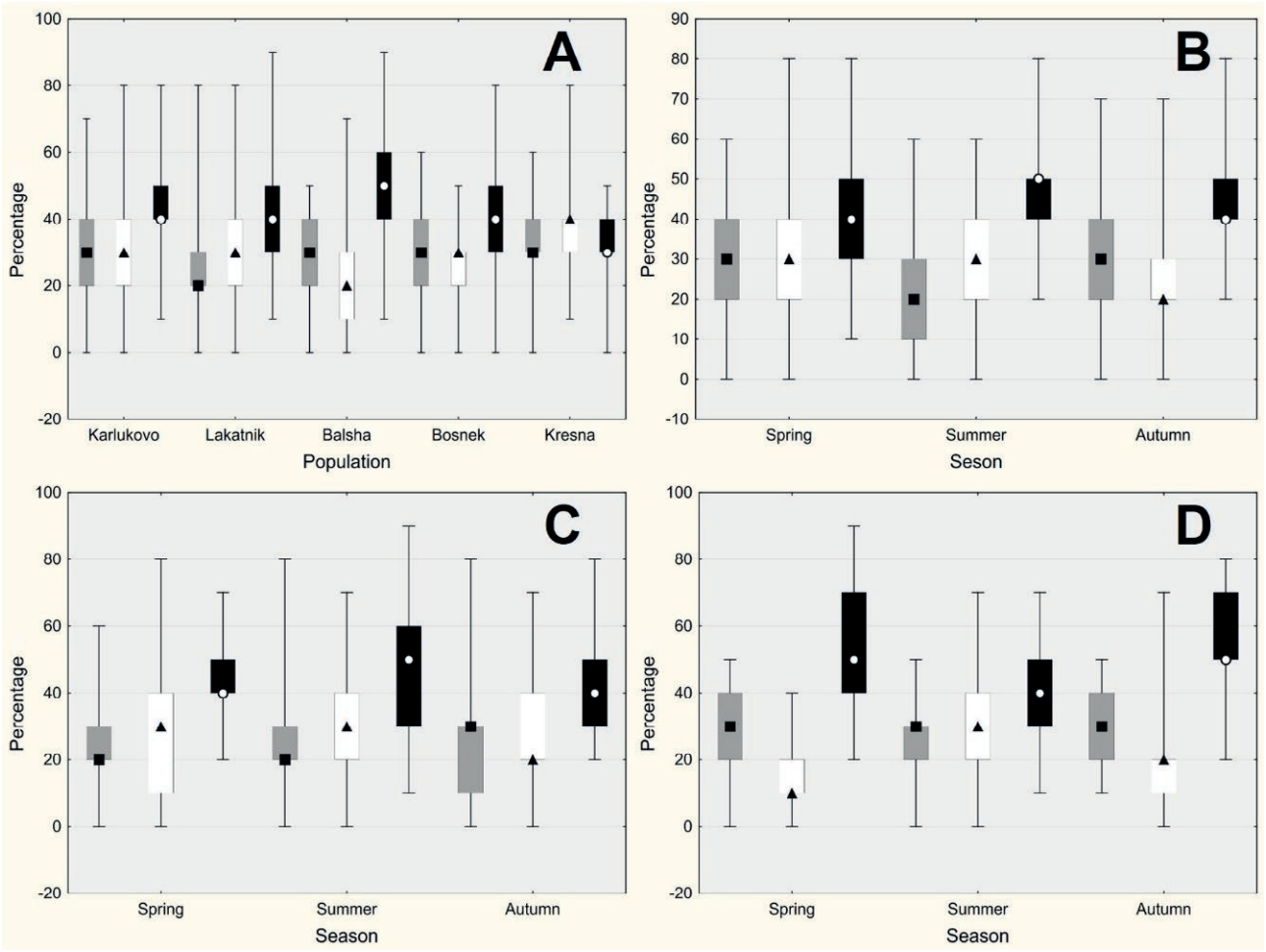

Fig. 5. Comparison of the microhabitat characteristics, presented as the percentage of trees/shrubs (grey), grasses (white), and stones/rocks (black) in the places of observations of *V. ammodytes*. A) Five studied sites with the combined data from the different seasons; different seasons for Karlukovo (B), Lakatnik (C), and Balsha (D). Bosnek and Kresna Gorge are not presented, due to the insufficient sample size for these populations.

at the threshold of statistical significance (P = 0.05; Table 3). The presence of stones/rocks was the highest in site 3, while it was the lowest in site 5 (Fig. 5A).

Seasonal variations in microhabitat use

Seasonal variations in the characteristics of the microhabitats used by *V. ammodytes* were present only in sites 1 and 3. In site 1 the presence of all three components (trees/shrubs, grasses, and stones/rocks) varied across seasons (Fig. 5B). The presence of trees/shrubs was the lowest in summer and the results between summer and autumn were statistically significant (Table 4). The presence of grasses decreased in autumn and the results between summer and autumn were statistically significant (Table 4). The presence of stones/rocks in summer was slightly higher than in the other two seasons and statistically significant differences were present between summer and spring (Table 4). In site 3, the presence of both grasses and stones/rocks differed significantly in summer, compared to spring and autumn (Table 4). The presence of grasses increased in the summer microhabitats of vipers, in contrast to that of stones/rocks, which decreased during this season (Fig. 5D).

DISCUSSION

In the five study sites, *V. ammodytes* showed a very narrow spatial niche, exhibiting a preference for different types of stony and rocky habitats and microhabitats, cov-

Table 3. Results of Kruskal-Wallis H tests assessing differences in three microhabitat characteristics (Trees/Shrubs, Grasses, Stones/rocks) among the five different populations.

Trees/Shrubs: Kruskal-Wallis H test: H = 20.56, P = 0.004, n = 648				
	Lakatnik	Balsha	Bosnek	Kresna
Karlukovo	1	1	0.99	0.02
Lakatnik	–	0.11	0.12	0.0009
Balsha	0.11	–	1	0.48
Bosnek	0.12	1	–	1
Grasses: Kruskal-Wallis H test: H = 58.06, P < 0.0001, n = 648				
	Lakatnik	Balsha	Bosnek	Kresna
Karlukovo	1	< 0.00001	1	0.005
Lakatnik	–	0.0003	1	0.0009
Balsha	0.0003	–	0.03	< 0.00001
Bosnek	1	0.03	–	0.008
Stones/rocks: Kruskal-Wallis H test: H = 75.62, P < 0.0001, n = 648				
	Lakatnik	Balsha	Bosnek	Kresna
Karlukovo	1	0.003	0.21	< 0.00001
Lakatnik	–	0.004	0.37	< 0.00001
Balsha	0.004	–	0.00003	< 0.00001
Bosnek	0.37	0.00003	–	0.05

ered with herbaceous and shrubby vegetation (Fig. 1). In contrast, the species clearly avoided bare habitats, dark deciduous forests, and agricultural habitats without or with very low presence of stones (Fig. 1). Our results are in agreement with the available literature about habitat use of *V. ammodytes* (Tuleshkov, 1959; Bruno, 1967; Beshkov, 1993; Stumpel and Hahn, 2001; Heckes et al., 2005; Plasinger et al., 2014; Mebert et al., 2015; Ghira, 2016).

Interpopulation variations in habitat and microhabitat use

Although there were some clear differences in habitat use and spatial niche breadth between the different populations in the current study, no latitude-based patterns were evident. Interestingly, it seems that the availability of suitable habitats was not the only factor to explain the interpopulation variations in habitat use. For instance, even though the OU habitat type H7 was the most abundant habitat in sites 1, 2, and 4, and its abundance was equal between the first two, in sites 1 and 4 (Fig. 2) this habitat was used much more often (and thus, was locally classified as OU), than in site 2, where it was classified as RU (Fig. 1). Similarly, the PR habitat type H2 was only slightly less abundant in site 1 compared to site 3 (Fig. 2). However, in site 1 this habitat was used much more rarely (and was classified as RU) than in site 3, where it was one of the most preferred habitats (Fig 1), at least in spring and autumn (see below). Therefore, it appears that habitat use does not depend solely on the availability of suitable habitats, but probably on a combination of factors. Such factors might be the local characteristics,

Table 4. Results of Kruskal-Wallis H tests between the microhabitat characteristics in the places of observations of *V. ammodytes* during the different seasons in the population around Karlukovo (second row) and Balsha (sixth row). The p-values from the post-hoc tests testing for differences in the presence of the three microhabitat components between the different seasons in the two populations are presented in rows 3-5 and 8-10, respectively. Sp – spring; Su – summer; Au – autumn.

Karlukovo									
	Shrubs: Kruskal-Wallis H test: H = 15.58, P = 0.0004, n = 220			Grasses: Kruskal-Wallis H test: H = 12.04, P = 0.002, n = 220			Stones/rocks: Kruskal-Wallis H test: H = 8.55, P = 0.01, n = 220		
	Su	Au		Su	Au		Su	Au	
Sp	0.09	0.55	Sp	1	0.07	Sp	0.03	1	
Su	–	0.00004	Su	–	0.003	Su	–	0.08	
Balsha									
	Shrubs: Kruskal-Wallis H test: H = 3.99, P = 0.14, n = 147			Grasses: Kruskal-Wallis H test: H = 23.33, P < 0.00001, n = 147			Stones/rocks: Kruskal-Wallis H test: H = 19.99, P < 0.00001, n = 147		
	Su	Au		Su	Au		Su	Au	
Sp	0.19	0.56	Sp	0.00002	1	Sp	0.0004	1	
Su	–	1	Su	–	0.0002	Su	–	0.0001	

habitat structure, and microclimatic conditions of the site (Reinert, 1984; Burger and Zappalorti, 1989; Kurek et al., 2018), population dynamics (Viitanen, 1967; Prestt, 1971; Luiselli et al., 1994; Charland and Gregory, 1995), or food abundance in the different habitats (Luiselli et al., 1994; Madsen and Shine, 1996; Luiselli, 2006).

In contrast to habitat use, there were some latitude-based patterns in vipers' microhabitat utilization. In the populations from the northern and central parts of western Bulgaria (sites 1-4), vipers were found mainly in stony-rocky microhabitats with less presence of shrubs and grasses, a pattern also reported for populations from other parts of the species range (Mebert et al., 2015; Ghira, 2016). Going south, however, to the southernmost population (site 5), vipers were found in microhabitats with more shrub and grass presence, equal to that of the stones/rocks. The structure and conditions (e.g., vegetation, light exposure, temperature, humidity) of the different microhabitats within a particular habitat may differ (Connell, 1961; Lugo et al., 1999; Petren, 2001; Bailey, 2009; Keith et al., 2020) and this might be why latitude-based differences were evident in microhabitat but not in habitat use. The observed differences in microhabitat use might be due to one of several reasons, or to a combination of most or all of them. First of all, these patterns might be a consequence of the specific characteristics of the different studied areas. Sites 1-4 were located in karst terrains, while site 5 in the Kresna Gorge was situated in a grassy-shrubby area. Secondly, the thermal conditions of the environment might also affect these patterns. The valley of Struma River in south-western Bulgaria, in which the Kresna Gorge is located, falls into the continental-Mediterranean zone, which is characterized by overall higher temperatures (Kopralev, 2002). Ambient temperatures in the stony/rocky-dominated microhabitats in this area might become too high, causing vipers to select more grassy and shrubby areas that provide more suitable temperatures. It is important to state, however, that the karst terrains in northern Bulgaria (i.e., Karlukovo) are also characterized by overall high temperatures (Nedyalkov et al., 2024), so this hypothesis seems less plausible. Another possible reason for the observed geographic differences in vipers' microhabitat use could be the effect of interspecific competition. In the northern and central parts of western Bulgaria, snake species richness is lower (up to six different species coexisting in sympatry and/or sintopy) than that in south-western Bulgaria, where up to 12 different species coexist in sympatry and/or sintopy (Beshkov, 1978, Petrov and Beshkov, 2001; Stojanov et al., 2011). It is possible that the stronger interspecific competition in this area, with species such as *Malpolon insignitus* (Geoffroy Saint-Hilaire, 1827), *Platyceps najadum* (Eichwald, 1831) and *Dolichophis caspius* (Gmelin, 1789), which all share similar habitats and diets with *V. ammodytes* (Beshkov, 1978) may drive the latter to use suboptimal microhabitats. Microhabitat segregation is known to reduce competition between ecologically similar species and/or species with similar diets, which share the same habitat (Luiselli, 2006; Martínez-Freiría et al., 2010; Mebert et al., 2015; Dyugmedzhiev et al., 2019). Further studies are needed, however, to evaluate this hypothesis.

Seasonal variations in habitat and microhabitat use

Our results, showing some seasonal variations in habitat use of *V. ammodytes*, are in agreement with the results of Beshkov (1993). Such seasonal shifts in habitat use are well-documented for other European viper species (Duguy, 1963; Viitanen, 1967; Prestt, 1971; Saint Girons, 1980; Naulleau et al., 1998; Anderson, 2003; Wollesen and Schwartze, 2004; Graitson, 2008). Our results however suggest that these seasonal variations in habitat use are much more complex than the basic seasonal pattern described by Beshkov (1993) (see Introduction), and dependent on the local characteristics of the area, inhabited by a particular population. The seasonal variations were most prominent in sites 1 and 3. In site 1, vipers hibernating dens were usually located in habitat H12 (Dyugmedzhiev et al., 2020). Shortly after spring emergence, vipers moved from their dens to the adjacent, more open and sunny habitat H7, where they were found until mid-autumn. During summer, only pregnant females remained close to the hibernating areas, although they inhabited H7 and not H12. Around the beginning of October, all vipers again returned close to the hibernating areas, where they were usually found basking in H7, but near their hibernating dens in H12 (usually between 20-100 m). By the second part of October and the first half of November, vipers moved to their hibernating dens in H12, where they spent the warm parts of the days basking.

A similar pattern was evident in a different habitat type (H2) in site 3. In this site, vipers used a big abandoned old quarry as a hibernating area. Vipers inhabited this quarry from the period of spring emergence until the end of the mating period (usually around mid to late May (Dyugmedzhiev et al., 2020). After this period, only pregnant vipers as well as a few immature individuals were detected in this habitat, until the second half of September, when the rest of the vipers started to return (Dyugmedzhiev et al., 2020). As it appears, from late spring until autumn, most vipers migrate from the quarry to the adjacent habitats. However, because we were

not able to detect a sufficient number of individuals in the vast area of those adjacent habitats, and none of the individuals captured there were identified as previously captured in the quarry, the true patterns and scale of this seasonal migration cannot be ascertained at this stage. Although it was evident that in site 2, habitats H1 and H7 were the vipers "preferred" areas during summer, our data is not comprehensive enough to point out the spring and autumn "preferred" habitats.

According to Beshkov (1993), the seasonal shifts in habitat use of *V. ammodytes* could be explained by the search for optimal thermal and solar radiation conditions, water sources, shelters, etc. However, food availability in the different habitat types might also play a role in these patterns (Viitanen, 1967; Prestt, 1971; Luiselli et al., 1994; Madsen and Shine, 1996; Luiselli, 2006). It is possible that spring/autumn habitats might have a more limited food base, such as small rodents, lizards, and centipedes, which are the most common prey of *V. ammodytes* (Beshkov, 1977; Luiselli, 1996; Dyugmedzhiev, 2020; Anđelković et al., 2021; Tomović et al., 2022). The fact that most vipers rarely use those habitats during summer, which is the most active feeding period, especially for adult vipers (Dyugmedzhiev, 2020), might be considered as an argument in support of this hypothesis. Similarly to the current study, some seasonal differences in microhabitat utilization were also reported for *V. ammodyes* from Serbia, Montenegro, and North Macedonia (Crnobrnja-Isailović et al., 2007) as well as for the ecologically similar *Vipera latastei* (Brito, 2003). These variations are most likely to be a consequence of the respective seasonal changes in habitat use.

Study limitations

There are some issues, coming from the method used to evaluate habitat preference, that need to be treated with caution. First of all, since the search effort was not even across each habitat type, it is possible that the use of some habitat types could be underestimated. Furthermore, the small overall areas of some habitat types, such as the abandoned buildings (H3) might cause an overestimation of the habitat preference compared to habitats with large areas (such as the rocky/stony areas overgrown with grass and shrubs, H7). Regarding the asphalt roads (H18), it is difficult to get a clear idea, based on the Ivlev's index values alone, since the only vipers that we found in this habitat type were dead ones (and they were excluded from the analyses). In any case, it appears that the roads are acting like a barrier, disrupting the vipers' home range.

CONCLUSIONS

Vipera ammodytes is a highly petrophilic species and in the studied areas showed a clear preference for various stony and rocky habitats and microhabitats, overgrown with herbaceous and shrub vegetation, while it avoided bare habitats, dark deciduous forests as well as cultivated agricultural lands. Habitat and microhabitat use seems to depend on a combination of many other factors such as season, locally specific characteristics like habitat structure and availability, population dynamics, food availability, physical and microclimatic conditions, and possibly the extent of the interspecific competition.

ACKNOWLEDGEMENTS

This work was partially supported by the Bulgarian Ministry of Education and Science under the National Research Program "Young scientists and postdoctoral students - 2" approved by DCM № 206 / 07.04.2022. All fieldwork was carried in accordance to Ministry of Environment and Water of Bulgaria Permit № 520/23.04.2013 and № 656/08.12.2015. We would like to thank Andrei Stoyanov (who sadly passed away in June 2016) and Georgi Popgeorgiev for the valuable advice and recommendations during this study; Kostadin Andonov and Nikola Stanchev for the help with some of the field work; Deyan Duhalov for providing initial information about the abandoned quarry; Nikolay Todorov for designing a special box, which facilitated the safe photographing of the vipers. We thank the anonymous reviewers and the subject editor whose comments and suggestions helped to improve the manuscript.

SUPPLEMENTARY MATERIAL

Supplementary material associated with this article can be found at <http://www-9.unipv.it/webshi/appendix/index.html> manuscript number 15928

REFERENCES

Anđelković, M., Nikolić, S., Tomović, L. (2021): Reproductive characteristics, diet composition and fat reserves of nose-horned vipers (*Vipera ammodytes*). Herpetol. J. **31**: 151-161.

Andersson, S. (2003): Hibernation, habitat and seasonal activity in the adder, *Vipera berus*, north of the Arctic Circle in Sweden. Amphibia-Reptilia **24**: 449-457.

Bailey, R.G. (2009): Ecosystem geography (Second ed.). New York, Springer.

Beshkov, V. (1977): Izsledvaniya varhu biologiyata i ekologiyata na zmiite v Maleshevskata planina (Yugozapadna Bulgaria). III. Varhu hranata i razmnozhavaneto na pepelyankata (*Vipera ammodytes meridionalis* Boulenger). Ekologiya **4**: 3-12.

Beshkov, V. (1978): Biologichni i ekologichni izsledvaniya varhu zmiite v Maleshevskata planina. Unpublished doctoral dissertation. Institute of Zoology, Bulgarian Academy of Sciences, Sofia.

Beshkov, V. (1993): Varhu sezonnata I denonoshtna aktivnost na pepelyankata *Vipera ammodytes* (L.) v Bulgaria. Herpetologiya **1**: 3-12.

Brito, J.C. (2003): Seasonal variation in movements, home range, and habitat use by male *Vipera latastei* in Northern Portugal. J. Herpetol. **37**: 155-160.

Bruno, S. (1967): Sulla *Vipera ammodytes* (Linnaeus 1758) in Italia. Memorie del Museo Civico di Storia Naturale di Verona **15**: 289-336.

Burger, J., Zappalorti, R.T. (1989): Habitat use by pine snakes (*Pituophis m. melanoleucus*) in the New Jersey pine barrens: individual and sexual variation. J. Herpetol. **23**: 68-73.

Charland, M.B., Gregory, P.T. (1995): Movements and habitat use in gravid and nongravid female garter snakes (Colubridae: *Thamnophis*). J. Zool. **236**: 543-561.

Connell, J.H. (1961): The influence of interspecific competition and other factors on the distribution of the barnacle *Chthamalus stellatus*. Ecology **42**: 710 - 723.

Cooper-Bohannon, R., Rebelo, H., Jones, G., Cotterill, F.(W.), Monadiem, A., Schoeman, M. C., Taylor, P., Park, K. (2016): Predicting bat distributions and diversity hotspots in southern Africa. Hystrix **27**: 38-48.

Crnobrnja-Isailović, J., Ajtić, R., Tomović, L. (2007): Activity patterns of the sand viper (*Vipera ammodytes*) from the Central Balkans. Amphibia-Reptilia **28**: 582-589.

Duguy, R. (1963): Biologie de la latence hivernale chez *Vipera aspis*. Vie et Milieu **14**: 311-444.

Dyugmedzhiev, A. (2020): Prostranstvena ekologiya na pepelyankata *Vipera ammodytes* (Linnaeus, 1758) v Zapadna Bulgaria. Unpublished doctoral dissertation. National Museum of Natural History, Bulgarian Academy of Sciences, Sofia.

Dyugmedzhiev, A.V., Popgeorgiev, G.S., Tzankov, N.D., Naumov, B.Y. (2020): Population estimates of the Nose-horned Viper *Vipera ammodytes* (Linnaeus, 1758) (Reptilia: Viperidae) from five populations in Bulgaria. Acta Zool. Bulgar. **72**: 397-407.

Dyugmedzhiev, A., Naumov, B., Tzankov, N. (2021): Thermal ecology of the Nose-horned Viper (*Vipera ammodytes* (Linnaeus, 1758)) under natural conditions. North-Western Journal of Zoology **17**: 44-56.

Dyugmedzhiev, A., Slavchev, M., Naumov, B. (2019): Emergence and dispersal of snakes after syntopic hibernation. Herpetozoa **32**: 149-157.

Dyugmedzhiev, A., Tzankov, N., Natchev, N., Naumov, B.Y. (2018): A non-traumatic multi-operational method for individual documentation and identification of nose-horned vipers (*Vipera ammodytes* (Linnaeus, 1758) (Squamata, Viperidae)) allows reliable recognition of recaptured specimens. Biharean Biologist **12**: 92-96.

Ghira, I. (2016): Ecologia, etologia şi distribuţia geografică a viperei cu corn (*Vipera ammodytes ammodytes L., 1758)* în România. Unpublished doctoral dissertation. Presa Universitară Clujeană, Cluj.

Graitson, E. (2008): Éco-éthologie d'une population de vipères péliades (*Vipera b. berus* L.) dans une région de bocage du sud-ouest de la Belgique. B. Soc. Herpétol. Fr. **128**: 3-19.

Hall, L.S., Krausman, P.R., Morrison, M.L. (1997): The habitat concept and a plea for standard terminology. Wildllife Soc. B. **25**: 173-182.

Hammer, Ø., Harper, D.A.T., Ryan, P.D. (2001): PAST: Paleontological statistics software package for education and data analysis. Palaeontol. Electron. **4**: 4.

Heckes, U., Gruber, H.-J., Stumpel, N. (2005): *Vipera* (*Vipera*) *ammodytes*. In: Handbuch der Reptilien und Amphibien Europas, Bd 3/2B, Schlangen (Serpentes) III Viperidae, pp. 81-151. Joger, U., Stümpel, N., Eds., Aula-Verlag, Wiebelsheim.

Huey, R.B., Peterson, C.R., Arnold, S.J., Porter, W.P. (1989): Hot rocks and not-so-hot rocks: retreat- site selection by garter snakes and its thermal consequences. Ecology **70**: 931-944.

Ioannidis, Y, Bousbouras, D. (1997): The space utilization by the reptiles in Prespa National Park. Hydrobiologia **351**: 135-142.

Keith, D.A., Ferrer-Paris, J.R., Nicholson, E., Kingsford, R.T. (2020): The IUCN Global Ecosystem Typology 2.0: Descriptive profiles for biomes and ecosystem functional groups. IUCN, Gland, Switzerland. https://doi.org/10.2305/IUCN.CH.2020.13.en

Kenward, R.E. (1992): Quantity versus quality: programmed collection and analysis of radio-tracking data. In: Wildlife Telemetry. Remote Monitoring and Tracking of Animals, pp. 231-246. Priede, I.G., Swift, S.M., Eds., Ellis Horwood, London.

Kopralev, I. (2002): Geografiya na Bulgaria. Sofia, For-Com Publishers.

Krebs, C.J. (1999): Ecological Methodology. Second Edition. Menlo Park, California, Addison Wesley Longman.

Kurek, K., Król, W., Najberek, K., Ćmiel, M., Solarz, W., Bury, S., Baś, G., Najbar, B., Okarma, H. (2018): Habitat use of the aesculapian snake at different spatial scales. The Journal of Wildlife Management **82**: 1746-1755.

Lugo, A.E., Brown, S.L, Dodson, R., Smith, T.S., Shugart, H.H. (1999): The Holdridge life zones of the conterminous United States in relation to ecosystem mapping. J. Biogeogr. **26**: 1025-1038.

Luiselli, L. (1996): Food habits of an alpine population of the sand viper (*Vipera ammodytes*). J. Herpetol. **30**: 92-94.

Luiselli, L. (2006): Resource partitioning and interspecific competition in snakes: the search for general geographical and guild patterns. Oikos **114**: 193-211.

Luiselli, L., Capula, M., Rugiero, L., Anibaldi, C. (1994): Habitat choice by melanistic and cryptically coloured morphs of the adder, *Vipera berus*. B. Zool. **61**: 213-216.

Madsen, T., Shine, R. (1996): Seasonal migration of predators and prey- a study of pythons and rats in tropical Australia. Ecology **77**: 149-156.

Martínez-Freiría, F., Lizana, M., do Amaral, J.P., Brito, J.C. (2010): Spatial and temporal segregation allows coexistence in a hybrid zone among two Mediterranean vipers (*Vipera aspis* and *V. latastei*). Amphibia-Reptilia **31**: 195-212.

Mebert, K., Jagar, T., Grželj, R., Cafuta, V., Luiselli, L., Ostanek, E., Golay, P., Dubey, S., Golay, J., Ursenbacher, S. (2015): The dynamics of coexistence: Habitat sharing vs. segregation patterns among three sympatric montane vipers. Biol. J. Linn. Soc. **116**: 364-376.

Morrison, M.L. (2009): Restoring wildlife: Ecological concepts and practical applications. Washington, DC, Island Press.

Naulleau, G., Bonnet, X., Duret, S. (1996): Déplacements et domaines vitaux des femelles reproductrices de vipères aspic *Vipera aspis* (Reptilia, Viperidae) dans le centre ouest de la France. B. Soc. Herpétol. Fr. **78**: 5-18.

Naulleau, G., Duguy, R., Saint Girons, H. (1998): Le système espace-temps au cours du cycle annuel chez les Viperinae. B. Soc. Zool. Fr. **123**: 53-60.

Nedyalkov, N., Kodzhabashev, N. Pandakov, P., Popgeorgiev, G. (2024): New records of *Suncus etruscus* (Soricidae, Mammalia) and its current status in Bulgaria. Historia naturalis bulgarica **46**: 189-194.

Neumeyer, R. (1987): Density and seasonal movements of the adder *(Vipera berus* L., 1758) in a subalpine environment. Amphibia-Reptilia **8**: 259-276.

Petren, K. (2001): Concept of habitat and niche. In: Encyclopaedia of biodiversity, vol. 3, pp. 303-315. Levin, S.A., Ed., Academic Press, Cambridge, Massachusetts.

Petrov, B., Beshkov, V. (2001): Zemnovodni (Amphibia) i vlechugi (Reptilia) v Kresnenskiya prolom. In: Biorznoobrazie na Kresnenskiya prolom (YuZ Bulgaria), pp. 297-303. Beron, P., Ed., BAN, Sofia.

Plasinger, I., Righetti, D., Di Cerbo, A.R. (2014): La Vipera dal corno (*Vipera ammodytes* Linnaeus, 1758) in Alto Adige. In: X Congresso Nazionale Societas Herpetologica Italica, pp. 271-278. Doria, G., Ed, Ianieri, Genoa.

Popgeorgiev, G., Spasov, S., Kornilev, Y. (2015): SmartBirds – Information system with biological information, BSPB. Retrieved from http://www.smartbirds.org.

Prestt, I. (1971): An ecological study of the viper, *Vipera berus*, in southern Britain. J. Zool. **164**: 373-418.

Reinert, H.K. (1984): Habitat variation within sympatric snake populations. Ecology **65**: 1673-1682.

Reinert, H.K. (1993): Habitat selection in snakes. In: Snakes: Ecology and Behavior, pp. 201-240. Seigel, R.A., Collins, J.T., Novak, S.S., Eds., McGraw-Hill, New York.

Reinert, H.K., Kodrich, W.R. (1982): Movements and habitat utilization by the massasauga, *Sistrurus catenatus catenatus*. J. Herpetol. **16**: 162-171.

Rohlf, F.J. (1988): NTSYS-pc: Numerical taxonomy and multivariate analysis system. New York, Exeter Publishing.

Saint Girons, H. (1952): Ecologie et éthologie des Vipères de France. Ann. Sci. Nat. Zool. **14**: 263-341.

Saint Girons, H. (1980): Biogéographie et évolution des vipers européennes. Compte Rendu des Séances de la Société de Biogêographie **496**: 146-172.

Saint Girons, H. (1997): Utilisation de l'espace vital par *Vipera aspis* (Reptilia, Viperidae) dans une région de bocage de l'ouest de la France. B. Soc. Herpétol. Fr. **84**: 5-14.

Seigel, R.A. (1986): Ecology and conservation of an endangered rattlesnake (*Sistrurus catenatus*) in Missouri, USA. Biol. Conserv. **35**: 333-346.

Shine, R. (1986): Sexual differences in morphology and niche utilization in an aquatic snake, *Acrochordus arafurae*. Oecologia **69**: 260-267.

Speybroeck, J., Beukema, W., Bok, B., Voort, J.V.D. (2016): Field guide to the amphibians and reptiles of Britain and Europe. London, Bloomsbury Publishing Plc,.

Stojanov, A., Tzankov, N., Naumov, B. (2011): Die Amphibien und Reptilien Bulgariens. Frankfurt am Main, Chimaira.

Strugariu, A., Zamfirescu, Ş.R., Gherghel, I., Sahlean, T.C., Moraru, V., Zamfirescu, O. (2011): A preliminary study on population characteristics and ecology of the critically endangered meadow viper *Vipera ursinii* in the Romanian Danube Delta. Biologia **66**: 175-180.

Stumpel, H., Hahn, C. (2001): Die Hornotter *Vipera ammodytes* (Linnaeus, 1758) in Südtirol, Italien. Herpetofauna **23**: 9-18.

Sweet, S.S. (1985): Geographic variation in *Pituophis* and *Crotalus*. J. Herpetol. **19:** 55-67.

Thomas, B. (2004): Die Kreuzotter (*Vipera b. berus* [L.]) im Toten Moor in der Region Hannover. Mertensiella **15**: 175-185.

Tomović, L., Anđelković, M., Golubović, A., Arsovski, D., Ajtić, R., Sterijovski, B., Nikolić, S., Crnobrnja-Isailović, J., Lakušić, M., Bonnet, X. (2022): Dwarf vipers on a small island: body size, diet and fecundity correlates. Biol. J. Linn. Soc. **20**: 1-13.

Tuleshkov, K. (1959): Prinos kam prouchvaneto ekologiyata na pepelyankata (*Vipera ammodytes* (L.) v Bulgaria. Izvestiya na Zoologicheskiya institut s muzey **8**: 169-180.

Viitanen, P. (1967): Hibernation and seasonal movements of the viper, *Vipera berus* (L.), in southern Finland. Ann. Zool. Fenn. **4**: 472-548.

Vitt, L.J., Caldwell, J.P. (2014): Herpetology. An Introductory Biology of Amphibians and Reptiles. Fourth Edition. Amsterdam, Elsevier.

Webb, J.K., Shine, R. (1998): Using thermal ecology to predict retreat-site selection by an endangered snake species. Biol. Conserv. **86**: 233-242.

Weinmann, K., Beck, C., Madl, R., Penner, J., Soun, P., Wollesen, R., Joger, U. (2004): Zur Ökologie und Raum-Zeit-Einbindung einer Kreuzotterpopulation (*Vipera berus* [L.]) im hessischen Spessart. Mertensiella **15**: 191-212.

Wolda, H. (1981): Similarity Indices, Sample Size and Diversity. Oecologia **50**: 296-302.

Wollesen, R., Schwartze, M. (2004): Vergleichende Betrachtungen zweier linearer Kreuzotter-Habitate (*Vipera berus* [Linnaeus, 1758]) in der norddeutschen Tiefebene. Mertensiella **15**: 164-174.

Acta Herpetologica 19(2): 97-122, 2024
DOI: 10.36253/a_h-15648

The tooth-bearing skeletal elements of the Italian urodeles, a comparative tool for osteological identification

Sara Monti[1,*], Loredana Macaluso[2,3], Massimo Delfino[1,4]

[1] *Dipartimento di Scienze della Terra, Università di Torino, Via Valperga Caluso 35, I-10125 Torino, Italy*
[2] *Museo Regionale di Scienze Naturali, Via Giolitti 36, 10123, Torino, Italia*
[3] *Sciences Collections, Martin Luther University Halle-Wittenberg, Domplatz 4, 06108 Halle (Saale), Germany*
[4] *Institut Català de Paleontologia Miquel Crusafont (ICP-CERCA), Edifici ICTA-ICP, c/ Columnes, s/n, Campus de la UAB, E-08193 Cerdanyola del Vallès, Barcelona, Spain*
**Corresponding author.* Email: sara.monti957@edu.unito.it

Submitted on: 2024, 31st January; revised on: 2024, 22nd March; accepted on: 2024, 8th May
Editor: Andrea Villa

Abstract. Urodele osteology is characterised by simplified skulls, loss of several bones and a specific sequence of cranial and limb ossification. The relatively few studies devoted to the comparative analysis of isolated urodele bones are mostly focused on the vertebrae and occipital complexes, and to a lesser extent humeri. The tooth-bearing skeletal elements (premaxillae, maxillae, dentaries, and vomers) are strongly neglected in this respect, despite being robust and as such sometimes found as fossils. Herein, we provide for the first time a comparative study of dentigerous bones, focusing on the Italian urodeles. Thirteen of the 19 species present in Italy, representing all genera except one, were analysed, for a total of 70 dry-prepared skeletons. The morphology of dentigerous skeletal elements of Italian urodeles is described and pictured, providing diagnostic characters and dichotomous keys for the identification at the genus level in most cases, and species level in some. The diagnostic morphological characters were included in a phylogenetic analysis, the results of which demonstrate that the tooth-bearing elements can have a phylogenetic value useful for assessing the relationships of living taxa.

Keywords. Osteology, urodeles, phylogeny, dentigerous bones.

INTRODUCTION

The Italian geographic province (Lanza and Corti, 1996) shows the highest amount of urodele endemism in Europe (Macaluso et al. 2021a, b, 2023a), including three endemic genera (*Salamandrina*, *Speleomantes*, and *Euproctus*; Lanza et al., 2007). How and when these taxa reached the Italian Peninsula is not yet fully understood as the Italian fossil record of urodeles is poor, mostly composed of isolated remains identified at best to the genus level, in a chronologic range spanning from the Miocene to the Holocene (among others, Abbazzi et al., 2004; Colombero et al., 2017; Delfino, 2004; Delfino et al., 2011; Delfino and Bailon, 2000; D'Orazi Porchetti et al., 2012; Macaluso et al., 2021a; Venczel and Sanchiz, 2006; Villa et al., 2018, 2020, 2021). Besides the rarity of fossils, our knowledge of the fossil record of urodeles is hindered by the limited studies on the osteology of the extant species. In fact, even if some studies focus on extensive and comprehensive descriptions of one taxon or a few taxa, few studies were devoted to the comparative analysis of isolated bones that represent nearly the entire Italian fossil record. At a European scale, the only inclusive and comparative studies are focused on vertebrae, otic-occipital complexes, and humeri (Ratnikov and Litvinchuk, 2007, 2009; Ratnikov, 2015; Macaluso et al.,

ISSN 1827-9635 (print)
ISSN 1827-9643 (online)

www.fupress.com/ah

2023b), which are the most commonly found elements in the fossil record thanks to their general robustness (Monti, 2021; Macaluso et al., 2022). Among the skull elements (the second most common skeletal district in the fossil record composed of isolated remains; Monti, 2021; Macaluso et al., 2022), tooth-bearing skeletal elements (premaxillae, maxillae, dentaries, and vomers) are easily found because of their peculiar morphology and relative thickness. Despite being easily recognised as belonging to Urodela or Amphibia due to the pedicellate teeth (Schoch, 2014), a generic or specific attribution is rarely reached because of a lack of comparative studies on the dentigerous elements. The aim of the current work is to provide taxonomically significant diagnostic characters at least at the genus level, and, when possible, at the species level, for Italian urodeles based on isolated dentigerous bones, as well as a dichotomous key for identification. Moreover, to provide a scaffold for the inclusion in phylogenies of extinct taxa, the most robust diagnostic morphological characters are included in a character matrix to test whether or not the tooth-bearing elements carry phylogenetic value useful for assessing the relationships of living (and therefore also extinct) taxa.

MATERIAL AND METHODS

The morphology of dentigerous skeletal elements of Italian urodeles is described based on disarticulated dry-prepared skeletons, housed in the Massimo Delfino Herpetological collection (MDHC) of the Museo di Geologia e Paleontologia dell'Università di Torino (MGPTU), at the Department of Earth Sciences of the University of Turin, and in the Museo Regionale di Scienze Naturali di Torino (MRSN). Thirteen of the 19 species present in Italy are considered, including two families, Plethodontidae and Salamandridae, and seven genera, for a total of 70 specimens (Table S1) and approximately 560 bones. All Italian genera are represented except *Proteus*, which is not included in this study due to its peculiar and derived palatal morphology (noteworthy is the absence of maxillae; Fabre et al., 2020) and will be the subject of future studies. All the missing species belong to the genus *Speleomantes*: this study includes *Speleomantes ambrosii*, *Speleomantes italicus*, and *Speleomantes strinatii*, whereas the species *Speleomantes supramontis*, *Speleomantes sarrabusensis*, *Speleomantes flavus*, *Speleomantes genei*, and *Speleomantes imperialis* are missing. For some taxa (*S. ambrosii, S. italicus*), only one specimen has been studied, whereas for others (*Salamandra salamandra, Triturus carnifex*) as many as 11 specimens were examined. Moreover, for *Salamandra atra*, the only available vomer was broken. For *S. italicus* MDHC 301, only the left maxilla and the dentaries are present. *Euproctus platycephalus* MDHC 405 does not preserve any dentigerous bone except for the dentaries. As such, it is important to underline that the characters concerning poorly represented species should be taken with caution due to the limited number of available specimens. Bones were photographed with a Leica M205 microscope equipped with the Leica application suite v3.3.0 or v4.10 at the Department of Earth Sciences of the University of Turin. Terminology follows Vater (2003), Buckley et al. (2010), and Villa et al. (2014).

Comparative and phylogenetic analysis

Dichotomous keys for identification and diagnostic characters were obtained comparing the descriptions and the observations made on the different taxa and are reported in the discussion section below. We performed statistical counts on the teeth number using Excel v2307.

A character matrix, including 13 species-level operational taxonomic units and 33 newly created osteological characters (supplementary file F1), was built with Mesquite v3.61 (Maddison and Maddison, 2019). All characters are related to the dentigerous bones (see Table S2 for the list of the characters). The hynobiid *Pseudohynobius flavomaculatus* was scored as outgroup, owing to its phylogenetic distance from the other operational taxonomic units (Duellman and Trueb, 1994; Kohono et al., 1991; Pyron and Wiens, 2011) and basing the scoring on the descriptions and pictures by Jia et al. (2021).

The phylogenetic analysis was run using TNT v1.6 (Goloboff and Morales, 2023) using the New Technology search with all algorithms selected, the consensus stabilised five times with a factor of 75, and 1000 trees in memory, followed by a second round of tree bisection and reconnection.

RESULTS

Terminology and general morphology

The anatomical structures cited in the text are illustrated in Fig. 1.

Premaxilla. Premaxillae are paired bones placed at the anterior end of the skull; they articulate medially with each other, laterally with the maxillae and posteriorly with the vomers. They can be separated or fused together, and they are formed by three main parts: alary process, pars dentalis, and pars palatina. The alary process is thin, dorsally elongated and curved in posterodorsal direction; it con-

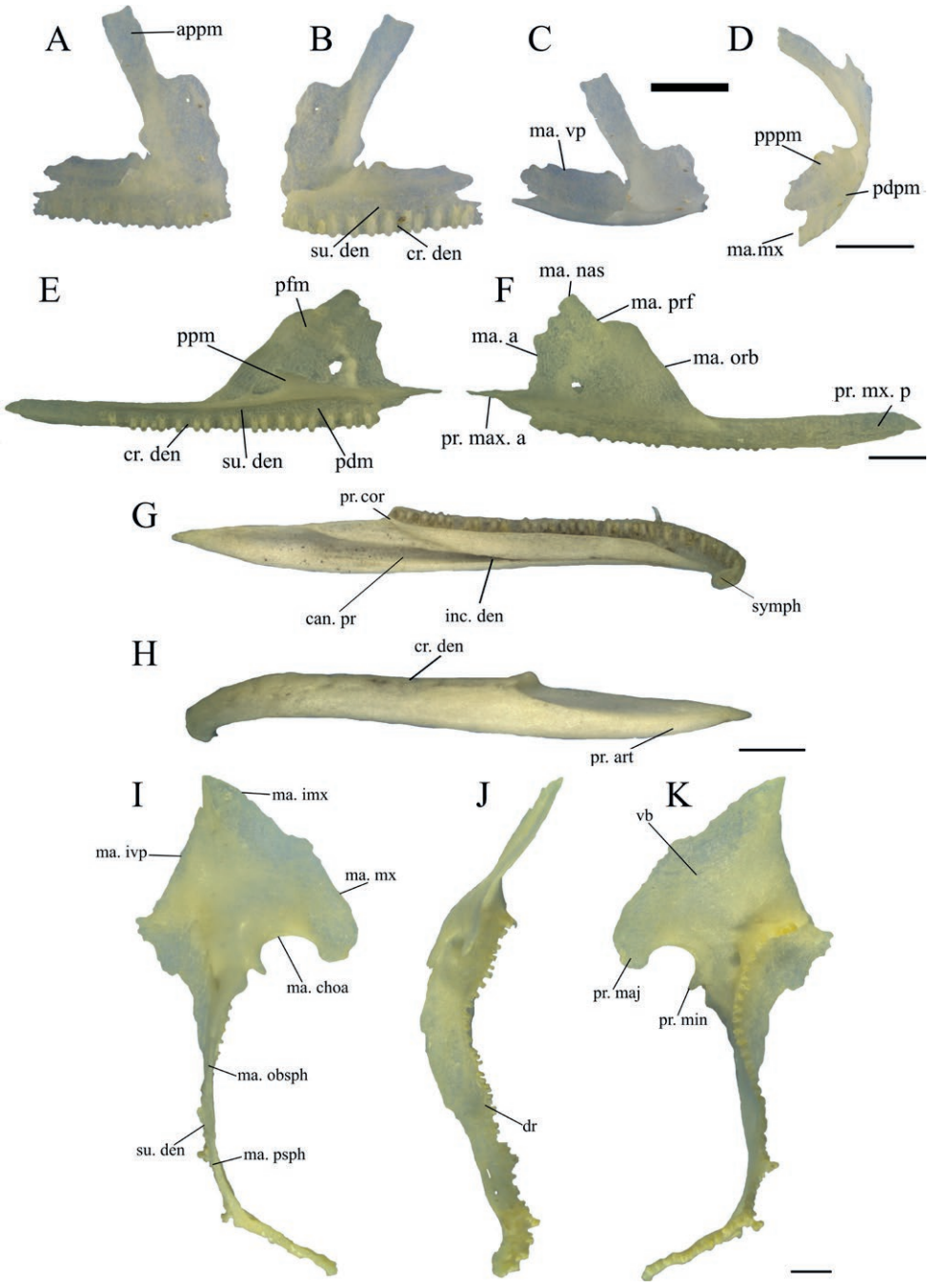

Fig. 1. Terminology followed for the dentigerous bones. A-D: right premaxilla of *Salamandra atra* (MDHC 394) in anterior (A), posterior (B), dorsal (C) and lateral (D) views. Abbreviations: appm, alary process of the premaxilla; cr. den, crista dentalis; ma. mx, margo maxillaris; ma. vp, margo vomeropalatinum; pdpm, pars dentalis of the premaxilla; pppm, pars palatina of the premaxilla; su. den, sulcus dentalis. E-F: left maxilla of *Salamandra lanzai* (MDHC 362) in medial (E) and lateral (F) views. Abbreviations: cr. den, crista dentalis; ma. a, margo anterioris; ma. nas, margo nasalis; ma. orb, margo orbitalis; ma. prf, margo praefrontalis; pdm, pars dentalis of the maxilla; pfm, pars facialis of the maxilla; ppm, pars palatina of the premaxilla; pr. mx. a, processus maxillaris anterior; pr. mx. p, processus maxillaris posterior; su. den, sulcus dentalis. G-H: left dentary of *Euproctus platycephalus* (MDHC 507) in medial (G) and ventrolateral (H) views. Abbreviations: can. pr, canalis primordialis; cor, processus coronoideus; inc. den, incisura dentalis; pr. art, processus articularis; su. den, sulcus dentalis; symp, symphysis. I-K: left vomer of *Salamandra salamandra* (MDHC 205) in dorsal (I), lateral (J) and ventral (K) views. Abbreviations: dr, dentigerous ridge; ma. choa, margo choanalis; ma. imx, margo intermaxillaris; ma. ivp, margo intervomeropalatinum; ma. mx, margo maxillaris; ma. obsph, margo orbitosphenoideum; ma. psph, margo parasphenoideum; pr. maj, processus vomeropalatinus major; pr. min, processus vomeropalatinus minor; su. den, sulcus dentalis; vb, body of the vomer. Scale bars: 1 mm.

tacts the anterior end of the frontal, and its posterior half is partially overlapped by the nasal. The pars dentalis bears a variable number of pedicellate teeth, which can be seen in anterior and lateral views, and it is slightly curved, usually thicker than the alary process; the dorsal margin can be straight or irregular. The pars dentalis articulates with the maxilla through the margo maxillaris. The pars palatina is always visible in posterior view. The margo vomeropalatinum can be straight or may show some irregularities.

Maxilla. Maxillae are paired bones, which articulate anteriorly with the premaxillae, dorsally with the prefrontals and nasals and medially with the vomers; their posterior end does not contact the pterygoid and extends only slightly beyond the posterior margin of the eye, without reaching the quadrate. Maxillae are formed by three main parts: pars facialis, pars dentalis, and pars palatina. The pars facialis develops in dorsal direction, it has a trapezoidal shape with irregular margins, and it can be smooth or sculptured. It articulates with the prefrontal and the nasal through respectively the margo praefrontalis and the margo nasalis and with the premaxillae through the processus maxillaris anterior. The margo anterioris and the margo orbitalis can be straight or irregular. The pars dentalis is narrow, regular and elongated and bears a variable number of pedicellate teeth that can be visible both in lateral and medial views; the pars dentalis can be straight or curved posterodorsally. The sulcus dentalis is visible on the medial surface of the pars dentalis, dorsally to the teeth. The pars palatina allows the whole maxilla to articulate with the corresponding premaxilla and can have variable shapes.

Dentary. Dentaries are elongated, paired and curved bones. They are robust and they are the primary bones forming the mandible. They touch each other anteromedially at the symphysis and their posterior portion articulates medially with prearticulars and articulars. The processus articularis is laminar. Posteriorly the bone is flat and smooth, with a pointy or rounded shape. The dorsal and ventral margins of the bone tend to fold up and they can be fused to a varying degree; due to the folding, the two margins are thicker than the bone between them. The two margins cover the canalis primordialis, which runs along the whole medial surface of the dentary. The space between the two margins is called the incisura dentalis, that is straight and regular and narrows in the anterior part due to the margins approaching. The latter come in contact in some species. The crista dentalis bears a variable number of pedicellate teeth, extending up to the processus coronoideus, a little triangular or trapezoidal expansion that sometimes is absent and likely changes significantly throughout ontogeny.

Vomer. Vomers are paired elements that articulate anterolaterally with the premaxillae through the margo intermaxillaris and with the maxillae through the margo maxillaris. Dorsally, the vomers articulate with the parasphenoid and orbitosphenoids through respectively the margo parasphenoideum and the margo orbitosphenoideum. The two vomers do not touch each other. This bone is made by two parts: the body of the vomer and the dentigerous ridge. The body of the vomer has a triangular or a claw hammer shape and it develops in a posterior direction; it is smooth on both the dorsal and ventral surfaces, and it keeps the same thickness throughout. The body of the vomer shows a concavity on the margo choanalis, bounded by the processus vomeropalatinus major and the processus vomeropalatinus minor, which can be variably pronounced or even absent. Only in *Speleomantes*, the concavity is bounded by the processus vomeropalatinus major and the dentigerous ridge. The dentigerous ridge is elongated and bears a variable number of pedicellate teeth that are regularly visible in lateral view. Dorsally to the teeth there is a very shallow sulcus dentalis. In *T. carnifex* and *S. salamandra*, there can be an aberrant condition with some supernumerary teeth developing outside the normal dental line.

Descriptions

In this section, the morphology of premaxillae (Figs 2, 3), maxillae (Figs 4, 5), dentaries (Figs 6, 7), and vomers (Fig. 8) are described for each taxon. The counts of the tooth positions are summarized in Table S3 (and discussed below in the section "Variation in the number of tooth positions").

Plethodontidae
Speleomantes

The species of the genus *Speleomantes* are grouped into a single description, emphasizing the differences between species.

Premaxilla (Fig. 2A-H). The premaxillae of the only studied specimen of *S. italicus* are missing. In *Speleomantes*, the two premaxillae are not fused together. Only in *S. strinatii* MDHC 225, the two premaxillae are fused together: they are connected by a thin bridge well visible in anterior and posterior views on the ventral third of the medial margin of the alary process. This bridge is pierced by one foramen. The whole premaxilla of *Speleomantes* is three times higher than long. In lateral view, it shows an expansion that extends along its dorsal half. The dorsal half of the alary process ends with a rounded tip. The pars dentalis is of the same thickness as the alary process and it is straight. The margo maxillaris is medially round-

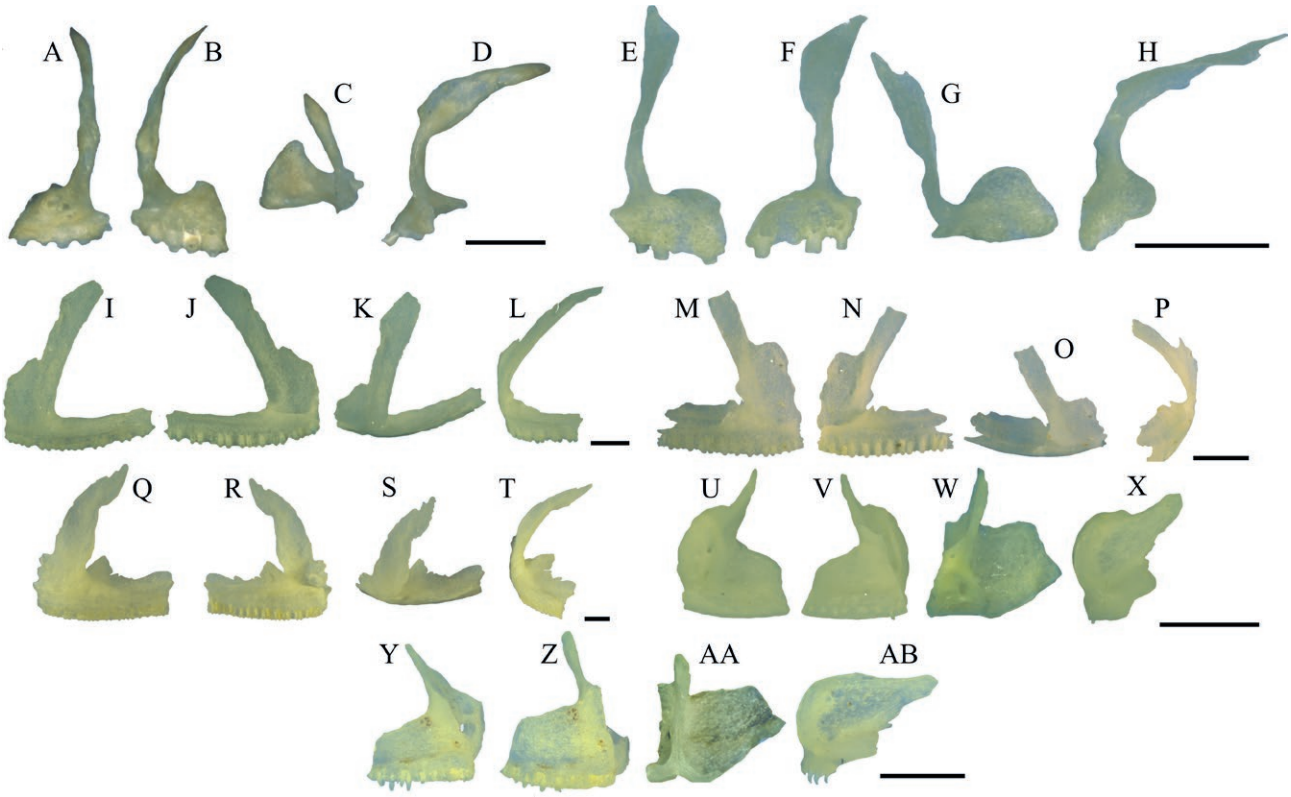

Fig. 2. Premaxillae of Italian salamanders. A-D: right premaxilla of *Speleomantes ambrosii* (MDHC 301) in anterior (A), posterior (B), dorsal (C) and lateral (D) views; E-H: left premaxilla of *Speleomantes strinatii* (MDHC 486) in anterior (E), posterior (F), dorsal (G) and lateral (H) views; I-L: left premaxilla of *Salamandra lanzai* (MDHC 362) in anterior (I), posterior (J), dorsal (K) and lateral (L) views; M-P: right premaxilla of *Salamandra atra* (MDHC 394) in anterior (M), posterior (N), dorsal (O) and lateral (P) views; Q-T: left premaxilla of *Salamandra salamandra* (MDHC 205) in anterior (Q), posterior (R), dorsal (S) and lateral (T) views; U-X: left premaxilla of *Salamandrina perspicillata* (MDHC 406) in anterior (U), posterior (V), dorsal (W) and lateral (X) views; Y-AB: left premaxilla of *Salamandrina terdigitata* (MDHC 333) in anterior (Y), posterior (Z), dorsal (AA) and lateral (AB) views. Scale bars: 1 mm.

ed. In posterior view, the pars palatina is developed in posterior direction, but it is not visible in anterior view, as it is covered by the dorsal half of the pars dentalis. It is subtriangular in shape, enlarging posterolaterally.

Maxilla (Fig. 4A-L). In *S. ambrosii*, the pars facialis extends along the middle third of the crista dentalis. In *S. italicus* and *S. strinatii*, the pars facialis extends respectively along the second fourth and the second and third fifths (MDHC 225) or the middle third (MDHC 486 and MDHC 521) of the crista dentalis. It has a smooth surface, both in lateral and medial views. In lateral view, it shows a shallow concavity on the margo orbitalis and another one on the margo anterioris; these cavities are absent in *S. italicus*. The margins are rather straight in *S. ambrosii* and *S. italicus*, and irregular in *S. strinatii*. The right pars facialis of MDHC 225 shows one foramen. The teeth run for the whole length of the pars dentalis, including the processus maxillaris anterior. As such, the pars facialis does not reach the anterior end of the tooth row. The pars palatina runs along the whole dorsomedial margin of the pars dentalis. This pars is very small, with the same width for almost its entire length; it ends anteriorly in a flat and abrupt processus maxillaris anterior, with regular margins.

Dentary (Fig. 6A-L). The margins fold up covering the anterior third of the canalis primordialis, which runs across the whole medial surface of the dentary, so that in medial view the incisura dentalis opens only along its posterior two thirds. In *S. strinatii*, only the ventral margin of the dentary folds up, thickening and covering a small part of the canalis primordialis. In medial view, the processus coronoideus has a parallelogram-like shape, with smooth edges. In *S. italicus*, the processus coronoideus is almost absent. The symphysis shows an anterodorsal bulge in medial view. In ventral view, in *S. strinatii*, the ventral margin is thicker than the dorsal one.

Vomer (Fig. 8A-F). The vomers of *S. italicus* are missing. In ventral view, the body of the vomer has a

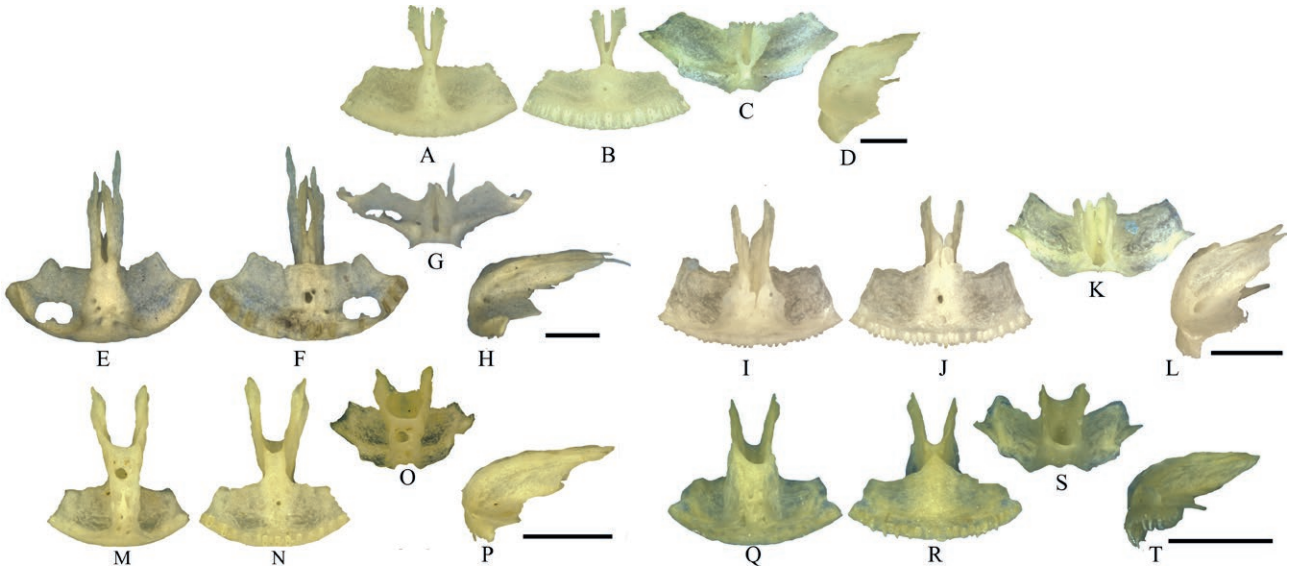

Fig. 3. Premaxillae of Italian newts. A-D: premaxilla of *Triturus carnifex* (MDHC 85) in anterior (A), posterior (B), dorsal (C) and left lateral (D) views; E-H: premaxilla of *Euproctus platycephalus* (MDHC 507) in anterior (E), posterior (F), dorsal (G) and left lateral (H) views; I-L: premaxilla of *Ichthyosaura alpestris* (MDHC 416) in anterior (I), posterior (J), dorsal (K) and left lateral (L) views; M-P: premaxilla of *Lissotriton vulgaris* (MDHC 132) in anterior (M), posterior (N), dorsal (O) and left lateral (P) views; Q-T: premaxilla of *Lissotriton italicus* (MDHC 482) in anterior (Q), posterior (R), dorsal (S) and left lateral (T) views. Scale bars: 1 mm.

triangular shape, with a laterally directed tip. In dorsal and medial views, the margo choanalis shows a concavity bounded by the processus vomeropalatinus major and the dentigerous ridge. The dentigerous ridge is mediolaterally directed, slightly posteriorly curved, forming with the margo intervomeropalatinum an acute angle. In lateral view, the dentigerous ridge is curved. The margo intervomeropalatinum and the margo maxillaris are regular and rather straight.

Salamandridae
Salamandrinae
Salamandra lanzai

Premaxilla (Fig. 2I-L). The two premaxillae are not fused together. The premaxilla is as long as or slightly shorter than high. In anterior view, the alary process ends abruptly. Still in the same view, the pars dentalis is thick, rectangular and curved posterolaterally, with either one or two foramina on its dorsal half. In dorsal view, the ventral half of the premaxilla is thickened at the articulation with the opposite premaxilla. In anterior view, the margo maxillaris is vertical. The margo vomeropalatinum is generally straight in dorsal view, but it can show some irregularity. The dorsal margin of the pars dentalis expands in posterior direction and, together with the expansion of the alary process, it forms a cavity, open on the anterior side. Dorsally to this cavity, there is another smaller one (missing on the right premaxilla of MDHC 362). The pars palatina is extremely small and cannot be seen in anterior view. In posterior view, the pars palatina keeps the same width for all its length, except for a widening at midlength.

Maxilla (Fig. 4M-P). In lateral view, the pars facialis bears one to three foramina and has a variable thickness. The pars facialis extends along the anterior half of the pars dentalis. In lateral and medial views, the margo anterioris is particularly irregular, with sharp edges, whereas the margo orbitalis is more regular and straight. Only the posterior fourth of the length of the pars dentalis is toothless. The pars palatina runs along the whole dorsomedial margin of the pars dentalis; it keeps the same width for almost its entire length, forming a triangular and sharp processus maxillaris anterior, with irregular margins. The pars facialis does not significantly extend on the processus maxillaris anterior, but it ends together with the tooth row anteriorly. In ventral view, the pars palatina of the left maxilla of MDHC 361 expands medially with a V-shaped tip, whereas the pars palatina of MDHC 363, MDHC 465, and MDHC 450 forms a medial triangular expansion with irregular margins by the posterior margin of the pars facialis. This triangular expansion is interrupted by one or two foramina, well visible in ventral view.

Dentary (Fig. 6M-P). The symphysis is semicircular in medial view. The dorsal and ventral margins are not

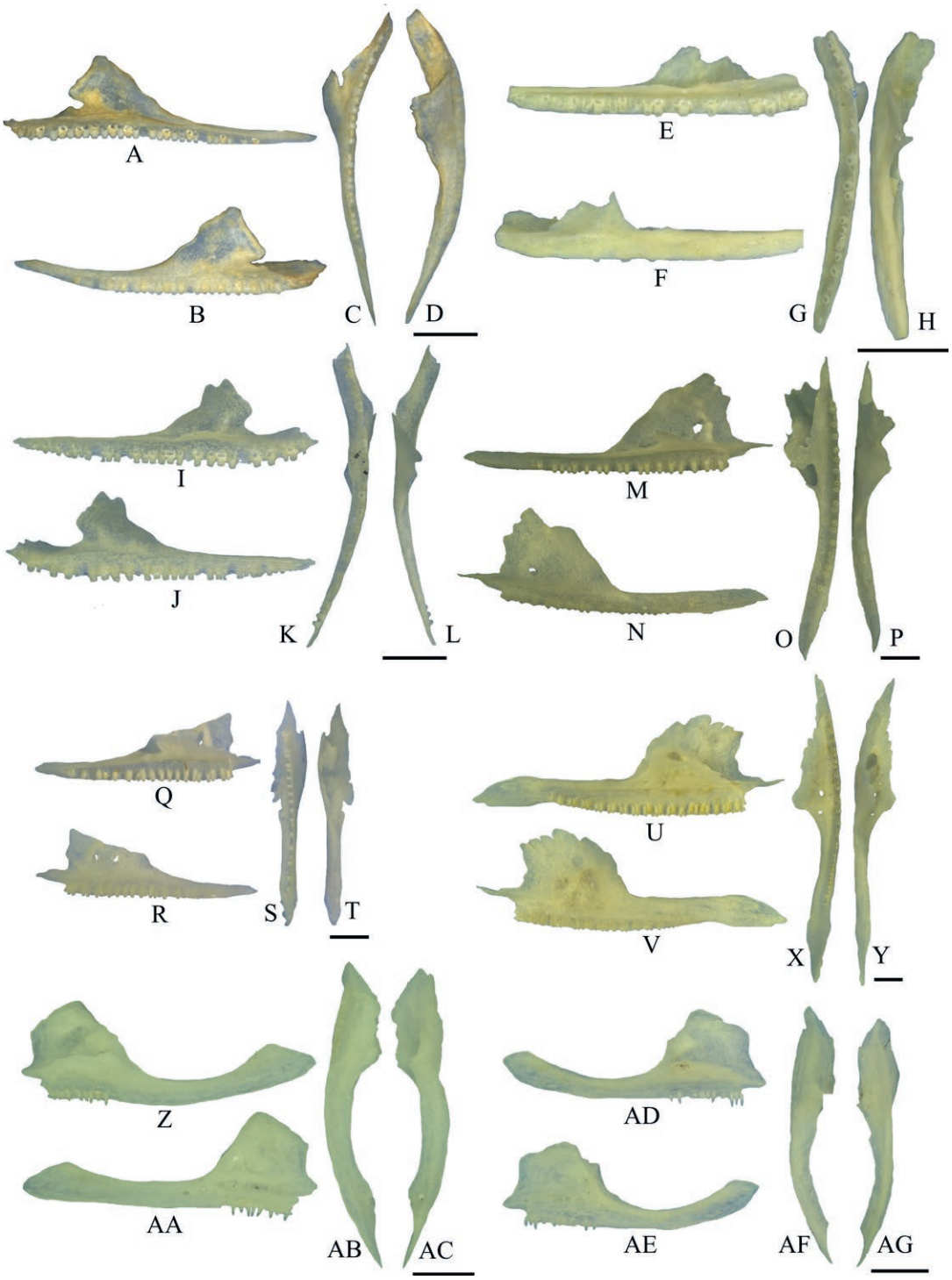

Fig. 4. Maxillae of Italian salamanders. A-D: right maxilla of *Speleomantes ambrosii* (MDHC 301) in medial (A), lateral (B), ventral (C) and dorsal (D) views; E-H: left maxilla of *Speleomantes italicus* (MDHC 61) in medial (E), lateral (F), ventral (G) and dorsal (H) views; I-L: left maxilla of *Speleomantes strinatii* (MDHC 486) in medial (I), lateral (J), ventral (K) and dorsal (L) views; M-P: left maxilla of *Salamandra lanzai* (MDHC 362) in medial (M), lateral (N), ventral (O) and dorsal (P) views; Q-T: left maxilla of *Salamandra atra* (MDHC 394) in medial (Q), lateral (R), ventral (S) and dorsal (T) views; U-Y: left maxilla of *Salamandra salamandra* (MDHC 205) in medial (U), lateral (V), ventral (X) and dorsal (Y) views; Z-AC: right maxilla of *Salamandrina perspicillata* (MDHC 300) in medial (Z), lateral (AA), ventral (AB) and dorsal (AC) views; AD-AG: left maxilla of *Salamandrina terdigitata* (MDHC 333) in medial (AD), lateral (AE), ventral (AF) and dorsal (AG) views. Scale bars: 1 mm.

fused together, so that in medial view the incisura dentalis is fully open. Conversely, in MDHC 465, the two margins are fused together and the incisura dentalis is not visible. In medial view, the processus coronoideus is particularly small and it has a parallelogram-like shape, with smooth edges (in MDHC 362, it is almost not visible).

Vomer (Fig. 8G-I). In dorsal view, the body of the vomer has a triangular shape, with a tip facing anteriorly. In dorsal view, the margo maxillaris forms a continuous convex anterolateral margin. The body of the vomer develops in posterodorsal direction. The processus vomeropalatinus minor is poorly developed. The dentigerous ridge forms an angle of ca. 130° with the margo intervomeropalatinum in ventral and dorsal views. In ventral view, the dentigerous ridge is elongated and has a slightly sigmoid shape, with an anteromedially directed anterior end and a posterolaterally directed posterior end. The width of the dentigerous ridge is the same in the anterior two thirds of its length, whereas the posterior third can become narrower. Almost all vomers are broken.

Salamandra atra

Premaxilla (Fig. 2M-P). The two premaxillae are not fused together. The premaxilla is as long as or slightly shorter than high. In anterior view, the alary process ends abruptly. A medial cavity is present on the medial margin of this process. Still in anterior view, the pars dentalis is as thick as the alary process, rectangular and curved posterolaterally. The left premaxilla of MDHC 394a bears one foramen. In dorsal view, the ventral half of the premaxilla is thickened at the articulation with the opposite premaxilla. In anterior view, the margo maxillaris is vertical. The margo vomeropalatinum is straight in dorsal view. The dorsal margin of the pars dentalis expands in posterior direction and, together with the expansion of the alary process, it forms a cavity, open on the anterior side. The pars palatina is poorly developed but can be seen in anterior view too. In posterior view, the pars palatina develops in dorsal direction and keeps the same width for all its length, except for a widening at midlength.

Maxilla (Fig. 4Q-T). In lateral view, the pars facialis bears one or two foramina and has a variable thickness. The pars facialis extends along the anterior half of the pars dentalis. In MDHC 394a, in lateral and medial views, the margo anterioris is particularly irregular, with sharp edges, whereas the margo orbitalis is more regular and straight. Conversely, in MDHC 394b, both margins are straight. Only the posterior fifth of the length of the pars dentalis is toothless. The pars palatina runs along the whole dorsomedial margin of the pars dentalis; it narrows at the anterior end, forming a triangular and sharp processus maxillaris anterior with irregular margins. The pars facialis does not significantly extend on the processus maxillaris anterior, but it ends together with the tooth row anteriorly. In ventral view, the pars palatina forms a medial triangular expansion with irregular margins by the posterior margin of the pars facialis. This triangular expansion is pierced by two foramina, well visible in ventral view. In the left maxilla of MDHC 394a, the medial margin of the pars palatina is broken at the level where the foramina should be located, resulting in the presence of a medially open concavity in place of the latter. The right maxilla of MDHC 394b is broken, thus, the presence of foramina or cavities cannot be evaluated.

Dentary (Fig. 6Q-T). The symphysis is semicircular in medial view. The dorsal and ventral margins are fused together in the anterior half of the dentary, so that in medial view the incisura dentalis opens only along its posterior half. Conversely, in MDHC 394b, the two margins do not completely fold up; they rise in the anterior half, giving to the bone a concave shape. In this same specimen, the canalis primordialis is, thus, fully visible. In the posterior half, the two margins are almost flat, and the bone widens. On the left dentary of MDHC 394a, there are no tooth positions on the anterior fourth of the bone. In medial view, the processus coronoideus is particularly small and it has a parallelogram-like shape, with irregular edges. Even if MDHC 394b shows unfolded margins, the latter are still thicker than the rest of the bone in this specimen as well.

Vomer (Fig. 8J). Vomers of MDHC 394a and the right vomer of MDHC 394b are missing, so the description is based on the broken left vomer of MDHC 394b. In dorsal view, the body of the vomer has a triangular shape, with a tip facing anteriorly. In the same view, the margo maxillaris forms a continuous convex anterolateral margin. The body of the vomer develops in posterodorsal direction. The processus vomeropalatinus minor is poorly developed. The dentigerous ridge forms an angle of ca. 130° with the margo intervomeropalatinum in ventral and dorsal views. In ventral view, the dentigerous ridge is elongated and has a slightly sigmoid shape, with an anteromedially directed anterior end and a posterolaterally directed posterior end. The width of the dentigerous ridge is the same in the anterior two thirds of its length, whereas the posterior third can become narrower. In ventral view, the dentigerous ridge bears on the anterior third some teeth that are not visible in lateral and dorsal views. This happens because the lateral margin of the body of the vomer expands ventrally to cover the dentigerous ridge.

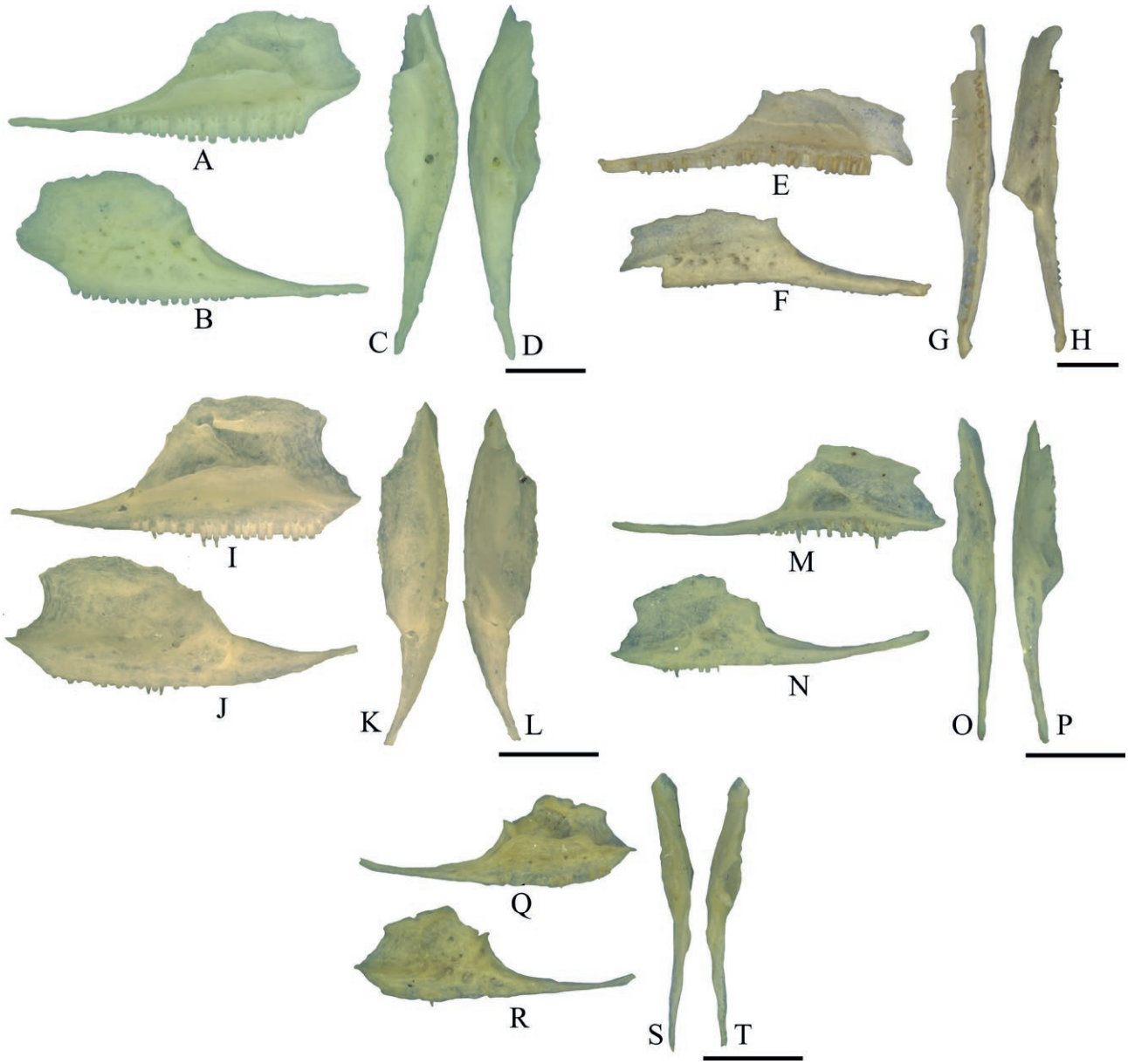

Fig. 5. Maxillae of Italian newts. A-D: left maxilla of *Triturus carnifex* (MDHC 38) in medial (A), lateral (B), ventral (C) and dorsal (D) views; E-H: left maxilla of *Euproctus platycephalus* (MDHC 507) in medial (E), lateral (F), ventral (G) and dorsal (H) views; I-L: left maxilla of *Ichthyosaura alpestris* (MDHC 416) in medial (I), lateral (J), ventral (K) and dorsal (L) views; M-P: left maxilla of *Lissotriton vulgaris* (MDHC 132) in medial (M), lateral (N), ventral (O) and dorsal (P) views; Q-T: left maxilla of *Lissotriton italicus* (MDHC 482) in medial (Q), lateral (R), ventral (S) and dorsal (T) views. Scale bars: 1 mm.

Salamandra salamandra

Premaxilla (Fig. 2Q-T). The two premaxillae are not fused together. The premaxilla is as long as or slightly shorter than high. In anterior view, the alary process ends with a dorsal rounded or sharp tip. In posterior view, on the dorsal half of the pars dentalis, the medial margin can form two or three triangular expansions. In dorsal view, on the dorsal half of the pars dentalis, foramina can be either present or absent, varying in number from zero to three. In lateral view, in both premaxillae of MDHC 23, in the left premaxilla of MDHC 124, and in the right premaxilla of MDHC 227, there is a cavity on the medial margin of the alary process. In anterior view, the pars dentalis is of the same thickness of the alary process, rectangular and, in dorsal view, it curves posterolaterally. In

dorsal view, the ventral half of the premaxilla is thickened at the articulation with the opposite premaxilla. In anterior view, the margo maxillaris is vertical. The margo vomeropalatinum is straight in dorsal view. In the same view, the dorsal margin of the pars dentalis expands in posterior direction and, together with the expansion of the alary process, it forms a cavity, open on the anterior side. Posterior to this cavity, there is another smaller cavity (absent in MDHC 23, MDHC 227, MDHC 234, and MDHC 396). The pars palatina is poorly developed but can be seen in anterior view too. In posterior view, the pars palatina develops in dorsal direction and keeps the same width for all its length; only at midlength, it widens and forms a triangular expansion.

Maxilla (Fig. 4U-Y). In lateral view, the pars facialis bears two to six foramina and has a variable thickness. The pars facialis extends along the anterior third of the pars dentalis. In lateral and medial views, the margo anterioris is particularly irregular with sharp edges. The margo orbitalis is irregular too. In MDHC 124 and MDHC 387, the margo anterioris is vertical, forming a right angle in the ventral end, whereas in MDHC 234 and MDHC 235, it is semicircular. The pars dentalis can be straight or bend posteroventrally in the posterior half (the anterior half is always anterodorsally directed). Only the posterior fourth of the length of the pars dentalis is toothless. The pars palatina runs along the whole dorsomedial margin of the pars dentalis; it keeps the same width for almost its entire length, forming a triangular and sharp processus maxillaris anterior, with regular margins. The pars facialis does not significantly extend on the processus maxillaris anterior but it ends together with the tooth row anteriorly. In ventral view, the pars palatina forms a medial triangular expansion with irregular margins by the ventral half of the pars facialis. This triangular expansion is pierced by one to three foramina, well visible in ventral view. Between the pars palatina and the pars facialis, there are one to three cavities, well visible in dorsal view. In the left maxilla of MDHC 205 and MDHC 212, the cavities are not separated, resulting in a larger one. In dorsal view, both maxillae of MDHC 227 and the left one of MDHC 234 show one foramen, anteriorly to the cavities.

Dentary (Fig. 6U-X). The symphysis is semicircular in medial view. In dorsal view, the anterior third of the right dentary of MDHC 23 bends medially, forming an almost right angle. The anterior half of the dorsal and ventral margins are fused together, so that in medial view the incisura dentalis opens only along its posterior half. In MDHC 212 and the left dentary of MDHC 364, the margins are not fused in the second fourth of the dentary from the anterior end, so that the incisura dentalis opens in this part of the bone and closes again posteriorly. In MDHC 124, MDHC 234, MDHC 235, and MDHC 387, on the other hand, the margins fuse only in the anterior fourth of the dentary. In dorsal view, between the folding of the dorsal margin and the crista dentalis, there are two to four foramina. In medial view, by the processus coronoideus, the dorsal margin of the bone is completely flat. Still in the same view, the processus coronoideus is particularly small and it has a parallelogram-like shape, with smooth edges.

Vomer (Fig. 8K-M). In dorsal view, the body of the vomer has a triangular shape, with a tip facing anteriorly. In the same view, the margo maxillaris forms a continuous convex anterolateral margin. The body of the vomer develops in posterodorsal direction. In dorsal and ventral views, there are two concavities at the centre of the margo choanalis: the largest one is bounded by the processus vomeropalatinus major and the processus vomeropalatinus minor, which is small and pointy, whereas the smallest one is posteromedial to the processus vomeropalatinus minor. The left vomer of MDHC 212 and both vomers of MDHC 386 show just one concavity. In ventral view, the dentigerous ridge is elongated and has a slightly sigmoid shape, with an anteromedially directed anterior end and a posterolaterally directed posterior end. The width of the dentigerous ridge is the same in the anterior two thirds of its length, whereas the posterior third becomes narrower. The dentigerous ridge forms an angle of ca. 130° with the margo intervomeropalatinum in ventral and dorsal views. In lateral view, the dentigerous ridge is strongly curved. In ventral view, the dentigerous ridge bears on the anterior third some teeth that are not visible in lateral and dorsal view. This happens because the lateral margin of the body of the vomer expands ventrally to cover the dentigerous ridge. In ventral view, between the dentigerous ridge and the body of the vomer, there can be one to four cavities. The vomers of MDHC 386 do not show any cavity and the right vomer of MDHC 235 shows one foramen instead of the cavity. The teeth on the dentigerous ridge are not properly aligned in a row.

Salamandrininae

The species of the genus *Salamandrina* are grouped into a single description, emphasizing the differences between species.

Salamandrina

Premaxilla (Fig. 2U-AB). The two premaxillae are not fused together. The premaxilla is as long as or slight-

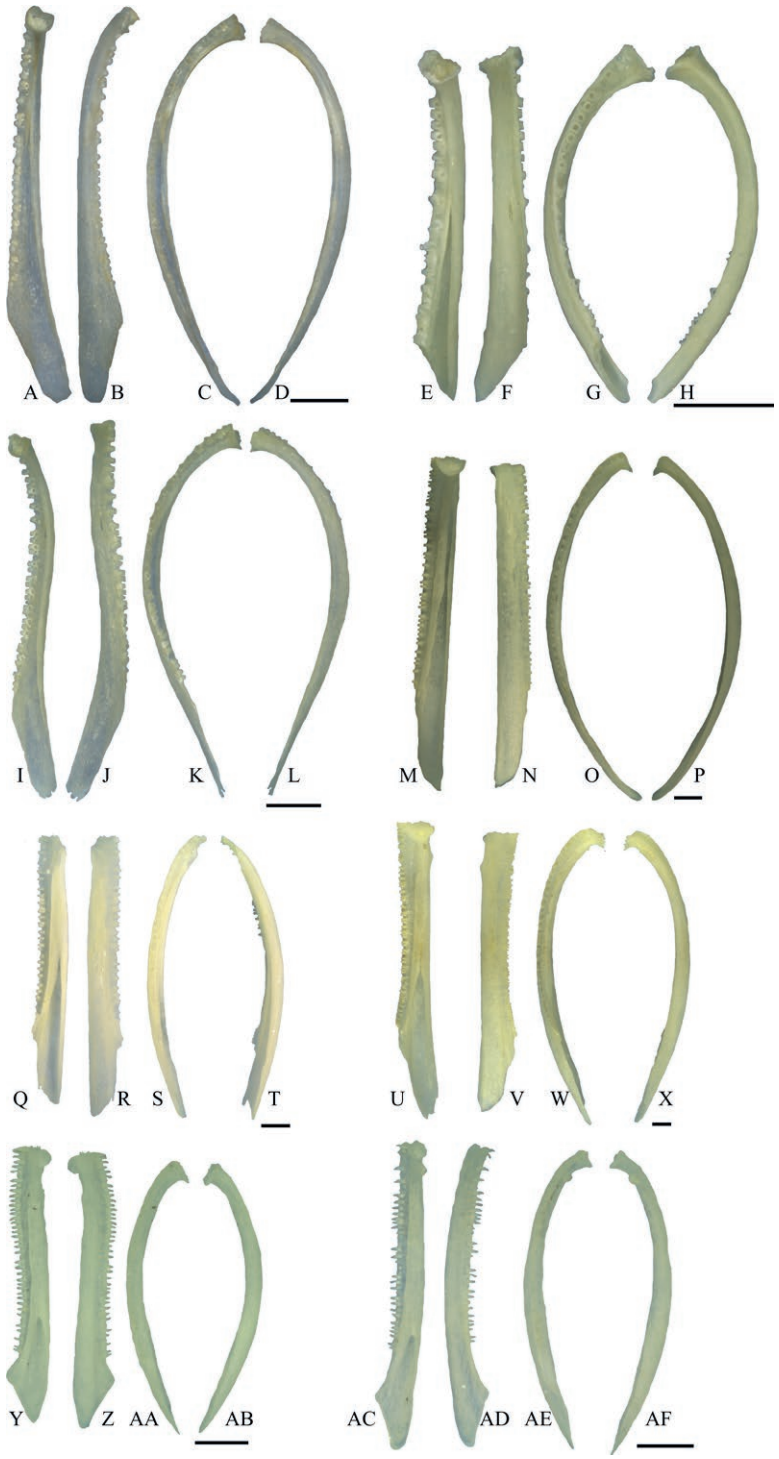

Fig. 6. Dentaries of Italian salamanders. A-D: left dentary of *Speleomantes ambrosii* (MDHC 301) in medial (A), lateral (B), dorsal (C) and ventral (D) views; E-H: left dentary of *Speleomantes italicus* (MDHC 61) in medial (E), lateral (F), dorsal (G) and ventral (H) views; I-L: left dentary of *Speleomantes strinatii* (MDHC 486) in medial (I), lateral (J), dorsal (K) and ventral (L) views; M-P: left dentary of *Salamandra lanzai* (MDHC 362) in medial (M), lateral (N), dorsal (O) and ventral (P) views; Q-T: left dentary of *Salamandra atra* (MDHC 394) in medial (Q), lateral (R), dorsal (S) and ventral (T) views; U-X: left dentary of *Salamandra salamandra* (MDHC 205) in medial (U), lateral (V), dorsal (W) and ventral (X) views; Y-AB: left dentary of *Salamandrina perspicillata* (MDHC 300) in medial (Y), lateral (Z), dorsal (AA) and ventral (AB) views; AC-AF: right dentary of *Salamandrina terdigitata* (MDHC 332) in medial (AC), lateral (AD), dorsal (AE) and ventral (AF) views. Scale bars: 1 mm.

ly shorter than high. In anterior view, the alary process shows a thickening on its medial margin, which extends for the two ventral thirds of the alary process and makes the whole process thick and sturdy. The expansion is visible also in lateral view, giving to the process a semicircular shape. In dorsal view, the ventral half of the premaxilla is thickened at the articulation with the opposite premaxilla. Between the ridge and the alary process there are one to four foramina. Only MDHC 495 shows no ridge or foramina. In anterior view, on the alary process one can find two to six foramina, which concentrate on the thick expansion. MDHC 495 shows no foramina in the alary process. In anterior view, the pars dentalis is thick, rectangular and curved posterolaterally. In anterior view, the margo maxillaris is vertical. The margo vomeropalatinum is straight in dorsal view. In posterior view, the pars palatina develops in dorsal direction, medially enlarging. The posterior half of the alary process is not visible in posterior view. In posterior view, the pars palatina of MDHC 407 is pierced by three foramina, whereas the left premaxilla of MDHC 342 bears one foramen. The pars palatina is well developed and it is visible in anterior view too. In lateral view, between the pars palatina and the pars dentalis, a foramen is visible at the dorsal margin of the pars dentalis. The cavities defined by the dorsal margin of the pars dentalis and the expansion of the alary process, which are present in the specimens of the genus *Salamandra*, are absent.

Maxilla (Fig. 4Z-AG). In lateral view, the pars facialis shows two to six foramina and has a variable thickness. In lateral view, the pars facialis shows one to four cavities, forming a shallow sculpturing composed only of depressions and with no crests (except for MDHC 228, that shows no cavity). The pars facialis extends along the anterior third of the pars dentalis. In medial view, the dorsal half of the pars facialis shows a triangular medial expansion. This expansion develops in dorsal direction in *Salamandrina perspicillata* and is not visible in lateral view, whereas it is posterodorsally directed and visible also in lateral view in *Salamandrina terdigitata*. The margo anterioris and the margo orbitalis are regular, except for the left maxillae of MDHC 228 and MDHC 300, which are the only maxillae with an irregular margo orbitalis. In medial view, the processus maxillaris posterior is thick and dorsoventrally expanded; it is also posterodorsally directed, giving a semicircular shape to the whole pars dentalis. In dorsal view, the pars dentalis shows one to three cavities; MDHC 492 and MDHC 495 do not show any cavity. In lateral view, the pars dentalis, along its length, shows one to three foramina; however, no foramina are present on the pars dentalis of the maxillae of MDHC 407, MDHC 492, and MDHC 494. Only the anterior fourth of the length of the pars dentalis is toothed. The pars palatina runs along the anterior third of the dorsomedial margin of the pars dentalis. In medial view, the pars palatina narrows at the anterior end, forming a triangular and sharp processus maxillaris anterior, with regular margins. The pars facialis extends more anteriorly than the tooth row, on the processus maxillaris anterior. In ventral view, the pars palatina has a semicircular shape with irregular margins. In dorsal view, between the pars palatina and the pars facialis, there are two cavities. Exceptions to this are the right maxillae of MDHC 406, in which the two cavities are replaced by two foramina, and MDHC 494, showing only one cavity.

Dentary (Fig. 6Y-AF). The symphysis is semicircular in medial view. Posteriorly, the bone is pointed. The dorsal and ventral margins are completely fused together, closing completely the incisura dentalis. In dorsal view, between the dorsal margin that folded up and the crista dentalis, the right dentary of MDHC 228 and both dentaries of MDHC 407 show one foramen. In medial view, by the processus coronoideus, the dorsal margin of the bone is completely flat. The processus coronoideus is almost absent in all specimens, but MDHC 300 displays a prominent and triangular process.

Vomer (Fig. 8N-S). In dorsal view, the margo maxillaris forms a continuous convex anterolateral margin, which can be provided with sharp edges. In dorsal view, the anteromedial tip of the body of the vomer forms an expansion followed by a deep concavity that interrupts the margo intervomeropalatinum, which is otherwise straight. This structure gives the vomer a characteristic shape that resembles a claw hammer. The body of the vomer develops in posterodorsal direction. The processus vomeropalatinus minor is short. In ventral view, the dentigerous ridge is elongated and curved, forming a lateral concavity and having an anterolaterally directed anterior end and a posterodorsally directed posterior end. The width of the dentigerous ridge is the same in the anterior two thirds of its length, whereas the posterior third becomes narrower. The dentigerous ridge forms an angle of ca. 180° with the margo intervomeropalatinum in ventral and dorsal views. In lateral view, the dentigerous ridge is straight (or slightly curved). In ventral view, the dentigerous ridge bears on the anterior fourth some teeth that are not visible in lateral and dorsal view. This happens because the lateral margin of the body of the vomer expands ventrally to cover the dentigerous ridge.

Pleurodelinae
Euproctus platycephalus

Premaxilla (Fig. 3E-H). The two premaxillae are fused together forming a single bone; they are connected

Fig. 7. Dentaries of Italian newts. A-D: left dentary of *Euproctus platycephalus* (MDHC 507) in medial (A), lateral (B), dorsal (C) and ventral (D) views; E-H: left dentary of *Triturus carnifex* (MDHC 85) in medial (E), lateral (F), dorsal (G) and ventral (H) views; I-L: left dentary of *Ichthyosaura alpestris* (MDHC 416) in medial (I), lateral (J), dorsal (K) and ventral (L) views; M-P: left dentary of *Lissotriton vulgaris* (MDHC 132) in medial (M), lateral (N), dorsal (O) and ventral (P) views; Q-T: left dentary of *Lissotriton italicus* (MDHC 482) in medial (Q), lateral (R), dorsal (S) and ventral (T) views. Scale bars: 1 mm.

through the whole medial margin of the pars dentalis and half of the alary process. The dorsal halves of the alary processes remain close along all their length. In anterior view, the alary process bears one (MDHC 508) or seven (MDHC 507) foramina and it is weakly sculptured. The pars dentalis is of the same thickness as the alary process and it is curved; it bears three foramina on the ventral margin and another larger one where the left and right partes dentalis meet. The margo maxillaris is concave. In posterior view, the pars palatina is well developed posterodorsally, and it is visible also in anterior view. It keeps approximately the same width for its entire length and has regular margins.

Maxilla (Fig. 5E-H). The pars facialis extends along the anterior half of the crista dentalis and it has a smooth surface in medial view, whereas in lateral view the surface is sculptured, with irregular pits and ridges. In lateral view, the right maxilla of both MDHC 508 and MDHC 509 show three larger cavities, whereas the left maxilla of MDHC 509 shows two smaller cavities. MDHC 507 hosts five larger cavities, positioned in a straight line on the ventral margin. The left maxilla of MDHC 508 bears two foramina. In medial view, the right maxilla of MDHC 508 shows three cavities on the anterior margin and a foramen between the pars dentalis and the pars facialis. Between the pars facialis and the pars dentalis, one (left maxilla of MDHC 507, MDHC 508, right maxilla of MDHC 509) or two (right maxilla of MDHC 507, left maxilla of MDHC 509) foramina can be seen. In lateral view, on the pars dentalis of MDHC 508, three cavities can be seen. In posterior view, the pars facialis of the left maxilla of MDHC 508 has two cavities and one foramen on the anterior margin. In lateral view, on the margo anterioris of MDHC 508, two pointed expansions are visible. In medial view, the processus maxillaris posterior is covered by a ridge formed by the pars palatina. Less than the posterior sixth of the pars dentalis is toothless. The pars palatina runs along the whole dorsomedial margin of the pars dentalis, keeping the same width for the anterior half of the latter. It narrows at the anterior end without meeting the pars facialis, so the triangular and sharp processus maxillaris anterior is formed just by the pars facialis. The pars facialis extends more anteriorly than the anterior end of the tooth row.

Dentary (Fig. 7A-D). In medial view, the processus articularis is as thick as the rest of the bone. Posteriorly, the bone is pointed. The anterior half of the dorsal and ventral margins are fused together, so that in medial view the incisura dentalis opens only along the posterior half of the dentary. In MDHC 508, the two margins are fused for the anterior two thirds. In lateral view, three to seven foramina are visible. In medial view, the processus coronoideus has a triangular shape with smooth edges. The symphysis shows a dorsal bulge in the same view.

Vomer (Fig. 8W-Y). In dorsal view, the body of the vomer has a triangular shape, with a tip facing anteromedially. Still in the same view, the margo maxillaris forms a continuous convex anterolateral margin. The body of the vomer develops in posterodorsal direction, forming a pointy extension. The processus vomeropalatinus minor is poorly developed. On the margo intervomeropalatinum, there is a triangular expansion dorsally directed. In ventral and dorsal views, the dentigerous ridge is straight and elongated; it forms an angle of ca. 180° with the margo intervomeropalatinum. In lateral view, the dentigerous ridge is straight (or slightly curved). The margo orbitosphenoideum forms an expansion that runs for the two anterior thirds of the dentigerous ridge; in the last third, it ends suddenly. All the teeth are visible in lateral and dorsal views.

Triturus carnifex

Premaxilla (Fig. 3A-D). The two premaxillae are fused together, forming a single bone. They are connected through the whole medial margin of the pars dentalis and half of the alary process. The premaxilla is as long as or slightly shorter than high. The dorsal halves of the alary processes end with a semicircular tip and point dorsolaterally, getting far from each other. In anterior view, the dorsal half of the pars dentalis is rough, with five to 17 foramina; in MDHC 18, MDHC 86, MDHC 357, and MDHC 491 the surface is sculptured, with irregular pits and ridges. There is a large foramen located at the meeting point of the partes dentalis of the left and right premaxillae. In anterior view, the rectangular pars dentalis is as thick as the alary process and it curves posterolaterally. In posterior view, the left pars dentalis of MDHC 38, and the right partes dentalis of both MDHC 85 and MDHC 87 show one foramen. In the same view, MDHC 357 shows numerous smaller pedicellate pleurodont teeth, that are not properly aligned in a row, probably for an aberrant condition. In anterior view, the margo maxillaris is vertical. The margo vomeropalatinum is straight in dorsal view. Between the alary process and the pars palatina, one to three foramina or an anterior cavity can be found; in this latter case, dorsally to the cavity there is another smaller one. In posterior view, the pars palatina is smooth, thinner than the pars facialis, and it keeps the same width for all its length, hiding the ventral fourth of the pars dentalis. The pars palatina is well developed in dorsal direction, being visible in anterior view too. The pars palatina of the left premaxilla of MDHC 353 shows one foramen.

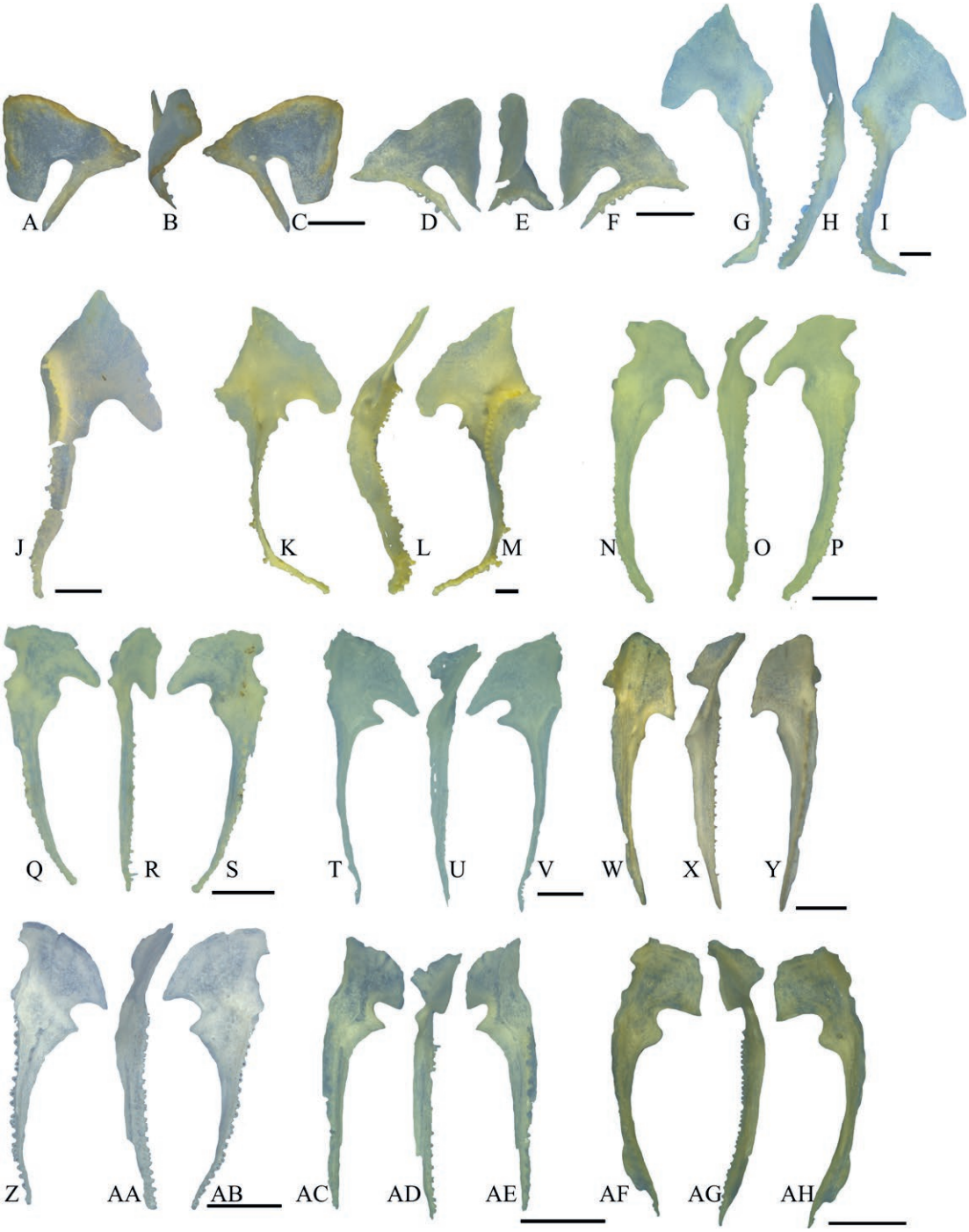

Fig. 8. Vomers of Italian urodeles. A-C: left vomer of *Speleomantes ambrosii* (MDHC 301) in dorsal (A), lateral (B) and medial (C) views; D-F: right vomer of *Speleomantes strinatii* (MDHC 486) in dorsal (D), lateral (E) and medial (F) views; G-I: left vomer of *Salamandra lanzai* (MDHC 362) in dorsal (G), lateral (H) and medial (I) views; J: left vomer of *Salamandra atra* (MDHC 394B) in ventral view; K-M: right vomer of *Salamandra salamandra* (MDHC 205) in dorsal (K), lateral (L) and medial (M) views; N-P: left vomer of *Salamandrina perspicillata* (MDHC 406) in dorsal (N), lateral (O) and medial (P) views; Q-S: right vomer of *Salamandrina terdigitata* (MDHC 332) in dorsal (Q), lateral (R) and medial (S) views; T-V: right vomer of *Triturus carnifex* (MDHC 85) in dorsal (T), lateral (U) and medial (V) views; W-Y: right vomer of *Euproctus platycephalus* (MDHC 507) in dorsal (W), lateral (X) and medial (Y) views; Z-AB: right vomer of *Ichthyosaura alpestris* (MDHC 416) in dorsal (Z), lateral (AA) and medial (AB) views; AC-AE: right vomer of *Lissotriton vulgaris* (MDHC 132) in dorsal (AC), lateral (AD) and medial (AE) views; AF-AH: right vomer of *Lissotriton italicus* (MDHC 482) in dorsal (AF), lateral (AG) and medial (AH) views. Scale bars: 1 mm.

Maxilla (Fig. 5A-D). In lateral view, the pars facialis is weakly to strongly sculptured (with irregular pits and ridges); the sculpturing in MDHC 18, MDHC 85, MDHC 87, and MDHC 145 is formed mainly by ridges, with pits (or foramina) rare or absent. In dorsal view, the anterolateral margin of the right maxilla of MDHC 353 shows a thin ridge that hosts two foramina. The pars facialis extends along the anterior half of the pars dentalis. In lateral and medial views, the margo anterioris and the margo orbitalis are irregular. In lateral view, the left pars dentalis of MDHC 85 shows 10 foramina distributed on a straight line. The posterior sixth of the pars dentalis is toothless, whereas in the anterior sixth of the bone, the pars dentalis is not present. In medial view, the teeth of MDHC 357 are not properly aligned in a row, probably as an aberrant condition. The pars palatina runs along the whole dorsomedial margin of the pars dentalis; it keeps the same width for the anterior half of the pars dentalis and it narrows at the anterior end, partly participating to the sharp processus maxillaris anterior, which shows regular margins. The pars facialis extends more anteriorly than the tooth row, on the processus maxillaris anterior. The pars palatina is pierced by one to eight foramina; however, in the right maxilla of MDHC 145 and both maxillae of MDHC 357, no foramen is visible. In some specimens, between the pars palatina and the pars facialis, there are one to five foramina, well visible in dorsal view. In dorsal view, on the pars dentalis, the right maxilla of MDHC 353 shows seven foramina positioned in a straight line.

Dentary (Fig. 7E-H). The symphysis is semicircular in medial view. Posteriorly, the bone is pointed. In dorsal view, in MDHC 357, the posterior fourth is curved toward the medial margin, forming a flat surface, which shows two cavities. The anterior half of the dorsal and ventral margins are fused together, so that in medial view the incisura dentalis opens only along its posterior half. The canalis primordialis of the left dentary of MDHC 18 and MDHC 357 is filled with the ossified Meckel's cartilage. In dorsal view, between the folded dorsal margin and the crista dentalis, there can be one (MDHC 85), two (MDHC 299) or three (MDHC 87, MDHC 261) foramina. In medial view, by the processus coronoideus, the dorsal margin of the bone is completely flat. MDHC 357 shows numerous smaller pedicellate pleurodont teeth, arranged chaotically on the crista dentalis and between the regular teeth. In medial view, the processus coronoideus has a parallelogram-like shape, with smooth edges; on the other hand, the processus is triangular in MDHC 85 and MDHC 87. Dentaries of MDHC 86 have no processus coronoideus.

Vomer (Fig. 8T-V). In dorsal view, the body of the vomer has a triangular shape, with a tip facing anteromedially. In dorsal view, the margo maxillaris forms a continuous convex anterolateral margin. The body of the vomer develops in posterodorsal direction, where it forms a pointy extension. In ventral view, the body of the vomer of MDHC 87 shows a cavity on the margo intervomeropalatinum. The processus vomeropalatinus minor is well developed and pointy. On the margo intervomeropalatinum, there is a dorsally directed and triangular expansion; the right vomer of MDHC 85 and the left vomers of both MDHC 299 and MDHC 491 bear a foramen on this expansion. In ventral view, the dentigerous ridge is straight and elongated. In lateral view, the dentigerous ridge is straight (or slightly curved). The width of the dentigerous ridge is the same in the anterior two thirds of its length, whereas the posterior third becomes narrower. The dentigerous ridge forms an angle of ca. 180° with the margo intervomeropalatinum in ventral and dorsal views. All the teeth are visible in lateral and dorsal views; however, the anterior fourth of the dentigerous ridge is shallower in both vomers of MDHC 85, MDHC 86, MDHC 87, MDHC 299, and MDHC 391, as well as the right vomer of MDHC 145 and MDHC 261, so much so that the teeth are not visible in ventral and lateral views in these specimens. This happens because the lateral margin of the body of the vomer expands ventrally to cover the dentigerous ridge.

Ichthyosaura alpestris

Premaxilla (Fig. 3I-L). The two premaxillae are fused together forming a single bone. They are connected through the whole medial margin of the pars dentalis and half of the alary process. The whole premaxilla is as long as or slightly shorter than high. The separated dorsal portions of the alary processes point dorsolaterally, getting far from each other. The pars dentalis is of the same thickness as the alary process and it is curved; it bears one foramen at the meeting point of the two alary processes. MDHC 416 bears two foramina instead, whereas MRSN A82 10 does not bear any foramen. In anterior view, both partes dentalis of MDHC 416 bear four foramina, positioned in a straight line; the two lines (one on the right and one on the left premaxillae) are symmetrical. In anterior view, in MRSN A82 10B, the dorsal half of the pars dentalis bear five foramina, where the two premaxillae meet. The margo maxillaris is concave. In posterior view, the pars palatina is well developed dorsoposteriorly, and it is visible also in anterior view. It keeps approximately the same width for all its length with regular margins.

Maxilla (Fig. 5I-L). The pars facialis extends along the anterior half of the crista dentalis. In medial view, the

pars facialis has a smooth surface, except for the presence of one to six foramina. Between the pars facialis and the pars palatina of the left maxilla of MDHC 352 and the right maxilla of MRSN A82 10, a large foramen can be seen. In lateral view, the margo anterioris is regular. The teeth portion that is visible also in anterior and lateral views is more fragile than the one that is adherent to the crista dentalis. The posterior half of the pars dentalis is toothless. The pars palatina runs along the whole dorsomedial margin of the pars dentalis, keeping the same width for the anterior half of the latter; it narrows at the anterior end, partly participating to the sharp processus maxillaris anterior, which shows regular margins. The pars facialis extends more anteriorly than the tooth row, on the processus maxillaris anterior. The pars palatina is pierced by two to eight foramina.

Dentary (Fig. 7I-L). The symphysis is semicircular in medial view. In medial view, the processus articularis is as thick as the rest of the bone. Posteriorly, the dentary is rounded. The dorsal and ventral margins are completely fused together in MDHC 352, whereas in MDHC 416 they are fused for the anterior half, so that in medial view the incisura dentalis opens only along its posterior half. In medial view, the processus coronoideus has a triangular shape.

Vomer (Fig. 8Z-AB). In dorsal view, the body of the vomer has a triangular shape, with a tip facing anteromedially. In ventral view, the body of the vomer of MDHC 416 shows numerous little cavities. In dorsal view, the margo maxillaris is continuously convex. The body of the vomer develops in posterodorsal direction, forming a pointy extension. The processus vomeropalatinus minor is well developed and pointy. In ventral view, the margo interovomeropalatinum forms a concavity. Both in ventral and lateral views, the dentigerous ridge is straight (or slightly curved) and elongated. The dentigerous ridge forms an angle of ca. 180° with the margo intervomeropalatinum in ventral and dorsal views. The margo orbitosphenoideum forms an expansion that runs for the two anterior thirds of the dentigerous ridge; in the last third it ends suddenly. All the teeth are visible in lateral and dorsal views.

Lissotriton vulgaris

Premaxilla (Fig. 3M-P). The two premaxillae are fused together forming a single bone; they are connected through the whole medial margin of the pars dentalis and two ventral thirds of the alary process. The left (or right) half of the premaxilla is twice higher than long. The alary process is quite robust. The dorsal halves of the alary processes point dorsolaterally, getting far from each other. In anterior view, the dorsal half of the pars dentalis shows numerous little cavities. The pars dentalis is as thick as the alary process and it is curved. It bears a small foramen at the meeting point of the two alary processes. In MDHC 135, in the same place, there are two smaller cavities too, whereas in MDHC 168 and MDHC 260, there are two other smaller foramina. The margo maxillaris is concave. The pars palatina is well developed dorsoposteriorly, and it is visible also in anterior view. It keeps approximately the same width for all its length with regular margins. In dorsal view, MDHC 133, MDHC 135, MDHC 168, and MDHC 260 display a foramen between the alary process and the pars palatina.

Maxilla (Fig. 5M-P). The pars facialis extends along the anterior two thirds of the crista dentalis. It has a smooth surface in medial view, whereas in lateral view it shows a thickening on the posterior half. In medial view, under this thickening the pars facialis bears either no foramen or one to two foramina. Both maxillae of MDHC 132 and the right maxilla of MDHC 133 show a cavity on the medial surface of the pars facialis. Between the pars facialis and the pars palatina, a cavity or a foramen can be seen. In lateral view, the margo anterioris is irregular. In lateral view, MDHC 132, MDHC 133, MDHC 135, MDHC 168, and MDHC 259 show numerous cavities positioned in a straight line on the pars dentalis; other cavities are visible in dorsal view. The teeth are limited to the anterior half of the crista dentalis. The pars palatina runs along the whole dorsomedial margin of the pars dentalis. It keeps the same width for the anterior half of the pars dentalis and it narrows at the anterior end, without meeting the pars facialis, so that the triangular and sharp processus maxillaris anterior is formed just by the pars facialis. This latter portion of the bone extends more anteriorly than the tooth row, on the processus maxillaris anterior. The pars palatina is pierced by one to five foramina.

Dentary (Fig. 7M-P). The symphysis is semicircular in medial view. The anterior half of the dorsal and ventral margins are fused together, so that in medial view the incisura dentalis opens only along its posterior half. In dorsal view, three foramina are hosted between the folded dorsal margin and the crista dentalis in MDHC 135 and the right dentary of MDHC 259. The processus coronoideus is completely absent.

Vomer (Fig. 8AC-AE). The body of the vomer has a triangular shape, it is smooth on both the dorsal and ventral surfaces, and it keeps the same thickness throughout; also, it shows a tip facing anteromedially. It develops in posterodorsal direction, forming a pointy extension. In dorsal view, the margo maxillaris is continuously convex. On the anterolateral portion of the margo intervomeropalatinum,

a dorsally directed and triangular expansion is present. The processus vomeropalatinus minor is well developed and pointy. In dorsal view, the concavity bounded by the processus vomeropalatinus minor and the processus vomeropalatinus major shows a thickened margin. In ventral view, on the medial portion of the margo interovomeropalatinum, there is a shallow concavity. In the same view, the dentigerous ridge is straight and elongated. The margo orbitosphenoideum forms a medially directed expansion, which runs for the whole length of the dentigerous ridge. The dentigerous ridge forms an angle of ca. 180° with the margo intervomeropalatinum in ventral and dorsal views. In lateral view, the dentigerous ridge is straight (or slightly curved).

Lissotriton italicus

Premaxilla (Fig. 3Q-T). The two premaxillae are fused together forming a single bone. They are connected through the whole medial margin of the pars dentalis and the ventral half of the alary process. The whole premaxilla is as long as or slightly shorter than high. The dorsal halves of the alary processes point dorsolaterally, getting far from each other. In anterior view, the dorsal half of the pars dentalis shows numerous little cavities, located at the level of the fusion between the two alary processes. The pars dentalis is as thick as the alary process and is curved; in posterior view, it bears a small foramen located at the meeting point of the two alary processes. In contrast to this general condition, however, MDHC 477 and MDHC 482 show no foramina. The margo maxillaris is straight, with a small lateral tip anteriorly (visible in dorsal view). In posterior view, the pars palatina is well developed dorsoposteriorly, and it is visible also in anterior view. It keeps approximately the same width for all its length with regular margins.

Maxilla (Fig. 5Q-T). The pars facialis extends along the anterior half of the crista dentalis and it has a smooth surface in medial view. In lateral view, it is weakly sculptured. Between the pars facialis and the pars palatina, either a foramen or a cavity can be seen. In lateral view, the margo anterioris shows a concavity. In medial view, in MDHC 477, the processus maxillaris posterior is medially directed. In lateral view, the pars dentalis of MDHC 476 and MDHC 477 shows numerous cavities positioned in a straight line. The teeth are limited to the anterior half of the crista dentalis. The pars palatina runs along the whole dorsomedial margin of the pars dentalis and it is pierced by two or three foramina. It keeps the same width for the anterior half of the pars dentalis, and it forms a triangular and sharp processus maxillaris anterior. The pars facialis extends more anteriorly than the tooth row, on the processus maxillaris anterior.

Dentary (Fig. 7Q-T). The symphysis is semicircular in medial view. In MDHC 477, the anterior half of the bone is medially directed, whereas the rest of the bone is straight. The anterior two third (three fourth for MDHC 477) of the dorsal and ventral margins are fused together, so that in medial view the incisura dentalis opens only along its posterior half. The processus coronoideus is completely absent.

Vomer (Fig. 8AF-AH). The body of the vomer develops in posterodorsal direction, forming a pointy extension; it also has a triangular shape, with a tip facing anteromedially. In dorsal view the margo maxillaris is continuously convex. On the anterolateral portion of the margo intervomeropalatinum a dorsally directed triangular expansion is present. The processus vomeropalatinus minor is well developed and rounded. In dorsal view, the cavity in the middle of the margo choanalis presents a thicker margin. In ventral view, on the medial portion of the margo interovomeropalatinum, there is a shallow concavity. In the same view, the dentigerous ridge is straight and elongated. This ridge forms an angle of ca. 180° with the margo intervomeropalatinum in ventral and dorsal views. In lateral view, the dentigerous ridge is straight (or slightly curved). The margo orbitosphenoideum forms a medially directed expansion, which runs for the whole length of the dentigerous ridge.

Comparative and phylogenetic analyses

The teeth number for each element of each specimen is reported in Table S3. Concerning the phylogenetic analysis, as a result of the New Technology Search on the matrix with the 33 dentigerous bones characters, seven trees were retained, and six trees after the subsequent round of tree bisection and reconnection. The strict consensus of these latter six trees is showed in Fig. 9. The Consistency Index (CI) is 0.89; the Retention Index (RI) is 0.914. The consensus tree displays seven nodes, excluding the one from which the outgroup diverges from the other clades, and a polytomy at the base of a clade grouping all members of Pleurodelinae and *Salamandrina*. *Salamandra* and *Speleomantes* are subsequent sister taxa of the clade including Pleurodelinae and *Salamandrina*.

DISCUSSION

Diagnostic characters

Diagnostic characters for each group are provided below and the most important diagnostic characters at genus level are reported in Table S4. The diagnostic characters reach the taxonomic level that was possible to achieve based on the data available for the study. Thus, in

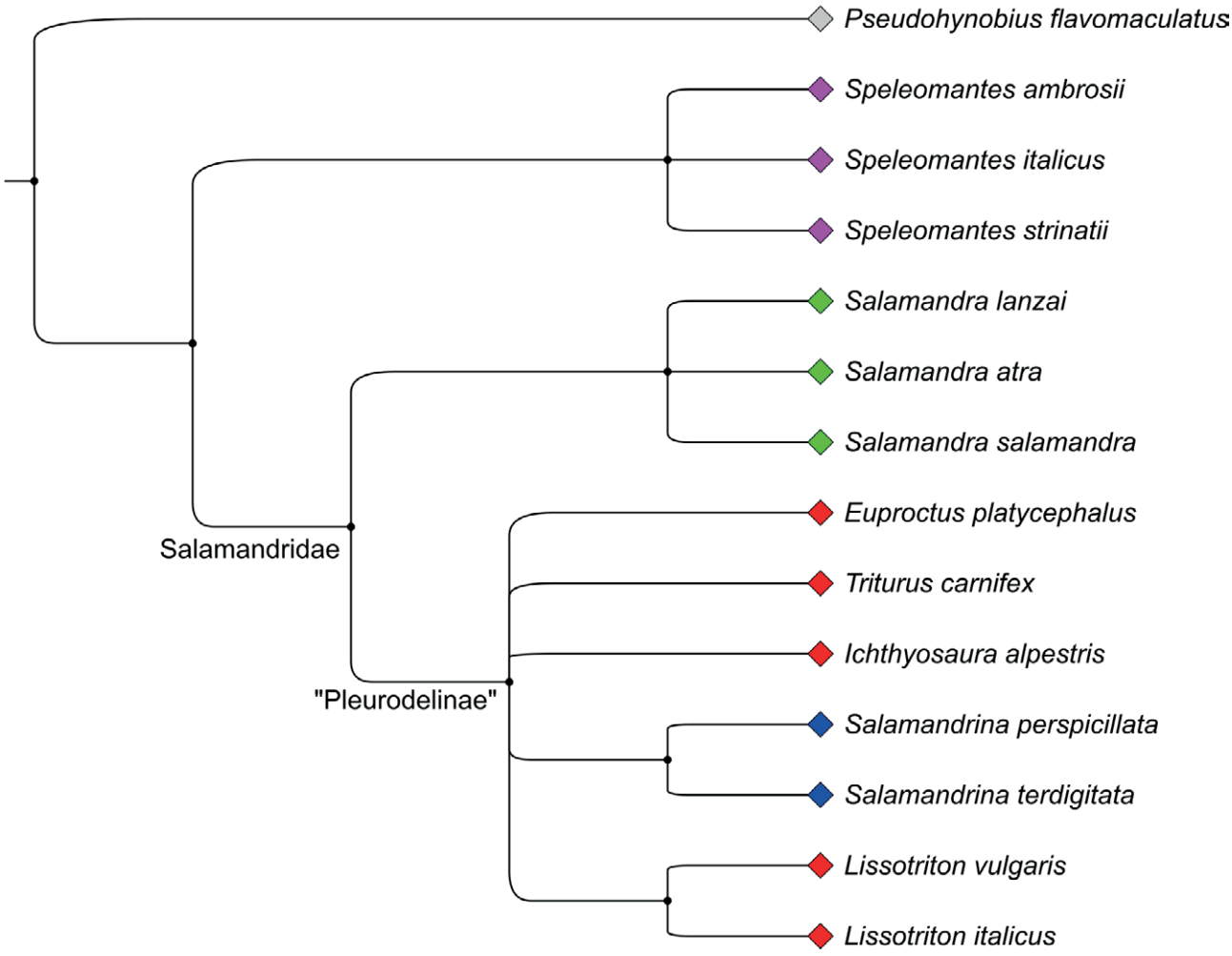

Fig. 9. Consensus tree obtained with a maximum parsimony phylogenetic approach using the matrix including the 33 dentigerous bones characters.

few cases the diagnostic characters allow identification to species, whereas in most cases they provide information at the genus level only. The dentary was revealed not to be highly diagnostic, so that the family was the only level possible to achieve in most cases, except for *Salamandrina* (see below). Characters for which the diagnostic value is uncertain (because of the limited number of available specimens) are highlighted with an asterisk (*).

Family Plethodontidae (monogeneric family in Europe so the diagnostic characters of the genus are valid also for the family)

Speleomantes

Premaxilla. Three times higher than long. Alary process particularly long and slender. Medial margin of ventral half of premaxilla without any thickening. Pars palatina developed in posterior direction, not visible in anterior view. Pars palatina subtriangular in shape, enlarging posterolaterally. Alary process of *S. ambrosii* with expansion extending along its dorsal half, not visible in anterior and posterior views*.

Maxilla. Whole length of pars dentalis with teeth, including processus maxillaris anterior. Pars palatina very small, with same width for almost its entire length. Processus maxillaris anterior absent (same in hynobiids). Pars facialis ending more posteriorly that anterior end of tooth row (same in hynobiids). No sculpturing in lateral view (same in hynobiids).

Dentary. Margin fused in anterior two thirds. Symphysis with dorsal bulge. Processus coronoideus generally absent in *S. italicus**.

Vomer. Concavity bounded by processus vomeropalatinus major and dentigerous ridge (same in hyno-

biids). Posteriorly curved dentigerous ridge in ventral view. Angle between dentigerous ridge and margo intervomeropalatinum less than 90° (same in hynobiids).

Family Salamandridae

Alary process of premaxilla rather short, and premaxilla with curved pars dentalis. Pars palatina generally visible in anterior view (either poorly developed or well developed; in *S. lanzai*, not visible in anterior view). Processus maxillaris anterior of maxilla present, pars facialis ends together with tooth row or more anteriorly (pars facialis participating or not significantly to processus maxillaris anterior). Dentary symphysis with semicircular shape (same in hynobiids). Concavity on vomer bounded by processus vomeropalatinus major and variably developed processus vomeropalatinus minor.

Salamandra

Premaxilla. Dorsal margin of pars dentalis forming a thin ridge. Same width of pars palatina for all its length, except for midlenght, where it widens and forms a triangular expansion. Dorsal margin of the pars dentalis and alary process forming an anterior concavity (same in hynobiids). *Salamandra salamandra* shows two or three triangular medial expansions on the pars dentalis. Pars palatina of *S. lanzai* extremely small and not visible in anterior view.

Maxilla. Pars facialis extended posteriorly to first third of pars dentalis. Posterior fourth to fifth of pars dentalis toothless. Pars palatina with medial triangular expansion with irregular margins (same in hynobiids). Processus maxillaris anterior formed mainly by pars palatina.

Vomer. Angle between dentigerous ridge and margo intervomeropalatinum ca. 130°. Sigmoid curvature of dentigerous ridge in ventral view. *Salamandra salamandra* shows two concavities on margo choanalis. Processus vomeropalatinus minor of *S. salamandra* small and pointy.

Salamandrina

Premaxilla. Medial margin of alary process thickened. Pars palatina medially enlarging.

Maxilla. Pars facialis posteriorly extended to first third of pars dentalis. Processus maxillaris posterior thick and dorsoventrally expanded. Anterior fourth of pars dentalis is toothed. Pars palatina runs along anterior third of dorsomedial margin of pars dentalis. Pars palatina semicircular (enlarging anteriorly and posteriorly) with irregular margins. Posterior half of pars dentalis dorsally curved. In all specimens of *S. perspicillata*, dorsal half of pars facialis shows triangular medial expansion, developed in mediodorsal direction and not visible in lateral view. Same expansion in two specimens of *S. terdigitata* posterodorsally directed, visible also in lateral view. Giving reduced sample (only eight specimens of *S. perspicillata* and four of *S. terdigitata* have been analysed), more in-depth study needed to confirm or refute diagnostic potential of this character.

Dentary. Dorsal and ventral margins completely fused or nearly so.

Vomer. Pars facialis hammer shaped. In lateral view, margo intervomeropalatinum forming small rounded dorsal expansion.

Subfamily Pleurodelinae

Premaxilla fused, with pars palatina with same width for all its length. Maxilla with processus maxillaris posterior pointy and thin, pars palatina with same width for anterior half of pars dentalis. Vomer with straight (or slightly curved) dentigerous ridge, margo intervomeropalatinum forming triangular dorsal expansion in lateral view (except for *Ichthyosaura*, in which more rounded than triangular). Extension of body of the vomer pointed.

Euproctus platycephalus (only Italian species in the genus, so the diagnostic characters of the species are valid also for the genus).

Premaxilla. Dorsal halves of alary process remain close along all their length*. Weakly sculptured in anterior view*.

Maxilla. Sculptured in lateral view*. Less than posterior sixth of pars dentalis toothless (same in hynobiids)*. Combination of processus maxillaris posterior pointy and thin and processus maxillaris anterior formed mainly by pars facialis*.

Vomer. Combination of processus vomeropalatinus minor poorly developed and margo intervomeropalatinum flat in lateral view*.

Triturus carnifex (only Italian species of the genus, so the diagnostic characters of the species are valid also for the genus).

Premaxilla. Sculptured in anterior view.

Maxilla. Posterior sixth of pars dentalis toothless.

Vomer. Combination of processus vomeropalatinus minor well developed and pointed and margo intervomeropalatinum flat in lateral view.

Ichthyosaura alpestris (only extant species in the genus, so the diagnostic characters of the species are valid also for the genus).

Premaxilla. Anterior margin of pars dentalis regular in dorsal view and rather trapezoidal in shape.

Maxilla. Combination of posterior half of pars dentalis toothless and processus maxillaris anterior formed by pars facialis and part of pars palatina.

Vomer. Combination of margo intervomeropalatinum forming small rounded dorsal expansion in lateral view and processus vomeropalatinus minor well developed and pointed.

Lissotriton

Premaxilla. Anterior margin of pars dentalis irregular in dorsal view and rather semicircular in shape. Premaxillae of *L. vulgaris* fused along whole medial margin of pars dentalis and two ventral thirds of alary process. Left (or right) half of premaxilla of *L. vulgaris* twice higher than long.

Maxilla. Combination of pars facialis extended to midlength of pars dentalis and pars palatina runs along anterior third of dorsomedial margin of pars dentalis. *Lissotriton italicus* weakly sculptured in lateral view, whereas *L. vulgaris* not sculptured. In *L. italicus*, processus maxillaris anterior formed by pars facialis and part of pars palatina.

Vomer. Margo intervomeropalatinum bearing shallow concavity, with ticker margin in dorsal view. Margo orbitosphenoideum of *L. italicus* forms expansion medially directed that runs for whole length of dentigerous ridge. Processus vomeropalatinus minor of *L. italicus* well developed and rounded.

Dichotomous key for identifications

Thanks to the diagnostic characters identified above, it has been possible to build a dichotomous key for the identification of the Italian urodele taxa. In few cases the identification reaches the species level, whereas in most cases it stops at the genus level. Characters that need to be confirmed with the study of a higher number of specimens are highlighted with an asterisk.

Premaxilla

1. Not Fused 2

- Fused 7

2. The pars palatina develops for the whole ventral half of the alary process, so that the posterior half of the alary process is not visible in posterior view ..... *Salamandrina* spp.

- The pars palatina develops posterodorsally, but the posterior half of the alary process is visible in posterior view . 3

3. The premaxilla is as long as or slightly shorter than high 4 (*Salamandra* spp.)

- The premaxilla is three times higher than long ..... 6 (*Speleomantes* spp.)

4. In posterior view, on the ventral half of the alary process, the medial margin can form two or three triangular expansions ..... *Salamandra salamandra*

- The alary process is thin, dorsally elongated and ends abruptly 5

5. The pars palatina is extremely small and cannot be seen in anterior view ..... *Salamandra lanzai*

- The pars palatina is poorly developed but can be seen in anterior view* ..... *Salamandra atra*

6. In lateral view, the alary process shows an expansion that extends along its dorsal half, not visible in anterior and posterior views* ..... *Speleomantes ambrosii*

- In anterior and posterior views, the alary process shows an expansion laterally directed that extends along its dorsal half* ..... *Speleomantes strinatii*

7. The dorsal portions of the alary processes remain close to each other along all their length .. *Euproctus platycephalus*

- The dorsal portions of the alary processes point dorsolaterally, getting far from each other 8

8. Ventral half of the alary process sculptured, with irregular pits and ridges ..... *Triturus carnifex*

- Ventral half of the alary process smooth or with a few foramina or cavities 9

9. Anterior margin of the pars dentalis smooth and regular in posterior view and rather trapezoidal in shape ..... *Ichthyosaura alpestris*

- Anterior margin of the pars dentalis irregular in posterior view and rather semicircular in shape 10 (*Lissotriton* spp.)

10. Left (or right) half of the premaxilla twice higher than long ..... *Lissotriton vulgaris*

- Premaxilla is as long as or slightly shorter than high ..... *Lissotriton italicus*

Maxilla

1. The posterior end of the pars dentalis is dorsally curved .... *Salamandrina* spp.

- The pars dentalis is straight 2

2. The teeth run for the whole length of the pars dentalis, including the processus maxillaris anterior. As such, the pars facialis does not reach the anterior end of the tooth row ..... *Speleomantes* spp.

- The pars facialis does not significantly extend on the processus maxillaris anterior, but it ends together with the tooth row anteriorly or the pars facialis extends more anteriorly than the tooth row, on the processus maxillaris anterior 3

3. The pars facialis does not significantly extend on the processus maxillaris anterior, but it ends together with the tooth row anteriorly ..... 4 (*Salamandra* spp.)

- The pars facialis extends more anteriorly than the tooth row, on the processus maxillaris anterior 6

4. The posterior fifth of the length of the pars dentalis is toothless* ..... *Salamandra atra*

- The posterior fourth of the length of the pars dentalis is toothless 5

5. The pars facialis extends along the anterior third of the pars dentalis ..... *Salamandra salamandra*

- The pars facialis extends along the anterior half of the pars dentalis ..... *Salamandra lanzai*

6. The pars palatina keeps the same width for the anterior half of the pars dentalis; it narrows at the anterior end, partly participating to the sharp processus maxillaris anterior, with regular margins ..... *Triturus carnifex*

- The pars palatina has the same width for almost its entire length; it either ends anteriorly in a flat, abrupt processus maxillaris anterior, with regular margins, or the pars palatina is subtriangular in shape, enlarging posterolaterally, or it has the same width for all his length except a widening at midlenght 7

7. No sculpturing on the pars facialis 8

- Pars facialis sculptured in lateral view, with irregular pits and ridges 9

8. Pars facialis extended for more than half of the pars dentalis ..... *Ichthyosaura alpestris*

- Pars facialis extended for half of the pars dentalis or less .. *Lissotriton vulgaris*

9. Processus maxillaris anterior formed just by the pars facialis ..... *Euproctus platycephalus*

- Processus maxillaris anterior formed by the pars palatina and the pars facialis ..... *Lissotriton italicus*

Vomer

1. In dorsal view, body of the vomer hammer shaped (see description above) ..... *Salamandrina* spp.

- In dorsal view, body of the vomer triangular 2

2. Processus vomeropalatinus minor is pointed and slender .. .. *Salamandra salamandra*

- Processus vomeropalatinus minor poorly or well developed and pointed or well developed and rounded 3

3. The dentigerous ridge forms an angle of ca. 130° with the margo intervomeropalatinum ..... *Salamandra* spp.

- The dentigerous ridge forms an angle of ca. 90° or ca. 180° with the margo intervomeropalatinum 4

4. The dentigerous ridge is mediolaterally directed, slightly posteriorly curved, forming with the margo intervomeropalatinum an angle of less than 90° ..... *Speleomantes* spp.

- The dentigerous ridge forms an angle of ca. 180° with the margo intervomeropalatinum 5

5. The processus vomeropalatinus minor is poorly developed ..... *Euproctus platycephalus*

- The processus vomeropalatinus minor is well developed 6

6. On the margo intervomeropalatinum there is a triangular expansion dorsally directed 7

- On the margo intervomeropalatinum there is a deep concavity or the margo intervomeropalatinum is straight .... *Ichthyosaura alpestris*

7. Processus vomeropalatinus minor rounded ..... *Lissotriton italicus*

- Processus vomeropalatinus minor forming a tip 8

8. Processus vomeropalatinus major particularly extended, giving the body of the vomer a trapezoidal shape .... *Triturus carnifex*

- Processus vomeropalatinus major short, giving the body of the vomer a rectangular shape ..... *Lissotriton vulgaris*

Dentary

1. The symphysis shows a dorsal bulge in medial view .... *Speleomantes* spp.

- The symphysis is semicircular 2

2. Dorsal and ventral margins fused for at least the anterior five sixths ..... *Salamandrina* spp.

- Dorsal and ventral margins unfused or fused for the anterior half or the anterior two third or less .... Pleurodelinae / *Salamandra* spp.

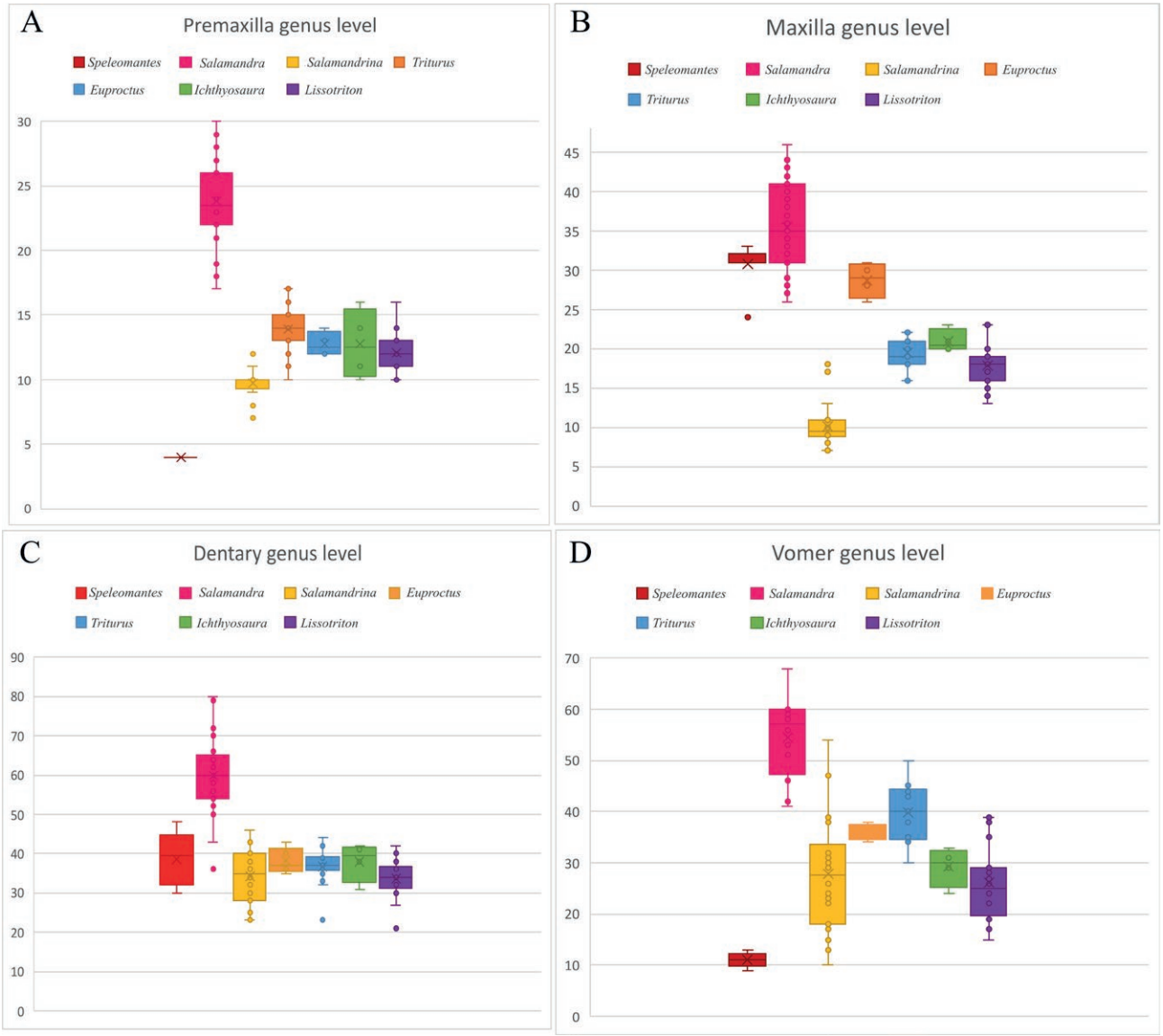

Fig. 10. Number of tooth positions in Italian urodele genera. A: tooth positions in the premaxilla at the genus level. In the fused ones, half of the premaxilla is considered. B: tooth positions in the maxilla at the genus level. C: tooth positions in the dentary at the genus level. D: tooth positions in the vomer at the genus level. The graphs are based on the data reported in Table S3.

Variation in the number of tooth positions

Urodeles (like most lissamphibians) have small and somehow delicate teeth that are attached to the inner side of the jaws (a condition called pleurodonty). Adult teeth usually have a zone of weakness, formed by fibrous, poorly mineralized tissue, giving sufficient flexibility to permit the crown to bent inwards into the oral cavity. This condition results from a developmental peculiarity of lissamphibians: the base of the tooth (pedicel of dentine) and its enamel-covered crown mineralize from separate centres and fail to fuse during tooth formation. This state is called pedicely (Schoch, 2014). As such, the number of teeth can be counted based on the number of pedicels (in other words, tooth positions) even though the crown is broken and lost, as it is the case in most of both dry-skeleton specimens and fossils. In general, the number of tooth positions is a character of uncertain value, as it changes during the different ontogenetic stages (Deban et al., 2000). However, through the data collected herein some consideration can be done. The number of teeth on the premaxilla (Fig. 10A) allows for the distinction of the genus *Speleomantes* (with a

mean of four tooth position for *S. ambrosii* and *S. strinatii*; the studied specimen of *S. italicus* does not preserve the premaxillae) and Salamandridae. *Salamandra* (with a mean of 22 tooth position for *S. lanzai*, 19 for *S. atra*, and 25 for *S. salamandra*) is also distinguishable from the subfamily Pleurodelinae (with a mean ranging from eight to 14 for the different genera). Among this latter clade, it is not possible to identify single genera based on teeth number. Similarly, *Salamandrina* has a small difference in the mean number of teeth in the premaxilla compared to the Pleurodelinae, but the difference is so small that it should not be considered as a possibly diagnostic character, given that the maximum number of teeth of *Salamandrina* overlaps with the minima of Pleurodelinae. As such, it seems that the number of teeth in the premaxilla can be a somehow reliable diagnostic character to distinguish *Salamandra* and *Speleomantes* from each other and from Pleurodelinae and *Salamandrina*. However, these three major groups can be already separated using many other diagnostic characters as seen above. Despite not being important for the diagnoses at species level, it seems that the number of teeth in the premaxilla possesses a quite significant phylogenetic value, separating taxa that are phylogenetically far and grouping together taxa that are close.

The number of tooth positions on the maxilla (Fig. 10B) divides the genera into three major groups based on average numbers: *Speleomantes*, *Euproctus*, and *Salamandra* (with an average number of tooth positions ranging from 24 to 36 in the different species of the genera), *Triturus*, *Ichthyosaura*, and *Lissotriton* (with a mean ranging from 12 to 18), and *Salamandrina* (from nine to 10). As such, the number of teeth in the maxilla could have a little diagnostic value, but the minimum number of tooth positions of *Speleomantes* is very close to the maxima of *Ichthyosaura*, *Lissotriton*, and *Triturus*, and the maximum number of tooth positions of *Salamandrina* overlaps the number of tooth positions of Pleurodelinae. As such, the number of tooth positions in the maxilla is not significant. Also, it has not much phylogenetic significance, given that for example *Salamandra* has a similar number to *Speleomantes* despite being very far phylogenetically from it (belonging to two different families that are separated by many branches of American and Asian taxa). Similarly, *Euproctus* is within the range of *Salamandra* and *Speleomantes*, despite belonging to the same subfamily of *Triturus*, *Lissotriton*, and *Ichthyosaura*.

The number of tooth positions in the dentary (Fig. 10C) shows a similar range in all the genera, only weakly separating *Salamandra* from the other genera. This makes again the dentary the dentigerous bone with the most conservative morphology within Italian urodeles. The number of tooth positions of the vomer (Fig. 10D) is very variable, and the ranges of all considered salamandrids extensively overlap. *Speleomantes* has a lower number of teeth, somehow as expected given that the morphology of the vomer is clearly dissimilar and shows a way shorter dentigerous ridge compared to Salamandridae.

Intra- and interspecific variation

Some characters observed in the tooth-bearing elements exhibit significantly more variability than others, like the position and the number of foramina and/or cavities, which are highly-variable intra- and interspecific characters: in every dentigerous bone there can be a varying number of foramina and/or depressions, or they can be completely absent. Concerning the margins of the bone, generally, the margo orbitalis of the maxilla is regular, whereas the margo anterioris is irregular. However, that is not true for all the species and even interspecifically: for example, in *S. atra* and *S. salamandra*, the two margins can be different in specimens of the same species. The dentary is particularly devoid of taxonomic significance in all the genera, even when considering variable identifying characters: the symphysis is different in *Speleomantes*, where it shows a dorsal bulge, but this character is also present (to a lesser extent and with a less regular shape) in *Triturus carnifex* MDHC 85. This suggests that the dorsal bulge could be a character showing a degree of intraspecific variation. Other characters in the dentary, such as the level of margin fusion, the thickness of the margins, and the general shape of the bone, are consistent across all species or are not significant, likely linked with different ontogenetic stages. As far as the vomer is concerned, in most specimens of *Triturus* all the teeth are visible in lateral view, but in some specimens (e.g. MDHC 261), the teeth are not visible due to the lateral margin of the body of the vomer expanding to a more ventral level than the dentigerous ridge.

Phylogenetic analysis

The phylogenetic analysis resulted in a well-supported Salamandridae clade, with *Speleomantes* excluded from it. The genera *Salamandra* and *Speleomantes* are monophyletic in the resulting tree. The two species of *Salamandrina* and the two Italian species of *Lissotriton* are also correctly grouped together. *Salamandra* is the sister group of the clade formed by *Salamandrina* and all the species of Pleurodelinae. The position of *Salamandrina*, in a polytomy with Pleurodelinae, is in line with the affinities pointed out by other morphological phylogenetic analyses (Marjanovic and Witzmann, 2015; Macaluso et al. 2022), but contrary to what is currently concluded by molecular phyloge-

netic studies (Zhang et al., 2008; Pyron and Wiens, 2011; Rancilhac et al. 2021). The general morphological affinity between *Salamandrina* and the newts (including several characters on the dentigerous bones as e.g. the straight dentigerous ridge of the vomer) could be the result of either shared plesiomorphic characters, which seems more likely at least in the case of the vertebrae (Macaluso et al. 2022, 2023b), or due to evolutionary convergence.

CONCLUSION

The present work successfully provides taxonomically significant diagnostic characters at the genus (and in some cases species) level for the extant Italian urodeles, including some taxa with poorly studied osteology, such as *Speleomantes* spp. and *Euproctus platycephalus*. Italian urodeles exhibit rather reliable diagnostic characters on premaxillae, maxillae, and vomers, but not in the dentaries, for which only the family level can be reached. Some characters are extremely variable, such as the number and the position of foramina and concavities and the regularity of the margins of the bones. The phylogenetic analysis based on newly defined characters on the tooth-bearing bones resulted in the recognition of the well-supported monophyletic Salamandridae and Pleurodelinae. *Salamandrina* was recovered as part of the Pleurodelinae clade, in agreement with previous phylogenetic analyses based on morphology, but in contrast with the results of the analyses based on molecular data.

ACKNOWLEDGMENTS

This work is supported by Fondi di Ricerca Locale dell'Università degli Studi di Torino 2020-2022. LM received fundings from the Alexander von Humboldt Foundation (Humboldt Research Fellowship). SM received help from Dr. Marco Pavia in the form of providing access to the collection and technical support. Andrea Villa, Hugues-Alexandre Blain, and an anonymous reviewer are thanked for the useful comments on a previous version of the manuscript. This is the publication number 378 of the Museo di Geologia e Paleontologia collections at the Università degli Studi di Torino.

SUPPLEMENTARY MATERIAL

Supplementary material associated with this article can be found at <http://www-9.unipv.it/webshi/appendix/index.html> manuscript number 15648

REFERENCES

Abbazzi, A., Angelone, C., Arca, M., Barisone, G., Bedetti, C., Delfino, M., Kotsakis, T., Marcolini, F., Palombo, M. R., Pavia, M., Piras, P., Rook, L., Torre, D., Tuveri, C., Valli, A. M. F., Wilkens, B. (2004): Plio-Pleistocene fossil vertebrates of Monte Tuttavista (Orosei, Eastern Sardinia, Italy), an overview. Riv. Itali. Paleontol. Stratigr. **110**: 681-706.

Buckley, D., Wake, M. H., Wake, D. B. (2010): Comparative skull osteology of *Karsenia koreana* (amphibia, caudata, plethodontidae). J. Morphol. **271**: 533-583.

Colombero, S., Alba, D., D'Amico, C., Delfino, M., Esu, D., Giuntelli, P., Harzhauser, M., Mazza, P.A.P., Mosca, M., Neubauer, T., Pavia, G., Pavia, M., Villa, A., Carnevale, G. (2017): Late Messinian mollusks and vertebrates from Moncucco Torinese, north-western Italy. Paleoecological and paleoclimatological implications. Palaeontol. Electron. **20**: 1-66.

Deban, S.M., Wake, D.B. (2000): Aquatic feeding in salamanders. In: Feeding: form, function and evolution in tetrapod vertebrates, pp. 65-94. Schwenk, K., Ed., Academic Press, San Diego.

Delfino, M. (2004): The Middle Pleistocene herpetofauna of Valdemino Cave (Liguria, North-Western Italy). Herpetol. J. **14**: 113-128.

Delfino, M., Bailon, S. (2000): Early Pleistocene herpetofauna from Cava Dell'Erba and Cava Pirro (Apulia, Southern Italy). Herpetol J. **10**: 95-110.

Delfino, M., Pitruzzella, G., Bailon, S. (2011): The Late Pliocene amphibians and reptiles from "Capo Mannu D1 Local Fauna" (Mandriola, Sardinia, Italy). Geodiversitas **33**: 357-382.

D'Orazi Porchetti, S., Sottili, G. (2012): A salamandrid from the middle Pleistocene of northern Latium (Fosso di San Martino, Rome, Italy). Boll. Soc. Paleontol. Ital. **51**: 7-13.

Duellman, W., Trueb, L. (1994): Biology of amphibians. Johns Hopkins University Press, Baltimore.

Fabre, A.C., Bardua, C., Bon, M., Clavel, J., Felice, R.N., Streicher, J.W., Bonnel, J., Stanley, E.L., Blackburn, D.C., Goswami, A. (2020): Metamorphosis shapes cranial diversity and rate of evolution in salamanders. Nat. Ecol. Evol. **4**: 1129-1140.

Goloboff, P., Morales, M. (2023): TNT version 1.6, with a graphical interface of MacOs and Linux, iincluding new routines in parallel. Cladistics **39**: 144-153.

Jia, J., Gao, K., Jiang, J., Bever, G., Xiong, R., Wei, G. (2021): Comparative osteology of the hynobiid complex *Liua-Protohynobius-Pseudohynobius* (Amphibia, Urodela): I. Cranial anatomy of *Pseudohynobius*. J. Anat. **238**: 219-248.

Kohno, S., Kuro-o, M., Ikebe, C. (1991): Cytogenetics and evolution of hynobiid salamanders. In: Amphibian cytogenetics and evolution, pp. 67-88. Green D.M., Sessions, S.K., Eds, Academic Press, San Diego.

Lanza, B., Corti, C. (1996): Evolution of the knowledge on the Italian herpetofauna during the 20th century. Boll. Museo St. Nat. Verona **20**: 373-436.

Lanza, B., Andreone, F., Bologna, M.A., Corti, C., Razzetti, E. (2007): Amphibia. Fauna d'Italia. Edizioni Calderini de Il Sole 24 Ore, Bologna.

Macaluso, L., Villa, A., Pitruzzella, G., Rook, L., Carnevale, G., Delfino, M. (2021a): A progressive extirpation: an overview of the fossil record of *Salamandrina* (Salamandridae, Urodela). Hist. Biol. **33**: 3723-3740.

Macaluso, L., Villa, A., Carnevale, G., Delfino, M. (2021b): Past, present, and future climate space of the only endemic vertebrate genus of the Italian peninsula. Sci. Rep. **11**: 22139.

Macaluso, L., Mannion, P., Evans, S., Carnevale G., Monti, S., Marchitelli, D., Delfino, M. (2022): Biogeographic history of Palearctic caudates revealed by a critical appraisal of their fossil record quality and spatio-temporal distribution. R. Soc. Open Sci. **9**: 220935.

Macaluso, L., Bertini, A., Carnevale, G., Eronen, J. T., Martinetto, E., Saarinen, J., Capasso, F., Delfino, M. (2023a): A combined palaeomodelling approach reveals the selective role as refugia of the Mediterranean peninsulas. Palaeogeogr. Palaeoclimatol. Palaeoecol. **625**: 111699.

Macaluso, L., Wencker, L., Castrovilli, M., Carnevale, G., Delfino, M. (2023b): A comparative atlas of selected skeletal elements of European urodeles (Amphibia: Urodela) for palaentological investigations. Zool. J. Linn. Soc. **197**: 569-619.

Maddison, W., Maddison D. R. (2019): Mesquite: a modular system for evolutionary analysis. Version 3.61.

Marjanovic, D., Witzmann, F. (2015): An extremely peramorphic newt (Urodela: Salamandridae: Pleurodelini) from the latest Oligocene of Germany, and a new phylogenetic analysis of extant and extinct salamandrids. PLoS ONE. **10**: e01370688.

Monti, S. (2021): Il record fossile e le origini dell'attuale diversità dei caudati paleartici. Bachelor's thesis, Università degli Studi di Torino.

Pyron, R., Wiens, J. (2011): A large-scale phylogeny of Amphibia including over 2800 species, and a revised classification of extant frogs, salamanders, and caecilians. Mol. Phylogenet. Evol. **61**: 543-583.

Ratnikov, V., Litvinchuk, S. (2007): Comparative morphology of trunk and sacral vertebrae of tailed amphibians of Russia and adjacent countries. Russ. J. Herpetol. **14**: 177-190.

Ratnikov, V., Litvinchuk, S. (2009): Atlantal vertebrae of tailed amphibians of Russia and adjacent countries. Russ. J. Herpetol. **16**: 57-68.

Ratnikov, V. (2015): Comparative humeral morphology of some Eurasian tailed amphibians (Amphibia, Urodela) for palaeontological studies. Acta Zool. Cracov. **58**: 101-119.

Rancilhac, L., Irisarri, I., Angelini, C., Arntzen, J. W., Babik, W., Bossuyt, F., Kunzel, S., Luddecke, T., Pasmans, F., Sanchez, E., Weisrock, D., Veith, M., Wielstra, B., Steinfartz, S., Hofreiter, M., Philippe, H., Vences, M. (2021): Phylotranscriptomic evidence for pervasive ancient hybridization among Old World salamanders. Mol. Phylogenet. Evol. **155**: 106967.

Schoch, R.R. (2014): Amphibian Evolution: The Life of Early Land Vertebrates. Wiley-Blackwell, Hoboken.

Vater, M. (2003): Anatómia kostrovej sústavy mloka vrchovského (*Triturus alpestris*) a jej ontogenéza (Vol. 132). PhD thesis, Praha: Přírodovědecká Faculta University Karlovi.

Venczel, M., Sanchiz, B. (2006): Lower Miocene Amphibians and Reptiles from Oschiri (Sardinia, Italy). Hantkeniana **5**: 72-75.

Villa, A., Andreone, F., Boistel, R., Delfino, M. (2014): Skull and lower jaw osteology of the Lanza's salamander, *Salamandra lanzai* (Amphibia, Caudata). In: Scripta Herpetologica. Studies on amphibians and reptiles in honour of Benedetto Lanza, pp. 171-200. Capula, M., Corti, C., Eds, Edizioni Belvedere, Latina.

Villa, A., Blain, H., Delfino, M. (2018): The Early Pleistocene herpetofauna of Rivoli Veronese (Northern Italy) as evidence for humid and forested glacial phases in the Gelasian of Southern Alps. Palaeogeogr. Palaeoclimatol. Palaeoecol. **490**: 393-403.

Villa, A., Bon, M., Delfino, M. (2020): Trapped in a roman well: Amphibians and reptiles from Tenuta Zuccarello near Marcon, Venice, Italy. Hist. Biol. **32**: 55-70.

Villa, A., Carnevale, G., Pavia, M., Rook, L., Sami, M., Szyndlar, Z., Delfino, M. (2021): An overview on the late Miocene vertebrates from the fissure fillings of Monticino Quarry (Brisighella, Italy), with new data on non-mammalian taxa. Riv. Ital. Paleontol. Stratigr. **127**: 297-354.

Zhang, P., Papenfuss, T., Wake, M., Qu, L., Wake, D. (2008): Phylogeny and biogeography of the family Salamandridae (Amphibia: Caudata) inferred from complete mitochondrial genomes. Mol. Phylogenet. Evol. **49**: 586-597.

Acta Herpetologica 19(2): 123-137, 2024
DOI: 10.36253/a_h-14527

Selection and daily occupancy of artificial retreat-sites by a declining Mediterranean island specialist, the European leaf-toed gecko *Euleptes europaea*

Julie Quessada[1,2,3,*], Vincent Riviere[3], Marc Cheylan[4], Alban Guillaumet[5]

[1] *Observatoire des Sciences de l'Univers de Rennes, Université de Rennes, Campus de Beaulieu, 263 Avenue Général Leclerc, 35042 Rennes, France*
[2] *Station d'Ecologie Théorique et Expérimentale (SETE), CNRS UAR2029, 2 route du CNRS, 09200 Moulis, France*
[3] *AGIR écologique, 147 ancienne route d'Esparron, 83470 Saint Maximin la Sainte Baume, France*
[4] *Ecole Pratique des Hautes Etudes, Paris Sciences Lettres University, 4-14 rue Ferrus, Paris, France*
[5] *Department of Biological and Environmental Sciences, Troy University, Troy, AL 36082, USA*
**Corresponding author.* Email: juliequessada@gmail.com / julie.quessada@agirecologique.fr

Submitted on: 2024, 13th March; revised on: 2024, 18th April; accepted on: 2024, 7th May
Editor: Enrico Lunghi

Abstract. The European Leaf-toed Gecko, *Euleptes europaea*, a rock-dwelling nocturnal gecko characteristic of Mediterranean Islands, is facing local extinctions and population decline at the margins of its range. Population monitoring through artificial retreat-sites (ARS) was implemented on French's Grand Rouveau and If islands to study the effects of management measures. We used Generalized Linear Models to identify: (i) the environmental variables (such as substrate, vegetation, and exposure to wind and sun) influencing the maximum number of individuals observed in ARS (studied in both islands); and (ii) the factors influencing ARS daily use (occupancy), including individual attributes such as age and weight, external temperature, and disturbance (Grand Rouveau only). The maximum number of geckos appeared to be determined by the thermal properties of ARS, as mediated by exposure to the dominant wind and sunlight, rather than by the structure of the habitat and nearby vegetation. An individual gecko's presence in an ARS was positively related to its presence in the same ARS on the previous day and negatively related to its age, the temperature of the previous night, and the number of days of disturbance. These results provide insights into the factors governing the selection and use of ARS by the European leaf-toed gecko and open perspectives on the use of ARS for the monitoring and conservation of this and other elusive terrestrial reptiles.

Keywords. Anthropogenic disturbance, gecko, habitat selection, Mediterranean islands, retreat-site, thermoregulation.

INTRODUCTION

Due to their isolation and unique environmental characteristics, including simplified food webs and small population sizes, islands are areas of high conservation value (Rodrigues et al., 2004, Gros-Désormeaux, 2012). They are often characterized by unique ecological assemblages, including many endemic and paleo-endemic species that have disappeared from the continent (Rodrigues et al., 2004, Blondel and Cheylan, 2008, Nias et al., 2010, Roberston et al., 2011, Gros-Désormeaux, 2012, Médail, 2017). With more than 10,000 islands and islets, about 5% of the world's total, the Mediterranean basin is a global hotspot for island environments (Blondel et al., 2010, Bellard et al., 2014, Médail, 2017) and one of 36 terrestrial biodiversity hotspots (Médail and Myers, 2004). Conservation challenges in the Mediterranean region include multiple forms of environmental exploitation and transformation, includ-

ISSN 1827-9635 (print)
ISSN 1827-9643 (online)

ing biological invasions, that are compounded by contemporaneous climate warming (e.g., Cheylan and Poitevin, 1994, Hulme et al., 2008, Underwood et al., 2009, Blondel et al., 2010, Médail, 2017, Lefebvre et al., 2019, Silva-Rocha et al., 2019, MedECC, 2020, Médail, 2022).

The European Leaf-toed Gecko *Euleptes europaea* (Gené, 1839), family Sphaerodactylidae, is endemic to the Mediterranean region and characteristic of Mediterranean Islands. Although its distribution has been described as a biogeographical enigma (Delaugerre and Cheylan, 1992), it is thought to have regressed from the continents resulting in a fragmented and mainly insular distribution (Delaugerre, 1981a, Delaugerre, 1981b, Renet et al., 2008, Vacher and Geniez, 2010, Fig. 1). Indeed, apart from a few continental stations in Tuscany (Italy), Liguria (Italy), Campania (Italy) and the Alpes-Maritimes (France), the species is only present on the islands of the western Mediterranean region: Corsica and Sardinia and their islets, the Galite archipelago (Tunisia), the Tuscan archipelago (Italy) and the islands of the Provencal coast (France) (Delaugerre et al., 2011, Di Nicola et al., 2022). The European Leaf-toed Gecko is the smallest species of gecko in Europe (on average 6-7 cm in length including tail, Arnold and Ovenden, 2014). It is an insectivorous and strictly nocturnal species avoiding light, which is active from dusk to dawn. It is a rock-dwelling species that lives in cracks and micro-cracks in rocks and buildings (Dardun, 2003). These natural shelters are of major importance for this poikilothermic species, which takes advantage of the heat stored by the rock to regulate its body temperature (Delaugerre, 1984). These cracks could also provide shelter from adverse weather conditions and diurnal predators (Delaugerre and Corti, 2020).

Having been qualified as a species pre-adapted to the island environment because of its low biomass and its ability to survive in very small populations, it is the vertebrate that is found on islands with the most drastic conditions in the Mediterranean regions, including very small area, reduced food web and low biomass (Delaugerre and Corti, 2020). However, this species is declining at the margins of its range and facing local extinctions both on islands and the continent (Dardun, 2003, Delaugerre, 2003, Salvidio and Delaugerre, 2003, Vacher and Geniez, 2010, Delaugerre et al., 2011, Corti *et al*, 2022). The exact causes of these declines are unknown but could be due to a combination of factors, including predation by the Black Rat *Rattus rattus* and the feral Cat *Felis catus* (Tranchant et al., 2003, Vacher and Geniez, 2010, Delaugerre et al., 2019), restoration of old buildings which serve as a refuge for the European Leaf-toed Gecko (AGIR écologique, 2016, Rennet and Monnet, 2021), competition with the Turkish Gecko *Hemidactylus turcicus* and the Common Wall Gecko *Tarentola mauritanica* (Linnaeus, 1758) (Renet and Monnet, 2021), introduction of new pathogens brought by the Common Wall Gecko (Delaugerre and Cheylan, 1992), abandonment of pastoralism leading to the closure of environments (Renet et al., 2013), urbanization (Renet et al., 2013), and

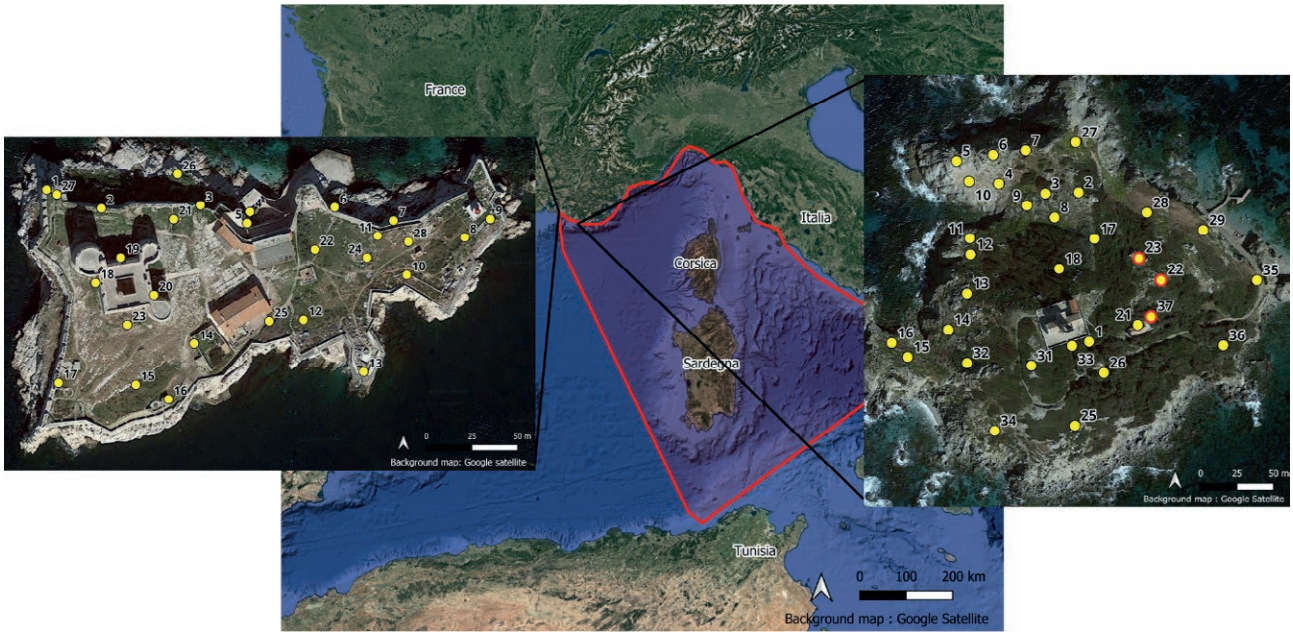

Fig. 1. Global distribution of the European Leaf-toed Gecko (in red) and locations of ARS on the left: If Island, and on the right Grand Rouveau Island. The three ARS used for the CMR protocol are circled in red.

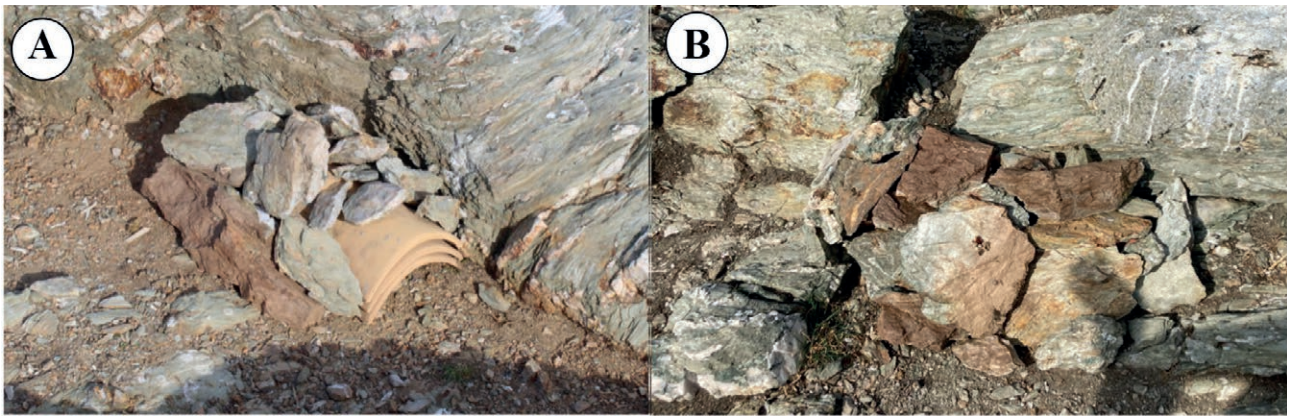

Fig. 2. A) Example of European Leaf-toed Gecko artificial retreat-site (ARS) left «open» to visualize the structure. B) Functional ARS completely covered with stones.

increase in the frequency of forest fires (Delaugerre and Cheylan, 1992). For these different reasons, the species is classified near threatened in the red list of Reptiles and Amphibians of the Mediterranean Basin and endangered in the red list of the Provence-Alpes-Côte d'Azur region in France (Cox et al., 2006, Marchand et al., 2017).

The European Leaf-Toad Gecko is an elusive species that is strictly nocturnal and can inhabit remote islands. As a consequence, the research on the species in activity, aiming for a better understanding of its ecology and conservation status, faces significant logistical challenges. A variety of monitoring techniques have been tested, including nighttime prospection with flashlights of potentially favorable rocky microsites (Delaugerre, 2002, Krebs et al., 2015, Couturier et al., 2020). However, nighttime prospections typically resulted in a small number of data points, insufficient for proper monitoring of the species (Vincent Rivière, pers. obs.). Because terrestrial ectotherms often use retreat-sites to regulate their body temperature and achieve their eco-physiological needs (Huey et al., 1989, Grillet et al., 2010), several studies have used artificial retreat-sites (ARS) to monitor reptiles or attempt to restore their habitat (Webb and Shine, 2000, Croak et al., 2010, Grillet et al., 2010, Moore et al., 2022). Monitoring of the European Leaf-toed Gecko using artificial retreat-sites was thus set up on the island of Grand Rouveau (Var, France) in 2014 and on the island of If (Bouches-du-Rhône, France) in 2016 (AGIR écologique, 2016, Cheylan et al., 2018) using three stacked roman roof tiles covered with stones (Fig. 2, Cheylan et al., 2018). These ARS were typically colonized rapidly (in less than a month) and their occupancy reached up to 76% on If Island, making these ARS a promising tool to monitor European Leaf-toed Gecko populations (AGIR écologique, 2016, Cheylan et al., 2018). But, to the best of our knowledge, no study has investigated the individual and environmental factors involved in the selection and daily use of ARS by the species.

Our overall objective is to provide important knowledge on the ecological preferences and life habits of the species that can be used to improve monitoring protocols and conservation measures targeted for the European Leaf-toad Gecko. Specifically, this study has two main objectives, namely identifying: (i) the environmental variables such as substrate, vegetation, and exposure to wind and sun influencing the maximum number of individuals observed in ARS; and (ii) the factors influencing ARS daily use (occupancy), including individual attributes such as age and weight, external temperature, and disturbance.

MATERIAL AND METHODS

Study sites

The island of If (43.279806°N, 5.325575°E) is part of the Frioul archipelago, off the coast of Marseille (Bouche-du-Rhône, France), in the heart of the Calanques National Park. In response to the restoration of the ramparts of If's castle, measures were taken to reduce the damage caused to the population of the European Leaf-toed Gecko on this island. Long-term monitoring of this population via artificial retreat-sites (ARS) has been implemented on If since September 2016 (AGIR écologique, 2016) in order to monitor the impact of the restoration and the effectiveness of the compensation measures. Twenty-seven ARS are currently positioned on If Island. They have been empirically arranged so that at least one ARS is placed within each main vegetation assemblage

of the island (Fig. 1a). Since 2016, European Leaf-toed Geckos are counted in every ARS 2 to 3 times a year.

The island of Grand Rouveau (43.08038°N, 5.76757°E) is part of the Embiez archipelago off the town of Six-Fours-Les-Plages (Var, France). Most of the land is owned by the Conservatoire du Littoral and its management is entrusted to the city of Six-Fours-Les-Plages, in association with the "Initiative pour les Petites Iles de Mediterranée" (PIM initiative) (AGIR écologique, 2021). Monitoring of the European Leaf-toed Gecko population by ARS started in 2014 on Grand Rouveau (Cheylan et al., 2018). Thirty-three ARS are currently positioned on the island, with at least one ARS within each main vegetation assemblage of the island (Fig. 1b). Since July 2014, European Leaf-toed Geckos are counted in every ARS 2 to 3 times a year, with at least one survey in the spring and one in autumn.

Field protocol for environmental variables and gecko numbers within retreat-sites

The collection of environmental data occurred in April 2021 for If Island and April 2022 for Grand Rouveau Island. The complete list of variables collected is provided in Table 1. The number of geckos was characterized by our response variable called *max_num* (see Table 1) which corresponds to the maximum number of individuals observed in the retreat-site since the beginning of the monitoring (2014 for Grand Rouveau Island and 2016 for If Island). On average, each ARS was surveyed 14.6 times (SD = 3.4), out of a maximum possible number of 19 between July 2014 and April 2022. The survey of an ARS is done by moving the ARS inside a box before opening it, in such a way that no individual can be missed or escape.

We verified that our response variable *max_num* did not depend on the number of sampling periods, used as a proxy for the time since installation of the ARS: Spearman's rank correlation coefficient, rho = -0.08, P = 0.56. Our data set included candidate variables measured within a radius of 5 or 10 meters around the site, variables describing the environmental conditions at the ARS itself, including classes of exposure to the major winds of the region (variables *N_WNW* and *ENE_ESE*) as well as sun exposure in classes at different orientations (*E*, *SE*, *S*, *SW*, and *W*) and cumulatively (S*un_pc*), as well as the distance in meters from the retreat-site to the sea (*Sea_d*) and to the nearest ARS (*Arti*_g), with the latter two measured in QGIS 3.16 (QGIS Development Team, 2022). Variables concerning wind and sun exposure are categorical (with 3 levels), whereas variables such as *Sun_pc*, *Sea_d* or *Arti_g* are numerical. For a complete description of variables in our data set, refer to Table 1.

Field protocol for Capture-Mark-Recapture and retreat-site occupancy

A protocol of Capture-Mark-Recapture (CMR) was carried out on the island of Grand Rouveau. All individuals of three ARS (#22, #23 and #37, see Fig. 1 for location) were captured during the daytime monitoring of April 14, 2022. These ARS were selected because they were adjacent to each other and held the highest number of geckos for the island. Each gecko was individually marked using water and pigment markers (edding 4040 CREATIVE marker) with a unique combination of leg marks (see Fig. S1 for an example of marked individuals). Because there is no known or suspected predator of the European Leaf-toad Gecko on either island, an increased predation risk due to colorful marking was not perceived as a significant issue for this study. For each marked individual, we recorded the site of capture as well as its weight and age class (see Table 2 for complete variable description). Sex was not recorded as it could not be safely determined for sub-adults and juveniles based on morphological features. All individuals were then returned to their ARS. These three ARS were surveyed daily for the next 4 days, allowing us to record the presence history of the marked individuals during these 4 recapture events. In addition, nighttime and daytime temperatures were obtained from the nearest weather station (at Cape Cépet, ~15 km from Grand Rouveau) using the website www.meteociel.fr. New arrivals during the protocol (n = 3 individuals) were processed in the same way and included in the study.

Statistical analyses for environmental variables and numbers within retreat-sites

All statistical analyses were performed with R 4.0.4 (R Core Team, 2021). The relationship between the maximum number of individuals observed in each ARS (our response variable *max_num*, see Table 1) and our set of candidate environmental variables was modeled using Generalized Linear Models and a negative binomial distribution (function *glm.nb* in R's MASS package). This distribution is suitable for over-dispersed discrete variables including many low-count data and a few high counts that stretch the distribution (Zuur et al., 2009). To reduce the risk of overfitting with our large, full set of 39 explanatory variables (for 60 data points), we used a conservative forward model selection approach as follows. First, starting from the (constant) null model, an explanatory variable was entered into the best model only if it resulted in a drop in the second-order AIC criterion (Akaike Information Criterion: Akaike, 1974),

Table 1. Description of environmental variables and gecko numbers within artificial retreat-sites (ARS). Legend: *max_num* is the response variable; explanatory variables calculated within a radius of 5 or 10 meters from the retreat-sites are identified at the end of the description with the notation '(5m)' and '(10m)', respectively; the variable G*en_sp* is actually referring to a set of 12 variables based on 12 plant species for which we determined whether they were dominant within the 5-meter radius of the ARS (value = 1) or not (0), such as *Atr.sp* referring to small bushes of *Atriplex sp.*, and *Hor.mur* to the grass *Hordeum murinum*; for the variable *Stru* (soil structure): 0 = a single substrate; 1: heterogeneous, with large substrate patches; 2: heterogeneous, with a mosaic of small patches; for sun exposure at different orientations (variables *E* to *W*): 0 = entirely shaded for this orientation, 1 = partially shaded for this orientation, 2 = entirely exposed for this orientation; for wind exposure of the retreat-site for the two major winds in this region (variables *N_WNW* and *ENE_ESE*): 0 = entirely protected from the wind; 1 = partially protected from the wind, 2 = entirely exposed to the wind. For each variable, its type (Num = numerical; Cat = categorical) and the values that it can take are presented as well. See text for details.

Variable	Description	Type	Values/Range
max_num	Maximum number of geckos observed in the ARS	Num	0 to x
Site	Island on which the ARS is located	Cat	If, Rouveau
Sea_d	Distance from the sea (in meters)	Num	0 to x
v0_5	Cover of the vegetation layer from 0 to 5 cm (5 m)	Num	0 to 100 %
v5_15	Cover of the vegetation layer from 5 to 15 cm (5 m)	Num	0 to 100 %
v15_40	Cover of the vegetation layer from 15 to 40 cm (5 m)	Num	0 to 100 %
v40	Cover of the vegetation layer above 40 cm (5 m)	Num	0 to 100 %
Goel	Number of yellow-legged gull (*Larus michahellis*) nests (5 m)	Num	0 to x
Pod.sp	Known presence of *Podarcis* lizards (*P. siculus* on If, *P. muralis* on Rouveau) on the ARS	Cat	0 / 1
Gen.sp	For 12 plant species, significant presence or not (5 m)	Cat	0/1
Rock	Cover of rocky substrate (5 m)	Num	0 to 100 %
Earth	Cover of other non-sandy and non-rocky natural substrate (5 m)	Num	0 to 100 %
Stone	Cover of construction stone (5 m)	Num	0 to 100 %
Sand	Cover of sandy substrate (5 m)	Num	0 to 100 %
Conc	Cover of concrete substrate (5 m)	Num	0 to 100 %
Stru	Soil structure (see legend for details)	Cat	0,1,2
Nat_g	Presence of natural (rocky) habitat for the species (10 m)	Cat	0 / 1
Arti_g	Distance from the nearest ARS (in meters)	Num	0 to x
Ant_g	Presence of anthropogenic habitat (10 m)	Cat	0 / 1
Mov	ARS moved since the beginning of the monitoring	Cat	0 / 1
Rep	ARS repaired since the beginning of the monitoring	Cat	0 / 1
E	Sun exposure of the ARS to the east	Cat	0,1,2
SE	Sun exposure of the ARS to the south-east	Cat	0,1,2
S	Sun exposure of the ARS to the south	Cat	0,1,2
SW	Sun exposure of the ARS to the south-west	Cat	0,1,2
W	Sun exposure of the ARS to the west	Cat	0,1,2
Sun_pc	Total sun exposure (sum of each direction of exposure)	Num	0 to 10
N_WNW	Wind exposure of the retreat-site to the 'Mistral' (dominant wind)	Cat	0,1,2
ENE_ESE	Wind exposure to the second major wind in the region	Cat	0,1,2

calculated using the AICc function in R's MuMIn package, and if the corresponding regression coefficient was significant at the 5% level (in the case of a factor with multiple levels, at least one contrast needed to be significant). In addition, to reduce the risk of detecting spurious correlations due to increased type I errors, we limited the number of interactions tested to seven potentially meaningful pairwise interactions among the set of variables retained after forward selection, excluding interactions between sun or wind exposure and the presence of a particular grass species. None of the seven tested interactions were significant (not shown) and thus none were included in the best model.

To assess model validity, we first used the *qresid* function of R's statmod package to obtain randomized quantile residuals which are normally distributed (Dunn and Smyth, 2018). Next, normality of the residuals was tested using a Shapiro-Wilk test (Shapiro and Wilk, 1965), the homogeneity assumption was tested using Levene's test (Levene, 1960) for each categorical variable included in the best model, independence was assessed by looking at the spatial distribution of the residuals, and

Table 2. Variables description for Capture-Mark-Recapture and ARS occupancy. *Pres* was our response variable, *Ind* was used as a random factor, and all other variables were used as candidate explanatory (fixed effect) variables. For each variable, its type (Num = numerical; Cat = categorical) and the values that it can take are presented.

Variable	Description	Type	Values / Range
Ind	Unique identifier of the individual	Cat	1 to 77
Pres	Presence or absence of the individual in the ARS	Cat	0/1
Pres-1	Presence or absence of the individual in the ARS on the previous day	Cat	0/1
Site	ARS where the individual was captured and returned	Cat	22, 23, 37
Weight	Weight (g) of the individual when first captured	Num	0.31 to 2.66
Age_class	Age class of the individual, based on morphological features. Adults and subadults could not be safely distinguished and thus they are grouped together.	Cat	Adult or juvenile
Night_temp	Temperature, in °C, of the night before the daily survey, as measured at 3 AM on the same day (data taken from www.meteociel.fr)	Num	9 to 20
Day_temp	Temperature, in °C, at 1 PM the day of the survey (www.meteociel.fr)	Num	17 to 22
D_site	Number of consecutive days of ARS disturbance	Num	1 to 5

R's *density* function was used to compare the distribution of observed *max_num* with those predicted by the model.

Statistical analyses for CMR and retreat-site occupancy

Because detection probability was always one (the survey method allows the detection of the total number of individuals present in an ARS) and we did not detect any movement between ARS, we did not attempt to estimate transition probabilities (using a multi-state CMR model), as initially planned; instead, we focused on individual occupancy, the probability for a gecko to be found at its shelter-site on any given night. To account for repeated measures of our binary response variable (*Pres*) over time, the influence of potential explanatory variables was assessed using Generalized Linear Mixed Models (GLMM) with the function *glmmTMB* in R's glmmTMB package, using a Bernoulli distribution and a logit transformation. The candidate variables included *Pres-1,* the presence or absence of the individual in the ARS on the previous day, to account for possible temporal autocorrelation. Only recapture data were analyzed in order to have *Pres-1* value available for every *Pres* value. The complete list of variables is provided in Table 2.

The selection of the optimal model explaining ARS daily use (occupancy) was performed using the top-down strategy which is adapted to mixed models (Zuur et al., 2009). To identify the random part of the model, we used REML estimators (REstricted Maximum Likelihood; see Bolker et al., 2009, *Zuur* et al., 2009) to compare four models with identical fixed effect structure (an additive model including all possible fixed effects factors) but different random effect structure, namely a different random intercept for each individual (1|Ind), a random slope for each individual that depended on the number of days of ARS disturbance (0 + D_site|Ind), as well as random intercepts and slopes that were either correlated (1 + D_site|Ind) or uncorrelated (1|Ind) + (0 + D_site|Ind). The optimal structure of the random component was selected using the AICc criterion (Akaike Information Criterion corrected for small numbers, Bolker et al., 2009, Hervé, 2014). The optimal fixed structure was then determined using forward model selection and Maximum Likelihood (ML) estimators, which are more relevant in the case of model comparisons with different fixed effects (Pinheiro and Bates, 2004, Millar, 2011). Although forward model selection did not include any interaction, we tested *a posteriori* whether the inclusion of potentially relevant pairwise interactions resulted in lower AICc; the model without any interaction was retained as the best model (not shown). Finally, the best model was fitted using REML estimators to get a more reliable estimate of the different parameters (Zuur et al., 2009).

To assess model validity, we used an approach adapted to GLMM models implemented in R's DHARMa package (Hartig, 2022). Instead of conventional residuals, the method uses simulated scaled residuals (obtained with the *simulateResiduals* function) that are bounded between 0 and 1. If the model has been specified correctly, a uniform (flat) distribution is expected for the scaled residuals (Hartig, 2022). We first tested whether the overall distribution, the number of outliers, and the dispersion of the scaled residuals conformed to expectations using the functions *testUniformity*, *testOutliers* and *testDispersion*, respectively. In addition, for all fixed-effect predictors included in the best model (after transforming numerical variables such as *Night_temp* into categorical predictors)

we used the *testCategorical* function to check for within-group deviations from uniformity and between-group deviation from homogeneity.

RESULTS

Environmental variables and numbers within retreat-sites

The best model included the variables *N_WNW*, *S*, *SW*, *Atr.sp*, and *Hor.mur* (Table 1 for variable description, Table 3, Fig. 3). A site completely exposed to the wind from N to WNW (level = '2' of *N_WNW*) held fewer individuals than a site partially or completely protected from the wind for this orientation (levels = '1' and '0', respectively; both $P < 0.001$, not shown), while moderate or partial exposure to N to WNW winds (level = '1') yielded higher values of *max_num* than any other situation (although the difference between levels '1' and '0' was not significant: Table 3). In addition, sites partially or completely exposed to the southern sun (levels '1' and '2' of variable *S*) had significantly larger numbers of European Leaf-toed Geckos than sites in the shade for this orientation (level = '0', both $P < 0.03$), while, moderate or partial sun exposure to the SW (level = '1' of variable *SW*) yielded significantly higher values of *max_num* than either a lack of or complete sun exposure for this orientation (levels '0' and '2' of variable *SW*, both $P < 0.001$, not shown). Finally, retreat sites that were surrounded by vegetation dominated by the grass *Hordeum murinum* or small bushes of *Atriplex* sp. held significantly larger numbers of European Leaf-toed Geckos than the sites which did not (Table 3).

Table 3. Coefficients and their Standard Error (SE) for the best model explaining the maximum numbers of European Leaf-toed Gecko observed within the ARS. For each categorical variable (*N-WNW*, *S*, and *SW*), the coefficients reflect the effect of a given level compared to the effect of level '0' that is included in the intercept (e.g., 0.15 is the predicted difference, on the log scale, between gecko number when the ARS is partially protected from the wind [N-WNW = 1] and when it is entirely protected from the wind [N-WNW = 0]); significance levels: '***': P < 0.001, '**': P < 0.01, '*': P < 0.05). See Table 1 for variable description.

Variable / Level	Coefficient	SE	z	P-value	
(Intercept)	1.10	0.19	5.62	1.86e-08	***
N-WNW / 1	0.15	0.25	0.58	0.56	
N-WNW / 2	-1.52	0.27	-5.64	1.71e-08	***
S / 1	0.83	0.29	2.82	0.005	**
S / 2	0.71	0.32	2.20	0.028	*
SW / 1	1.37	0.33	4.11	3.88e-05	***
SW / 2	-0.39	0.31	-1.25	0.21	
Atr.sp / 1	1.89	0.48	3.93	8.58e-05	***
Hor.mur / 1	0.88	0.27	3.20	0.001	**

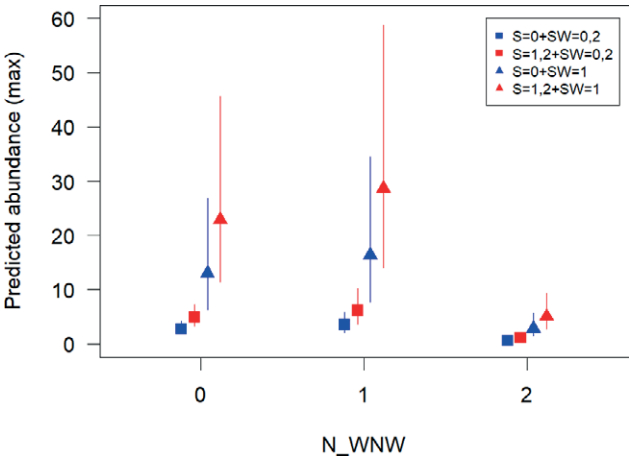

Fig. 3. Model-based predictions, including 95% confidence intervals, for the maximum number of geckos found in artificial retreat-sites (*max_num*) as a function of different parameter combinations; the predictions are based on the best model but after grouping modalities with similar effects to reduce the number of parameter combinations and provide greater clarity: S = 1,2 corresponds to S = 1 or S = 2, SW = 0,2 corresponds to SW=0 or SW=2. Atr.sp and Hor.mur were fixed to 0. See Table 1 for the description of variables.

The hypothesis that quantile residuals followed a normal distribution could not be rejected (Shapiro test, W = 0.99, P = 0.79). The null hypothesis that the variances did not differ among the different levels of each explanatory variable could not be rejected for any of the five explanatory variables in the best model (Levene's test: all $P > 0.05$). However, the existence of spatial autocorrelation in the residuals, notably at Grand Rouveau Island, suggests that the independence hypothesis is not respected (Fig. S2). We thus used the *glmmfields* function in R's glmmfields package to run the same (best) model while accounting for spatial autocorrelation (Anderson and Ward, 2019). The coefficients obtained were very similar to those obtained previously (not shown), suggesting that our results are also robust to this violation, although it should be noted that the contrast between the levels '0' and '2' of the variable *S* was no longer significant at the 5% threshold in the spatial model (estimate = 0.70, 95 %, CI = [-0.06; 1.47]). Finally, although the distribution of *y*-values predicted by the model resembles reality, the best model tends to underestimate the highest observed values (Fig. S3).

CMR and retreat-site occupancy

The total dataset of the CMR protocol consisted of 203 captures (first captures and recaptures) of 77 unique

individuals, with only 3 individuals being new arrivals (not captured during the first day but captured during one of the four days of recapture); 19 individuals were captured only during the first day, and not during any of the four days of recapture. On the first day, the ARS #22, #23 and #37, selected for the CMR protocol, were respectively occupied by 17, 36 and 21 unique individuals.

The best model identified by the top-down approach suggested that the probability of presence of geckos in their ARS (occupancy) was greater when the individual was present the previous day as well as for juveniles as compared to adults and subadults but was negatively related to the temperature of the previous night and the number of days of disturbance (Table 4 and Fig. 4). In addition, the random effect structure selected by AICc (0 + D_site | Ind; Akaike weight = 0.466) suggested the existence of between-individual variation in the response to disturbance.

The hypothesis that the distribution of the scaled residuals was uniform could not be rejected (one-sample Kolmogorov-Smirnov test: D = 0.037, $P = 0.80$) and no outlier was detected (DHARMa bootstrapped outlier test, $P = 1$). However, the dispersion of the residuals was lower than expected (dispersion = 0.728, $P < 0.001$), which resulted in a loss of statistical power (as opposed to overdispersion which results in inflated type I errors: Hartig, 2022). Such reduced power could explain, at least in part, the fact that some of the variables included in the final model (after selection by AICc) were not significant at the 5% level (see Table 4). For each of the fixed effects but one, we could not reject the null hypotheses of (within-group) uniform distribution and (between-group) homogeneity (one-sample Kolmogorov-Smirnov and Levene's tests, respectively: all $P > 0.37$, except *Pres-1* for which all $P < 0.01$).

Because *Pres-1* was the least significant variable included in the best model (Table 4: z = 1.29, $P = 0.20$), we investigated the influence of *Pres-1* by re-running all analyses after dropping it, yielding an alternative 'best model' called bm2. The difference in AICc between the best model and bm2 was less than 2 (ΔAICc = 1.9, Akaike weight for bm2 = 0.28). After dropping *Pres-1*, all explanatory variables retained the sign of their coefficient, but all became significant at the 5% level (compare with Table 4; *Night_temp*: Est = -0.10, z = -2.13, $P = 0.03$; *Age_class*: Est = 3.00, z = 2.02, $P = 0.04$; *D_site*: Est = -1.14, z = -4.73, $P < 0.001$), and none of the hypotheses examining the validity of the model could be rejected anymore (not shown). This suggested that our conclusions regarding the influence of fixed-effect variables are robust to the violations found when *Pres-1* is included.

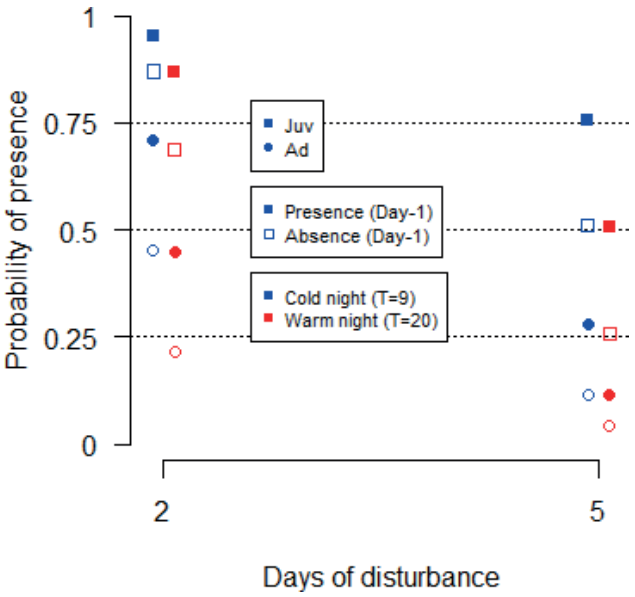

Fig. 4. Probability of presence (variable *Pres*) of a gecko in its ARS, as estimated from the best model's fixed effect coefficients and the inverse logit function, as a function of: (i) the number of days of disturbance (variable *D_site*; *x*-axis); we only show estimates for the two most extreme values, namely 2 and 5 days of disturbance; (ii) the individual's age class (Adult/Subadult or Juvenile, represented by circles or squares, resp.); (iii) presence or absence of the individual at the ARS on the previous day (filled or empty symbols, resp.); and (iv) the previous night's temperature; only the two most extremes temperatures in the data set are shown: T = 9 °C, shown in blue, and T = 20 °C, shown in red.

Table 4. Coefficients and their Standard Error (SE) on the logit scale for the best model explaining the probability of presence within the artificial retreat-site for an individual of European Leaf-toed Gecko; significance levels: '*': $P < 0.05$, '.': = $P < 0.1$. See Table 2 for variable description.

Variable / Level	Coefficient	SE	z	P-value	
(Intercept)	1.953	1.675	1.166	0.244	
Pres-1	1.090	0.847	1.287	0.198	
Night_temp	-0.101	0.044	-2.277	0.023	*
Age_class / Juvenile	2.088	1.153	1.811	0.070	.
D_site	-0.618	0.371	-1.665	0.096	.

DISCUSSION

Importance of the thermal properties of the retreat site

The first objective of this study was to determine the environmental variables affecting the number of European Leaf-toed Gecko present in the artificial retreat-sites. Consistent with studies in other reptiles (e.g., Huey, 1982), we found that three of the variables included in the best

model relate to exposure to the wind or sun, suggesting a strong influence of the thermal properties of the retreat-sites (Table 3; Discussion below). Indeed, for nocturnal poikilotherms that do not engage in direct insolation and spend the day in their retreat-sites such as the European Leaf-toed Gecko, the Turkish Gecko *Hemidactylus turcicus* (Hitchcock and McBrayer, 2006), the Broad-headed Snake *Hoplocephalus bungaroides* (Webb and Shine, 1998a), and the Marbled Southern Gecko *Christinus marmoratus* (Kearney and Predavec, 2000), thermoregulation depends on the choice of a retreat-site and the position occupied within that site (Huey, 1982, Webb and Shine, 1998a, Kearney and Predavec, 2000). Within their retreat-site, European Leaf-toed Geckos manage to maintain their body temperature above the atmospheric temperature even when inactive (Delaugerre, 1984).

Complex combined effect of exposure to the sun and wind on retreat site selection

As may have been anticipated, sites partially or completely exposed to the southern sun had more European Leaf-toed Geckos than sites in the shade for this orientation (Fig. 3). Interestingly, however, such difference was minimal for retreat-sites that were completely exposed to north to west-northwest winds (Fig. 3), locally called the 'mistral', and characterized by strong, cold, and dry winds (Guenard et al., 2005). Overall, sites completely exposed to the mistral held fewer geckos than other sites (see Results and Fig. 3). This suggests the mistral is a limiting factor for the European Leaf-toed Gecko, likely because exposure to strong winds, especially in open habitats, leads to a reduction of temperature for the substrate and reptiles' body through convection (Logan et al., 2015, Ortega et al., 2017). While ARS made of rocks and tiles can provide shelter from desiccation, protecting European Leaf-toed Geckos from direct wind and maintaining some moisture (Edgar et al., 2010), ARS should not be immune to wind-induced cooling.

Additional findings suggest that the sun and wind exposure act in combination to determine ARS quality for European Leaf-toed Gecko, although future studies directly investigating the thermal properties of ARS and the temperature of the geckos will be necessary to fully address this question. In the present study, more geckos were found in ARS that were partially exposed to the mistral and partially exposed to the southwestern sun, as compared to ARS that were either sheltered from or completely exposed to the mistral and southwestern sun (Results and Fig. 3). These results suggest that overheating is also a concern, and that only a narrow fraction of all possible environmental conditions provide optimal ARS conditions. Because of thermal inertia of the rock and slow heat absorption, nocturnal reptiles in retreat-sites tend to reach their optimal temperature in the afternoon (Webb and Shine, 1998a, Kearney, 2002). A complete absence of cooling provided by the mistral or a strong exposure to afternoon and evening sunshine could thus lead to temperatures beyond those optimal or even tolerable for the species (Walls, 1983, Kearney, 2002, Edgar et al., 2010). This may be particularly true during hot weather, raising the possibility of seasonal variation in the thermal properties of ARS. For instance, in summer the nocturnal gecko *Christinus marmoratus* prefers high-shaded rocks to medium and low-shaded ones and better tolerates low-shaded rocks when they are thick (Kearney, 2002). Anecdotal data suggest that more European Leaf-toed Geckos may be found in spring and fall, as compared to summer, in ARS of both Grand Rouveau and If islands (pers. obs), although future work will be needed to better understand possible seasonal variation in their patterns of activities.

Additional effect of surrounding vegetation on retreat site selection

In addition to variables related to sun and wind exposure, the best model also included the presence or absence of two plant groups: the bushy species of the genus *Atriplex* and the grass species *Hordeum murinum.* This result about *Atriplex sp.* is consistent with recent papers highlighting the importance of vegetated habitats, and especially woody habitat, for this gecko long-perceived as solely associated with rocky environments. Salvi *et al.* (2023) described observations and adaptations consistent with an agile arboreal locomotion and Deso *et al.* (2023) described the arboreal behavior of *E. europaea* on the alien *Eucalyptus sp.* species on two islands. It is worth noting, however, that *Atriplex sp*. were dominant (see Table 1 for definition) in two ARS only in our samples, suggesting that the inclusion of this variable in our best model might be an artifact of such a small sample size. Conversely, we are not aware of any study establishing a relationship between *E. europaea* and *Hordeum marinum* or any other grass species. Patches of *Hordeum* might shelter arthropods and thus provide a food supply for the European Leaf-toed Gecko, a hypothesis that requires further testing.

Model limitation for retreat site selection

The best model appears insufficient to precisely predict gecko numbers in the most favored retreat-sites.

First, the uncertainty around the estimates, as quantified by the amplitude of the confidence intervals, strongly increases when the estimated densities exceed approximately 15 individuals (Fig. 3). Second, the best model appears to slightly underestimate the densities in the best retreat-sites (Fig. S3). Although it is always possible that we missed an important environmental predictor (despite our large data set: Table 1), the small difference between observed and predicted values could be related to the gregarious behavior of the European Leaf-toed Gecko, whose individuals tend to group together within natural or artificial retreats (e.g., up to 35 individuals observed under the same ARS on If; see also Delaugerre and Cheylan, 1992, Delaugerre and Corti, 2020). If this is true, we may expect the difference between any two suitable retreat-sites to reflect local population size, taken as a proxy of the number of potential colonizers, rather than the thermal properties of the retreat-site itself. The fact that three adjacent sites at Grand Rouveau held the highest number of geckos for this island together with the presence of residual spatial autocorrelation (Fig. S2) may be consistent with that view, although future work will be needed to explore this hypothesis.

Effect of disturbance on retreat-site occupancy

Our daily surveys required a complete dismantling (and rebuilding) of the retreat-sites as well as the handling of individual geckos for identification. As may have been anticipated, such a disturbance was associated with a reduced probability of presence on the following day that was accounted for in the estimation of the other model parameters (Table 4; see also Fig. 4 for a comparison of two versus five days of disturbance). Since the CMR protocol was localized in space (3 artificial retreat-sites concerned out of 33 on the island) and time (5 days) and geckos can also find many suitable natural retreat-sites in the surrounding habitats, we do not expect any impact on the conservation status of the European Leaf-toed Gecko in Grand Rouveau Island.

Lack of movement between retreat-sites

We did not observe any movement between the three retreat-sites monitored. Every individual that was captured in one of our three retreat-sites either went missing for the rest of the study or was captured at least once more at the same site. Although the three sites are relatively far apart (distance: 21-41 meters), dispersal events can occur over more than 50 meters of rocky line in the European Leaf-toed Gecko (Delaugerre and Corti 2020). Similar dispersal distances were estimated in a slightly larger species, the Turkish Gecko *Hemidactylus turcicus*. Paulissen et al. (2013) found that some adults of Turkish Gecko exhibited movements up to 67 m, although the average movement when the individuals were recaptured after less than 30 days was only 5 m. Accordingly, besides site fidelity, several factors may explain a lack of movement between sites and future studies will be needed to assess their relative importance. First, the duration of the study may have been too short to detect movements between retreat-sites (only 4 days after the first capture). Second, movements may have occurred towards additional adjacent retreat-sites that have not been surveyed (see Fig. 1). Third, such movements between retreat-sites may be more likely in summer, as opposed to early in the season (in April), as higher temperatures may permit the species to wander away from the rocky environment and move through the vegetation (Delaugerre and Cheylan, 1992). To assess the possibility of movements between ARS, a longer CMR protocol using photo-identification could be valuable (see Monnet et al., 2022). This method, which is currently being tested for future studies, would have the advantages of avoiding daily manipulation and reducing the disturbance and the uncertainty due to shedding that can result in marking loss in long-term studies. Implementing it across an entire island could also enable us to estimate the abundance of the species on Grand Rouveau or If islands.

Temporal autocorrelation on retreat-site occupancy: retreat-site fidelity or lack of nocturnal activity?

As expected, the probability of an individual being present in the ARS on any given day was greater when that individual was already present in this ARS the previous day (e.g., Fig. 4). This could be explained in two non-mutually exclusive ways. First, individuals may not be active every night and therefore can be present several days in a row. Testing this hypothesis may be possible via video recording of artificial retreat-sites in order to follow the exits and re-entries of previously marked individuals over several nights (Deso & Reynier, 2024). Second, active individuals may tend to return to the same retreat-site from one night to the next (site fidelity). Other species of geckos tend to be faithful to their retreat-site, as demonstrated in *Hoplodactylus chrysosireicus*, *H. duvaucelii* (Flannagan, 2000), and *Gonatodes vittatus* (Quesnel et al., 2002).

Influence of outdoor temperatures on retreat-site occupancy

The presence within the retreat-sites was negatively related to the temperature of the previous night (Fig. 4),

which could be explained in several non-mutually exclusive ways. First, prey activity may be reduced during cold nights, reducing the incentive to leave the ARS (e.g., Lei and Booth, 2014 and references therein). Second, a decreased metabolic rate in response to cold temperatures could also lessen the incentive to forage and feed. In the Asian House Gecko *Hemidactylus frenatus*, the resting and post-feeding metabolic rates decreased with a decrease in temperature, and even in laboratory conditions with available living food, *H. frenatus* all but ceased its feeding activity below 17 °C, probably because their body temperature became too low to capture and digest prey efficiently (Lei and Booth, 2014). Third, European Leaf-toed Geckos may have a greater reliance on ARS for thermoregulation purposes when temperatures are lower. In agreement with that view, active individuals of the nocturnal Cap Verde Wall Gecko *Tarentola substituta* experienced significantly lower body temperature than inactive ones, and the body temperature of active geckos was correlated to air and soil temperatures, while the body temperature of inactive individuals was correlated to refuge temperature (Vasconcelos et al., 2012). Hence, geckos staying inside the ARS at night may benefit from its residual heat and conserve higher body temperatures. Fourth, individual geckos may be able to cover larger distances when temperatures are higher, allowing individuals to wander further away from their ARS; which, in turn, could give them the possibility, or force them, to identify and use a distinct retreat-site. Supporting the view that warm nights favor extended foraging opportunities, the Tree Dtella *Gehyra variegata* and the Eastern Stone Gecko *Diplodactylus vittatus* had longer spans of activity on hot nights (Bustard, 1967, Bustard, 1968), and the Tokay gecko *Gekko gecko* as well as the Gold Dust Day Gecko *Phelsuma laticauda* were significantly more mobile when temperatures were warmer (Ringenwald et al., 2021, Wehsener, 2019, respectively).

Difference between age classes on retreat-site occupancy

Juveniles appear to be more faithful to, or dependent on, artificial retreat-sites than older individuals (Fig. 4). A greater use of artificial retreat-sites by juveniles has also been observed in the gecko *Oedura lesueurii*, for which 82% of the individuals occupying artificial retreat-sites were juveniles (Webb and Shine, 2000). Future studies will be needed to understand this difference. For instance, adult and juvenile geckos may differ in their social behavior (Webb and Shine, 2000), in their thermoregulatory behavior or performance (but see Aparicio Ramirez et al., 2021, for a counter example in Crested Gecko *Correlophus ciliatus*), and in their response to predation risk by native or invasive predators such as the Black Rat *Rattus rattus*. In the French Mediterranean Bagaud Island, a successful eradication of the Black Rat was followed by an increase of observations of European Leaf-toed Geckos outside shelters for both juveniles and adults together with a significant increase in the overall number of juveniles (but not adults), suggesting the former age class may be the one most impacted by predation (Krebs et al., 2015). The impact of Black Rat on European Leaf-toed Gecko populations could be assessed by contrasting age-specific survival rates and population trajectories in islands with and without Black Rat while controlling for between-island differences in environmental conditions and gecko density. Partial rat control on a single island, which is considered on the island of Gargalo, could provide a suitable alternative.

ACKNOWLEDGEMENTS

The authors wish to thank the PIM Initiative (Initiative pour les Petites Îles de Méditerranée) for their constant support to this project via their program « îles sentinelles » and Michel-Jean Delaugerre for his feedback that helped improve an earlier version of this manuscript. The handling and the capture of the individuals were carried out under the permits DI-2018-130 and DI-2019-002 of the national park of the Calanques for the island of If and under the permit of May 13, 2020 granted by the prefect of the Var for the island of Grand Rouveau.

SUPPLEMENTARY MATERIAL

Supplementary material associated with this article can be found at <http://www-9.unipv.it/webshi/appendix/index.html> manuscript number 14527

REFERENCES

AGIR écologique (2016): Restauration du mur d'escarpe du Château d'If (Marseille, 13). Dossier scientifique accompagnant la demande de dérogation pour la capture, l'enlèvement, la destruction, la perturbation intentionnelle de spécimens de Phyllodactyle d'Europe, *Euleptes europaea* (Gené, 1839) (Rapport d'étude). Centre des Monuments Nationaux.

Akaike, H. (1974): A new look at the statistical model identification. IEEE Trans. Automat. Contr. **19**: 716-723.

Anderson, S. C., Ward, E. J. (2019): Black swans in space: modeling spatiotemporal processes with extremes. Ecology **100**: e02403.

Aparicio Ramirez, A., Perez, K., Telemeco, R. S. (2021): Thermoregulation and thermal performance of crested geckos (*Correlophus ciliatus*) suggest an extended optimality hypothesis for the evolution of thermoregulatory set-points. J. Exp. Zool. Part A **335**: 86-95.

Arnold, N., Ovenden, D. (2014): Le guide herpéto: 228 amphibiens et reptiles d'Europe. Delachaux et Niestlé.

Bellard, C., Leclerc, C., Courchamp, F. (2014): Impact of sea level rise on the 10 insular biodiversity hotspots: Sea level rise and insular hotspots. Global Ecol. Biogeog. **23**: 203-212.

Blondel, J., Cheylan, M. (2008): Lost species and animal survivors. In: Mediterranean Islands, pp. 41-45. Arnold, C., Ed, Survival Books, London

Blondel, J., Aronson, J., Bodiou, J. Y., Boeuf, G. (2010): The Mediterranean region: biological diversity in space and time. Oxford University Press Inc., New York

Bolker, B.M., Brooks, M.E., Clark, C.J., Geange, S.W., Poulsen, J.R., Stevens, M.H.H., White, J.-S.S. (2009): Generalized linear mixed models: a practical guide for ecology and evolution. Trends Ecol. Evol. **24**: 127-135.

Brooks, M.E., Kristensen, K., van Benthem, K.J., Magnusson, A., Berg, C.W., Nielsen, A., Skaug, H.J., Mächler, M., Bolker, B.M. (2017): glmmTMB Balances Speed and Flexibility Among Packages for Zero-inflated Generalized Linear Mixed Modeling. The R Journal **9**: 378-400.

Bustard, H.R. (1967): Activity cycle and thermoregulation in the Australian gecko *Gehyra variegata*. Copeia **1967**: 753-758.

Bustard, H.R. (1968): Temperature dependent activity in the Australian gecko *Diplodactylus vittatus*. Copeia **1968**: 606-612.

Cheylan, M., Poitevin, F. (1994): Conservazione di rettili e anfibi. In: La gestione degli ambienti costieri e insulari del Mediterraneo, pp. 275-336. Monballiu,X., Torre, A., Eds, Edizioni del Sole, Alghero (IT).

Cheylan, M., Rivière, V., Cheylan, A. (2018): Évaluation d'une méthode de suivi à long terme du gecko Euleptes europaea sur l'île du Grand Rouveau (archipel des Embiez, Var, France). Revue d'Écologie, 2018, **73**: 526-536.

Corti, C., Cecchi, L., Thévenet, M., Delaugerre, M.J. (2022): Reptiles and micro-insular environments of the Tuscan Archipelago (Italy). Naturalista sicil. **46**: 111-116.

Couturier, T., Debize, E., Le Mire Pecheux, L., Geoffroy, D., Moussay, C., Jailloux, A., Besnard, A. (2020): Suivi des tendances de l'occupation de l'espace par une espèce rare et cryptique: l'Eulepte d'Europe *Euleptes europaea* dans les Parcs nationaux des Calanques et de Port-Cros. (Rapport méthodologique, protocole version 1). Coopération OFB-CEFE.

Cox, N., Chanson, J., Stuart, S. (2006): The Status and Distribution of Reptiles and Amphibians of the Mediterranean Basin. IUCN, Gland, Switzerland and Cambridge, UK.

Croak, B.M., Pike, D.A., Webb, J.K., Shine, R. (2010): Using artificial rocks to restore nonrenewable shelter sites in human-degraded systems: colonization by fauna. Restor. Ecol. **18**: 428-438.

Dardun, J.Y. (2003): Problématiques de conservation du Phyllodatyle d'Europe *Euleptes europaea* sur les iles de Marseille (archipel du Frioul et de Riou). Unpublished doctoral dissertation. Université de Corse, Faculté des sciences et techniques.

Delaugerre, M.J. (1981a): Le point sur la répartition géographique de *Phyllodactylus europaeus* Gené. Bull. Soc. Herp. Fr. **18:** 14-16.

Delaugerre, M.J. (1981b): Sur l'histoire naturelle de *Phyllodactylus europaeus* Gené, 1838 (Gekkonidae Sauria Reptiles). Port-Cros: Etude d'une population naturelle. Trav. Sci. Parc Nat. Port-Cros **6**: 147-175.

Delaugerre, M.J. (1984): Sur l'écologie thermique des geckos *Phyllodactylus europaeus*, *Hemidactylus turcicus* et *Tarentola mauritanica* : rythmes d'activité, températures et activité, répartition altitudinale. Trav. sci. Parc Nat. Reg. Port-Cros **3**: 96–127.

Delaugerre M.J. (2002): Le Phyllodactyle d'Europe *Euleptes europaea* sur l'île de Port- Cros réflexion pour la mise au point d'un protocole de suivi des populations. Rapport Parc National de Port-Cros.

Delaugerre, M.J. (2003): Le phyllodactyle d'Europe sur l'ile de Port-Cros. Synthèse et mise à jour des carnets de terrains des recherches conduites entre 1975 et 1985. Parc National de Port-cros 24.

Delaugerre, M.J., Cheylan, M. (1992): Atlas de répartition des batraciens et reptiles de Corse.

Delaugerre, M.J., Corti, C. (2020): Tiny but "strong": the European Leaf-toed gecko, *Euleptes europaea*, a terrestrial vertebrate able to survive on tiny islets. Israel J. Ecol. Evol. **66**: 223-230.

Delaugerre M.J., Ouni, R., Nouira, S. (2011): Is the European Leaf-toed gecko *Euleptes europaea* also an African? Its occurrence on the Western Mediterranean landbrige islets and its extinction rate. Herpetol. Notes **4**: 127-137.

Delaugerre, M.J., Sacchi, R., Biaggini, M., Lo Cascio, P., Ouni, R., Corti, C. (2019): Coping with aliens: how a native gecko manages to persist on Mediterranean islands despite the Black rat? Acta Herpetol. **19**: 89–100.

Deso, G., Priol, P., Reynier, T., Renet, J. (2023): High occupancy of European leaf-toed gecko *Euleptes europaea* in two island stands of *Eucalyptus sp.*: tree

selection, co-occurrence and habitat effect. bioRxiv 2023.02.08.527781.

Deso, G., Reynier, T. (2024). Construction of a refuge wall with crevices to protect European leaf-toed geckos *Euleptes europaea* and young Turkish geckos *Hemidactylus turcicus* on the Ile du Levant, France. Herpetol. Bull. **167**: 20-24.

Di Nicola, M.R., Colombo, M., Russo, F. (2022): First record of european leaf-toed gecko *Euleptes europaea* (Gené, 1839)(Squamata, Sphaerodactylidae) in Campania (Italy). Rivista del Museo Civico di Scienze Naturali "Enrico Caffi" **35**: 79-82.

Dunn, P.K., Smyth, G.K. (2018): Generalized Linear Models With Examples in R, Springer Texts in Statistics. Springer New York, New York, NY.

Edgar, P., Baker, J., Foster, J. (2010): Reptile habitat management handbook. Amphibian and Reptile Conservation, Bournemouth.

Escofier, B. (1979): Traitement simultané de variables qualitatives et quantitatives en analyse factorielle. Cahiers de l'analyse des données **4**: 137-146.

Flannagan, H.J. (2000): Conservation Biology of the goldstripe gecko (*Hoplodactylus chrysosireticus*) and interactions with Duvaucel' s gecko (*Hoplodactylus duvaucelii*) on Mana Island, Cook Strait, New Zealand. Unpublished doctoral dissertation. Massey University, Palmerston North, New Zealand.

Grillet, P., Cheylan, M., Thirion, J.M., Doré, F., Bonnet, X., Dauge, C., Chollet, S., Marchand, M. A. (2010): Rabbit burrows or artificial refuges are a critical habitat component for the threatened lizard *Timon lepidus* (Sauria, Lacertidae). Biodivers. Conserv. **19**: 2039-2051.

Gros-Désormeaux, J.-R. (2012): La biodiversité dans des territoires insulaires, approche théorique et perspectives de développement. Developpement durable.

Guenard, V., Drobinski, P., Caccia, J.-L., Campistron, B., Bench, B. (2005): An Observational Study of the Mesoscale Mistral Dynamics. Boundary-Layer Meteorol. **115**: 263-288.

Hartig, F. (2022): DHARMa: residual diagnostics for hierarchical (multi-level/mixed) regression models. cran.r-project .https://cran.r-project.org/web/packages/DHARMa/vignettes/DHARMa.html [*accessed on 20 May 2022*]

Hervé, M. (2014): Aide-mémoire de statistique appliquée à la biologie. Construire son étude et analyser les résultats à l'aide du logiciel R.

Hitchcock, M.A., McBrayer, L.D. (2006): Thermoregulation in nocturnal ecthotherms: seasonal and intraspecific variation in the Mediterranean gecko (*Hemidactylus turcicus*). J. Herpetol. **40**: 185-195.

Huey, R.B. (1982): Temperature, physiology, and the ecology of reptiles. In: Biology of the Reptilia, Vol 12, Physiology (C), pp. 25-91. Gans, C., Pough, F.H., Eds, Academic Press, London.

Hulme, P.E., Brundu, G., Camarda, I., Dalias, P., Lambdon, P., Lloret, F., Medail, F., Moragues, E., Suehs, C., Traveset, A., Troumbis, A., Vilà, M. (2008): Assessing the risks to Mediterranean islands ecosystems from alien plant introductions. In: Plant Invasions: Human Perception, Ecological Impact and Management, pp. 39-56. Tokarska-Guzik, B., Brock, J.H., Brundu, G., Child, L., Daehler, C.C., Pyšek, P., Eds, Backhuys Publishers, Leiden, The Netherlands.

Kassambara, A. (2017): Practical Guide To Principal Component Methods in R*:* PCA, M (CA), FAMD, MFA, HCPC, factoextra (Vol. 2). Sthda.com.

Kearney, M. (2002): Hot rocks and much-too-hot rocks: seasonal patterns of retreat-site selection by a nocturnal ectotherm. J. Thermal Biol. **27**: 205-218.

Kearney, M., Predavec, M. (2000): Do nocturnal ectotherms thermoregulate ? A study of the temperate gecko *Christinus marmoratus*. Ecology **81**: 2984-2996.

Krebs, E., Abba, A., Gillet, P., Eudeline, R., Gauthier, J., Le Quilliec, P., Lorvelec, O., Martinerie, G., Vidal, E., Buisson, E. (2015): Réponses des populations de reptiles à l'éradication du rat noir (*Rattus rattus*) sur l'île de Bagaud (parc national de Port-Cros, Var, France). Revue d'Ecologie, Terre et Vie **70**: 99-109.

Lefebvre, G., Redmond, L., Germain, C., Palazzi, E., Terzago, S., Willm, L., Poulin, B. (2019): Predicting the vulnerability of seasonally-flooded wetlands to climate change across the Mediterranean Basin. Sci. Total Environ. **692**: 546-555.

Lei, J., Booth, D.T. (2014): Temperature, field activity and post-feeding metabolic response in the Asian house gecko, *Hemidactylus frenatus*. J. Thermal Biol. **45**: 175-180.

Levene, H. (1960). Test of homogeneity of variances. In: Contributions to probability and statistics: Essays in honor of Harold Hotelling, pp. 278-292. Olkin, I., Ghurye, S.G., Hoeffding, W., Madow, W.G., Mann, H.B., Eds, Stanford University Press, Palo Alto (USA).

Logan, M.L., Fernandez, S.G., Calsbeek, R. (2015): Abiotic constraints on the activity of tropical lizards. Funct. Ecol. **29**: 694-700.

Marchand, M. A., Roy, C., Renet, J., Delauge, J., Meyer, D., Hayot, C. (2017): Liste rouge régionale des amphibiens et reptiles de Provence-Alpes-Côte d'Azur. Publication du Conservatoire des Espaces Naturels.

Médail, F. (2017): The specific vulnerability of plant biodiversity and vegetation on Mediterranean islands in

the face of global change. Reg. Environ. Change. **17**: 1775-1790.

Médail, F. (2022): L'écosystème méditerranéen: états d'urgence. Pouvoirs **183**: 27-41.

Médail, F., Myers, N. (2004): Mediterranean Basin. In: Hotspots Revisited: Earth's Biologically Richest and Most Endangered Terrestrial Ecoregions, pp 144-147. Mittermeier, R.A., Gil, P.R., Hoffman, M., Pilgrim, J., Brooks, T., Goettsch Mittermeier, C., Lamoreux, J., da Fonseca, G.A.B., Eds, Cemex Books on Nature. CEMEX, Mexico.

MedECC (2020): Climate and Environmental Change in the Mediterranean Basin – Current Situation and Risks for the Future. First Mediterranean Assessment Report [Cramer, W., Guiot, J., Marini, K. (eds.)] Union for the Mediterranean, Plan Bleu, UNEP/MAP, Marseille, France.

Millar, R.B. (2011): Maximum likelihood estimation and inference: with examples in R, SAS, and ADMB. Statistics in practice. John Wiley & Sons Ltd, Chichester, UK.

Monnet, C., Dokhelar, T., Renet, J. (2022): Rapid colour changes in a tiny threatened gecko do not impede computer-assisted individual recognition. bioRxiv 2022.03.16.484634.

Moore, E., Nimmo, D.G., Wassens, S., Michael, D.R. (2022): Use of artificial bark covers to investigate the distribution and abundance of arboreal lizards in a floodplain environment. Aust. J. Zool. **69**: 125-135.

Nias, R.C., Burbidge, A.A., Ball, D., Pressey, R.L. (2010): Island arks: the need for an Australian national island biosecurity initiative. Ecol. Manag. Restor. **11**: 166-167.

Ortega, Z., Mencía, A., Pérez-Mellado, V. (2017): Wind constraints on the thermoregulation of high mountain lizards. Int. J. Biometeor. **61**: 565-573.

Paulissen, M.A., Meyer, H.A., Hibbs, T.S. (2013): Movement patterns and sociality of the Mediterranean gecko, *Hemidactylus turcicus*, in southwestern Louisiana. Southwest. Nat. **58**: 344-350.

Pinheiro, J.C., Bates, D.M. (2004): Mixed-effects models in S and S-PLUS. Statistics and computing. Springer, New York, Berlin, Heidelberg.

QGIS Development Team (2022): QGIS Geographic Information System. QGIS Association.

Quesnel, V.C., Seifan, T., Werner, N., Werner, Y.L. (2002): Field and captivity observations of the lizard *Gonatodes vittatus* (Gekkonomorpha: Sphaerodactylini) in Trinidad and Tobago. Living World, Journal of the Trinidad and Tobago Field Naturalists' Club **2002**: 8-18.

R Core Team (2021): R: A Language and Environment for Statistical Computing. R Foundation for Statistical Computing.

Renet, J., Gerriet, O., Jardin, M., Magne, D. (2008): Les populations de phyllodactyle d'Europe *Euleptes europaea* Gené, 1839 Reptilia Sauria Gekkonidae dans les Alpes Maritimes: premiers éléments sur leur répartition et leur écologie. Faune de Provence **24/25**: 117-126.

Renet, J., Gerriet, O., Kulesza, V., Delaugerre, M.J. (2013): Le Phyllodactyle d'Europe *Euleptes europaea* (Gené, 1839) (Reptilia, Squamata, Sphaerodactylidae) - Les populations continentales françaises ont-elles un avenir? Bull. Soc. Herp. Fr. **145/146:** 189-198.

Ringenwald, B.E., Bogacki, E.C., Narvaez, C.A., Stark, A.Y. (2021): The effect of variable temperature, humidity, and substrate wettability on Gecko (*Gekko gecko*) locomotor performance and behavior. J. Exp. Zool. Part A **335**: 454-463.

Roberston, P., Bainbridge, I., de Soye, Y. (2011): Priorities for conserving biodiversity on european islands. Presented at the Convention on the conservation of European wildlife and natural habitats, European Council, Strasbourg.

Rodrigues, A.S.L., Akçakaya, H.R., Andelman, S.J., Bakarr, M.I., Boitani, L., Brooks, T.M., Chanson, J.S., Fishpool, L.D.C., Da Fonseca, G.A.B., Gaston, K.J., Hoffmann, M., Marquet, P.A., Pilgrim, J.D., Pressey, R.L., Schipper, J., Sechrest, W., Stuart, S.N., Underhill, L.G., Waller, R.W., Watts, M.E.J., Yan, X. (2004): Global Gap Analysis: Priority Regions for Expanding the Global Protected-Area Network. BioScience **54**: 1092-1100.

Salvi, D., Berrilli, E., Bruni, G., Garzia, M., Gomes, V., Radi, G., Delaugerre, M.J. (2023): The secret life of a rock-dweller: arboreal acrobatics observed in the European leaf-toed gecko *Euleptes europaea*. Herpetozoa **36**: 135-141.

Salvidio, S., Delaugerre, M.J. (2003): Population dynamics of the european leaf-toed gecko (*Euleptes europaea*) in NW Italy: implications for conservation. Herpetol. J. **13**: 81–88.

Shapiro, S.S., Wilk, M.B. (1965): An analysis of variance test for normality (complete samples). Biometrika **52**: 591-611.

Silva-Rocha, I. R., Salvi, D., Carretero, M. A., Ficetola, G. F. (2019). Alien reptiles on Mediterranean Islands: A model for invasion biogeography. Divers. Distrib. **25**: 995-1005.

Tranchant, A., Vidal, E., Kayser, Y. (2003): Premières données sur le régime alimentaire du chat haret *Felis catus* en situation micro-insulaire méditerranéenne. Revue d'Ecologie, Terre et Vie, Société nationale de protection de la nature **58**: 411-418.

Underwood, E.C., Viers, J.H., Klausmeyer, K.R., Cox, R.L., Shaw, M.R. (2009): Threats and biodiversity in the mediterranean biome. Divers. Distrib. **15**: 188-197.

Vacher, J.-P., Geniez, M. (2010): Les reptiles de France, Belgique, Luxembourg et Suisse : Cahier d'identification. Cartes de distribution, Publications scientifiques du muséum. Biotope Éditions, Mèze.

Vasconcelos, R., Santos, X., Carretero, M.A. (2012): High temperatures constrain microhabitat selection and activity patterns of the insular Cape Verde wall gecko. J. Arid Environ. **81**: 18-25.

Walls, G.Y. (1983): Activity of the tuatara and its relationships to weather conditions on Stephens Island, Cook Strait, with observations on geckos and invertebrates. New Zeal. J. Zool. **10**: 309-317.

Webb, J.K., Shine, R. (1998a): Using thermal ecology to predict retreat-site selection by an endangered snake species. Biol. Conserv. **86**: 233-242.

Webb, J.K., Shine, R. (1998b): Thermoregulation by a Nocturnal Elapid Snake (*Hoplocephalus bungaroides)* in Southeastern Australia. Physiol. Zool. **71**: 680-692.

Webb, J.K., Shine, R. (2000): Paving the way for habitat restoration: can artificial rocks restore degraded habitats of endangered reptiles? Biol. Conserv. **92**: 93-99.

Wehsener, J.W. (2019): Foraging mode and the factors affecting foraging behavior in the diurnal arboreal gecko, *Phelsuma laticauda*. Unpublished Manuscript. Environmental Science Policy and Management, University of California, Berkeley, California 94720 USA.

Zuur, A.F., Ieno, E.N., Walker, N., Saveliev, A.A., Smith, G.M. (2009): Mixed effects models and extensions in ecology with R, Statistics for Biology and Health. Springer New York, New York, NY, USA.

Acta Herpetologica 19(2): 139-153, 2024
DOI: 10.36253/a_h-15232

The effect of climate change on spatio-temporal activity in burrowing frogs of the *Smilisca* group

Alondra Encarnación-Luévano[1], J. Jesús Sigala-Rodríguez[1], Gustavo E. Quintero-Díaz[2], Marcelo Silva Briano[3], Octavio Rojas-Soto[4,*]

[1] *Colección Zoológica, Departamento de Biología, Centro de Ciencias Básicas, Universidad Autónoma de Aguascalientes, Aguascalientes 20100, México*
[2] *Departamento de Biología, Centro de Ciencias Básicas, Universidad Autónoma de Aguascalientes, Aguascalientes 20100, México*
[3] *Laboratorio de Ecología, Departamento de Biología, Centro de Ciencias Básicas, Universidad Autónoma de Aguascalientes, Aguascalientes 20100, México*
[4] *Laboratorio de Bioclimatología, Red de Biología Evolutiva, Instituto de Ecología A. C., Xalapa, Veracruz 91073, México*
**Corresponding author.* Email: octavio.rojas@inecol.mx

Submitted on: 2023, 3rd October; revised on: 2024, 30th March; accepted on: 2024, 4th September
Editor: Raoul Manenti

Abstract. Measuring the potential effects of future climate changes on the spatio-temporal variance of optimal conditions for seasonal species is a key conservation issue. This study assesses the impact of climate change on the spatial and temporal patterns of optimal conditions for activity in two burrowing frogs, *Smilisca fodiens* and *S. dentata*. Ecological Niche Modeling was used to implement niche seasonality models, with calibration performed during the peak activity (July). These models were then transferred to current and future conditions for the remainder of the year, predicting future scenarios up to 2070 with an intermediate trajectory greenhouse gas concentration of 4.5 W/m^2. Climate change transferability was assessed for four potential scenarios: 1) high precipitation and low temperature, 2) high precipitation and high temperature, 3) low precipitation and low temperature, and 4) low precipitation and high temperature. We examined the impact across future projected areas and analyzed geographic change trends based on latitude, longitude, and elevation. For both species, the best scenario would involve increased precipitation in the future. However, the worst-case would be a combination of reduced precipitation and higher temperatures. Due to large area loss, northern populations of *S. fodiens* may be highly vulnerable. Concerning *S. dentata*, the outlook is worrisome, with all known populations experiencing losses in most months. Area gains may not help either species since they tend to occur at elevations above their known ranges. Using a seasonal approach in spatio-temporal analysis enhances comprehension of the behavioral adaptations of seasonal species and their vulnerability to current and future climatic variations.

Keywords. Ecological niche modeling, seasonal niche, distribution, anurans, estivation, global warming.

INTRODUCTION

Climate change is one of the leading environmental problems in species conservation (Hughes, 2000; van-Vuuren et al., 2007). Changes in temperature and precipitation patterns and in hydrological and nutrient cycles (IPCC 2014) are among the main factors threatening biodiversity, ecosystem functioning and resilience, and ecological services (Thomas et al., 2004; Bellard et al., 2012). These adverse effects include problems related to changes in the geographic distribution of species (reduction in range, extinction, or displacement to other areas; Sierra-Morales et al., 2021) and phenology (courtship and oviposition outside the reproductive period; IPCC 2014).

ISSN 1827-9635 (print)
ISSN 1827-9643 (online)

Whether species will be able to acclimatize or adapt quickly enough to cope with changing climate remains to be seen. Evidence of change has been documented, and the main mechanisms encountered are plasticity in physiology, morphology, and behavior, and, in a few cases, microevolutionary adaptations (Bellard et al., 2012; Pacifici et al., 2017). Whatever the mechanism is, species responses can be more clearly observed at the local scale (Walther et al., 2002) through altitudinal and latitudinal changes in the distribution of species throughout the year (e.g., Cohen and Jetz, 2023) and, to a lesser extent, adaptation through changes in physiology and behavior (Bellard et al., 2012). The latter is the less obvious change and the most complex and unlikely because it requires longer evolutionary times (Bodensteiner et al., 2021). Conversely, shifts in the distribution throughout the year may be more advantageous for species and are easy to detect. Distribution shifts have been observed in species with high dispersal capacity as they follow their optimal climatic requirements in the face of impending climate change, leading to population extinctions at the edges of their original ranges (e.g., Hughes, 2000; Thomas et al., 2004). Alternatively, some species have evolved cyclical climatic variations daily or seasonal (e.g., animal activity patterns; Bellard et al., 2012; Weatherhead et al., 2012; Rojas-Soto et al., 2021).

Most studies of species responses to climate change have concluded that the most common response is to track the niche by following environmental changes across the range; however, most of these studies have focused on species with a high ability to disperse (e.g., Peterson et al., 2002; Martínez-Meyer et al., 2004). For amphibians, a group of ectothermic vertebrates, an alternative response to climate change is temporal adjustments in activity following life history because their physiological mechanisms tend to be conserved traits (Navas et al., 2008; Weatherhead et al., 2012) and because they have a low dispersion capacity due to their strong dependence on moisture (Navas et al., 2008).

A good example of behavioral temporal responses to climatic variations throughout the year is the two burrowing species of the *Smilisca* group, which have modified their activity periods to adapt to temperate conditions and become seasonal species (Encarnación-Luévano et al., 2021). Unlike the other six species of *Smilisca*, *S. fodiens* and *S. dentata*, have adapted to more seasonal and xeric environments in the northernmost latitudes of the group (Duellman, 2001; Quintero-Díaz and Vázquez-Díaz, 2009; IUCN SSC Amphibian Specialist Group 2020; Fig. 1). They are morphologically adapted to burrowing (i.e., integumentary-cranial co-ossification of the skull, short limbs, reduced terminal discs in the fingers, and an inner metatarsal tubercle; Duellman, 2001) and to spending long periods of the year underground by slowing metabolism and cocoon formation (Ruibal and Hillman, 1981; Sullivan et al., 1996; Quintero-Díaz and Vázquez-Díaz, 2009). During the most favorable climatic months, individuals leave the burrows to feed and breed (Sullivan et al., 1996; Quintero-Díaz and Vázquez-Díaz, 2009). However, even in these months, *S. dentata* remain in the burrows during the warmest hours and become active when humidity increases or heat decreases (Quintero-Díaz and Vázquez-Díaz, 2009). The surface activity of the northernmost populations of *S. fodiens* is seasonal and is predictable from the temporal and geographic variation of suitable climatic conditions (Encarnación-Luévano et al., 2013). In an evolutionary context, the emergence of this behavioral novelty could allow adaptation to higher latitudes and extreme conditions. Indeed, there is evidence of niche conservation within this group of tropical origin when considering the seasonal niche of these burrowing species (i.e., limited to the period of activity outside burrows; Encarnación-Luévano et al., 2021).

Predicting the extent of climate change impacts on biodiversity has become one of the most important

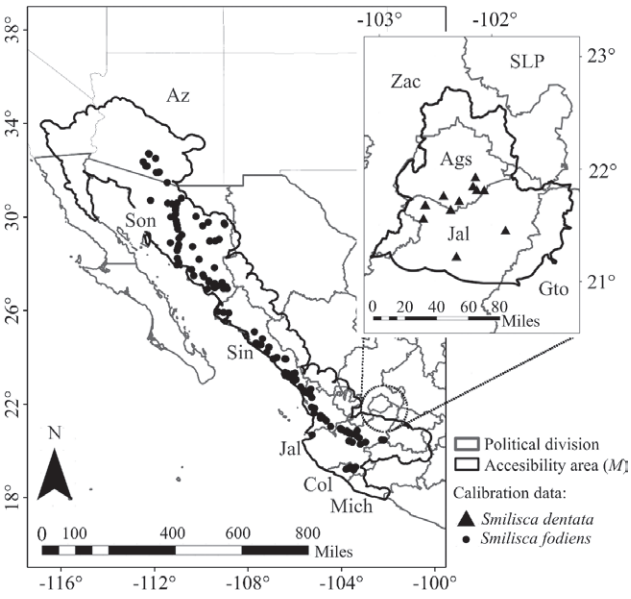

Fig. 1. The geographical location of the accessibility area and the presence of data used in the model calibration. We show both species hypothetical accessible areas (*M*, solid black line) employed in the calibration and model transfer. For *Smilisca fodiens* known historical records for July (black dots) goes from central-southern Arizona (AZ) along the Mexican Pacific coast through Sonora (Son), Sinaloa (Sin), Jalisco (Jal), Colima (Col) and Michoacán (Mich). Contrarily, for *S. dentata,* July records used in the calibration (black triangles) are restricted to a small portion of the Mexican Plateau, the South of Aguascalientes (Ags) and North of Jalisco.

conservation goals (i.e., changes in the direction and strength of species' ranges) (Dawsonn et al., 2011; Farooqi et al., 2022). Ecological niche modeling (ENM) and species distribution modeling (SDM) are the most commonly used techniques to achieve this goal. However, these approaches have primarily focused on the axis of spatial change (e.g., Peterson et al., 2002; Bellard et al., 2012). Subterranean habitats have functioned as optimal climate refugia for a wide range of high latitudes species (Scheffers et al., 2014; Rojas-Soto et al., 2021), and thus the behavioral adaptations of the *Smilisca* fossorial species should provide an adaptive advantage in the face of future climate change.

Our approach analyzes the potential impact of climate change on the spatial and temporal axes; this is important for seasonal species by considering their natural history, understanding their evolution and adaptation, and improving their conservation strategies. This has a crucial foundation within the ecological niche theory and its study through correlative models: the environmental limits estimated by ENM approach the *fundamental* niche but is in the *realized* niche where environments meet the presence of the species (Soberón and Peterson, 2005). Thus, we emphasize that it is in the temporal dimension where the real vulnerability of seasonal species can be effectively assessed. The main objective of this study was to analyze the potential effect of climate change on the temporal and geographic activity (i.e., outside burrows) via the ENM and SDM in *S. fodiens* and *S. dentata*.

MATERIAL AND METHODS

We performed a monthly analysis to track the environmental niche of July. We considered July because it is the month with the largest substantial data recorded in collections and literature for *S. fodiens*. It also is the month with the greatest number of individuals over several years of systematic fieldwork within the species *S. dentata* (unpublished data). We also assumed that this is the month with the optimal climatic conditions for feeding and reproduction in both species (Sullivan et al., 1996; Quintero-Díaz and Vázquez-Díaz, 2009; Encarnación-Luévano et al., 2013). The models calibrations were performed with July data and then transferred to current and future conditions for the remaining months of the year (Fig. 2). The transfer of the model was made towards four possible future scenarios until 2070, described by groups of general circulation models (GCMs; see Environmental Data section) for the study area using an intermediate trajectory greenhouse gas concentration of 4.5 W/m^2. We identified three combinations

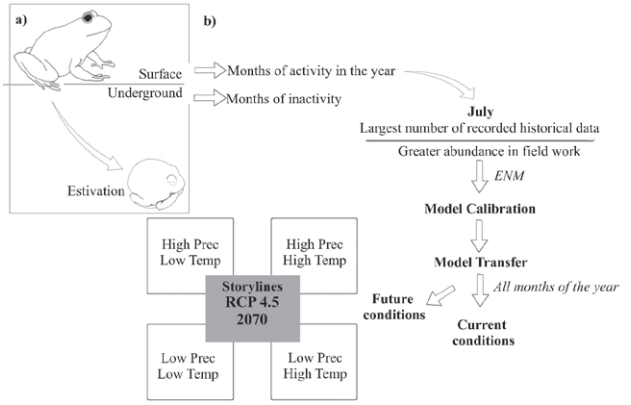

Fig. 2. Diagram of the calibration and transfer process. Calibration was done with July data assuming that it is in this month that the most suitable conditions for activity outside burrows are presented (*see* Methods). a) The time of inactivity for many burrowing species implies a period underground in aestivation (diagram adapted from Moreira et al., 2020). b) Then, the model was transferred into current and future conditions of all the months in the year towards four storylines (i.e., possible climate futures) to 2070 using an intermediate trajectory greenhouse gas concentration 4.5 W/m^2. The storylines result from the possible forms in which precipitation and temperature can vary at certain regions because of the uncertainty of the global circulation models (GCMs; Fajardo et al., 2020).

according to the decrease or increase of predicted areas in the future compared to current climate conditions: areas that will maintain their optimal conditions for the species (stable areas), new optimal areas (gain areas), and optimal areas that will be lost (loss areas). We analyzed impacts based on the area predicted in the future and the trend of geographic change according to three attributes: latitude, longitude, and elevation.

Biological data

The distribution of *Smilisca fodiens* extends from south-central of Arizona, south along the Mexican Pacific slope, from Sonora to northern Michoacán (Sullivan et al., 1996; Duellman, 2001; Fig. 1). *Smilisca dentata* has a more restricted range, with fewer records in southeastern Aguascalientes, northern Jalisco, and a small adjacent portion of the state of Zacatecas (Quintero-Díaz and Vázquez-Díaz, 2009; Ávila-Villegas and Flores de Anda, 2017; Villalobos-Juárez, 2023; Fig. 1). Presence data were obtained from online portals providing primary biodiversity data, including GBIF (https://doi.org/10.15468/dl.wtz7zr; https://doi.org/10.15468/dl.tf7n27), VertNet, and UNIBIO (http://vertnet.org/; http://unibio.unam.mx/, last accessed 04/02/2020), and from the literature. The analysis of the *S. dentata* data was more direct due

to the small number of localities recorded for the species and the author's experience from years of fieldwork and knowledge of historical data. Of the 17 historical records, nine were recorded in July. We add two records from July from new localities in Jalisco and Aguascalientes to the analysis. For *S. fodiens*, all records found in the databases mentioned above were evaluated and verified in geographic and ecological space through spatial correspondence and pairwise scatterplots in ArcGIS (ESRI, 2019), searching for inconsistencies and removing outliers, taking into account biology, ecology, and life history. After data cleaning, we recovered 448 records, of which 232 were for July only (47 for June, 113 for August, 42 for September, 10 for October, and four for November). Except for July, the monthly presence data of *S. fodiens* were used only as a reference to visualize the geographic correspondence in the monthly transfers as in Encarnación-Luévano et al. (2013).

Environmental data

To characterize the ecological niches, we obtained environmental data from the CHELSA database version 2.1 (Karger et al., 2017; https://chelsa-climate.org/timeseries/) with a spatial resolution of 30 arc-seconds (~1 km^2). Current conditions are from the period 1979-2013. This study's ecological niches were climatically delimited using the average monthly temperature and the total monthly precipitation. Using the mean temperature (hereafter Tmean) over the minimum and maximum temperatures has solid biological implications. We use Tmean to establish that *Smilisca fodiens* and *S. dentata* limit their activity outside burrows and avoid extreme temperatures. Therefore, the impact of climate change on these species can be focused on the temperature range that triggers feeding and reproductive activities. We also included the topographic variable of Slope to increase the niche dimensionality, as it is not directly correlated with precipitation and temperature like elevation (Parra et al., 2004). This variable was obtained from the digital elevation model GTOPO20, available at the EROS Data Center (http://eros.usgs.gov/).

The climate change scenarios correspond to the CHELSA-CMIP5 dataset. We selected the delta change climatology for 2061-2080 (i.e., downscaled climatology for 2070; Karger et al., 2017). These scenarios represent the climate simulations based on greenhouse gas's socioeconomic emission and concentration scenarios. The CMIP5 provides four climatic change scenarios in which concentration and emission pathways result in radiative forcings of 2.6, 4.5, 6, and 8.5 W/m^2, also referred to as Representative Concentration Pathways (RCP; van-Vuuren et al., 2007; IPCC, 2014). This study evaluated the 4.5 RCP, considered an intermediate scenario but the most likely given fossil fuel production (Höök et al., 2010). RCP4.5 is comparable to the B1 scenario in the IPCC's Third and Fourth Assessment Reports. It assumes a medium to low level of emission reduction policies, which means that greenhouse gas emissions will increase until 2100, when stabilization of gas emissions will be achieved, for example, at around 538 ppm CO_2 (IPCC, 2014). To explore the possible climate storylines in which ecological niches are transferred, we used GCMcomparer, via the code available on GitHub (https://github.com/marquetlab/GCM_compareR/issues/8; Fajardo et al., 2020). The storylines result from the possible ways precipitation and temperature can vary in a given region due to uncertainty in the general circulation models (GCMs; Fajardo et al., 2020). After testing 32 GCMs available in CHELSA, we find that the average ensemble predicts a future with less precipitation and up to 4°C warmer than the present. Considering the deviations of the GCMs from the mean, four storylines were proposed: 1) high precipitation and low temperature, hereafter Hprec-Ltemp, 2) high precipitation and high temperature, Hprec-Htemp, 3) low precipitation and low temperature, Lprec-Ltemp, and 4) low precipitations and high temperature, Lprec-Htemp (Fig. S1). From these GCM clusters, we selected those whose future climate information differed from the climatic mean of all GCMs and were also available at the resolution and trajectory of greenhouse gas concentrations. The GCMs were: 1) Hprec-Ltemp: gfdl_esm2g, mri_cgm3; 2) Hprec-Htemp: miroc_esm, csiro_access1, cesm1_cam5; 3) Lprec-Ltemp: inm_cm4, ncc_noresm1_m, giss_e2r; and 4) Lprec-Htemp: mohc_hadgem2_es, ipsl_cm5a_lr, and mpi_esm_ir.

Ecological niche modeling

We used Maxent (maximum entropy algorithm; Phillips et al., 2006), which fits a distribution of probabilities across the study area subject to the constraints of the environmental characteristics of known presences. To run Maxent, we used the R package kuenm (Cobos et al., 2019), which allows the inclusion of different sets of environmental predictions by evaluating many feature combinations with different regularization multipliers to find the best parameter combination, improving the quality and robustness of the predictions (Cobos et al., 2019). We used the presence data recorded for model calibration in July, which were 232 for *S. fodiens* and 11 for *S. dentata*. For *S. fodiens*, 20% of the total presence data were randomly sampled for model evaluation (see below). For *S. dentata*, all data sets were used for model calibration, con-

sidering the sensitivity of the estimators to the number of presences (Jiménez-Valverde, 2020, but see Pearson et al., 2007). Despite the low number of presences, the predictive capacity was improved by creating a number of replicates of the model (Breiner et al., 2015) and evaluating each one using the method proposed by Pearson et al., (2007). Models were calibrated across regions that were assumed to be historically accessible areas for both species (*M*, Barve et al., 2011, see Fig. 1). We consider the limited dispersal ability of amphibians and the boundaries of surrounding ecoregions (Olson et al., 2001) as a guide.

We analyzed the response of the model under current conditions with different parameters in kuenm (Cobos et al., 2019) to obtain the best response curves of the variables and, thus, improve the performance during the model transfers, as suggested by Guevara et al., (2017) and Shcheglovitova and Anderson (2013). In the cases where the response curves of the variables followed a normal distribution, we allowed an extrapolation mode during model transfers (Guevara et al., 2017). For *S. fodiens*, a normal distribution of the variables was obtained using the linear/quadratic/product features, with a regularization value of 0.2. To characterize the background during the model performance, we included the total number of pixels (i.e., 100074) of the extent of the calibration area (which Maxent sets to 10000 pixels by default). For *S. dentata*, we calibrated the model with linear/quadratic features, a regularization value of 0.1. As with the previous species, we used the total pixels in the calibration area extent to characterize the species background (i.e., 25718). This model was the only one in which a normal distribution was fitted for the precipitation response curve; however, this fit was not observed for the Tmean in any of the models. In most models, an increase in suitability was observed towards high-temperature values, indicating that values greater than 23 °C could reach the highest suitability values according to the maximum entropy algorithm. Therefore, we avoided extrapolation in *S. dentata* and instead allowed the algorithm to truncate during the transfers to future scenarios (Owens et al., 2013). Ten replicates were established per model combination.

Models were evaluated using kuenm_ceval function (Cobos et al., 2019) according to statistical significance estimated by the partial area under the receiver operating characteristic (partial ROC) and omission rates (E = a user-selected proportion of presence data that might present meaningful errors; Peterson et al., 2008). The partial ROC only evaluates models over the prediction spectrum and allows for differential weighting of the two error components (omission and commission; Peterson et al., 2008). Thus, the area under the curve (AUC) was limited to the proportional area over which the model made predictions, and we only considered models with omission errors < 5% (Peterson et al., 2008). Due to the small number of records for *S. dentata*, we additionally performed the jackknife test suggested by Pearson et al. (2007) to assess the ability of models to predict species occurrence when fewer than twenty-five occurrence records are available. The significance of this test was evaluated over *n* models, each excluding one locality from among the *n* available and assessing the model's success in predicting the excluded locality. The probability of these observed levels of success and failure was calculated according to Pearson et al. (2007).

Geographic transfers

The probability maps of the GCMs were averaged to have only one future prediction per storyline (see Environmental Data in Methods). We converted the final models to binary (presence-absence) maps using a threshold applied to the probability outputs for current and future scenarios to quantitatively analyze current and future projections. For *S. fodiens*, we applied the tenth percentile training presence threshold (> 0.242 = suitable conditions present). For *S. dentata*, we explored multiple thresholds to reduce overfitting; then, based on its monthly activity observed during the fieldwork, we chose the fixed cumulative value of 5 (> 0.183). All spatial processes were carried out in ArcGis (ESRI, 2019).

We plot the total number of pixels for each prediction, so the bar graphs show how the predicted area increases or decreases over a year under current and future conditions. To identify the type of impact, considering the areas that will be lost, gained, or stable in the future, we overlap and sum, in ArcGis, the binary layers of the current and future predictions. Lost areas were counted as pixels that corresponded only to the current prediction; conversely, gain areas were counted as pixels that corresponded only to the future prediction, and finally, stable areas were counted as all those pixels where the current and future predictions coincided. We then analyzed the correspondence in elevation, latitude, and longitude between the distribution of each type of impact and the distribution described by the July data used to calibrate the model (see the Methods/Biological Data section). To do this, we used the package ggplot2 in R (Wickham, 2016) to plot the variance of the data for each variable (i.e., elevation, latitude, and longitude) and compared the group medians to determine the similarities between the impact types and the July data median. We used the nonparametric median.test for independent samples, available in the agricolae package in R (de Men-

diburu, 2023). Assuming that the ideal for the species is the persistence of suitable conditions that guarantee reproduction and feeding in current localities, it would be desirable to find a similarity between the medians of elevation, latitude, and longitude of the stable or newly gained areas and the July presence data. On the contrary, it would be desirable that the median of elevation, latitude, and longitude of the loss areas be different from the median of the July presence data.

RESULTS

All our models performed well in predicting the presence of data used in the validation process for *S. fodiens* (AUC ratio = 1.424, P < 0.05; omission rate at 5% = 0.05) and *S. dentata* (AUC ratio = 1.876, P = 0; omission rate at 5% = 0). For the latter, we also observed a high success rate and statistical significance with the jackknife test (1, P < 0.001).

Under current conditions, the year period with a predicted area for activity outside of burrows is larger for *S. fodiens* than for *S. dentata*. The predicted area for *S. fodiens* ranges from June to October (Fig. 3a). For *S. dentata* from June to September (Fig. 4a). For both species, we found that June was the month with the smallest predicted area (i.e., the number of pixels), in contrast to July, which was the month with the largest area, and from which a gradual decrease was observed in the following months (Fig. 5).

In the future, the predicted area for *S. fodiens* was larger than that predicted under current conditions in almost every month; there was even a small increase in November (Fig. 3b). Conversely, for *S. dentata*, the pre-

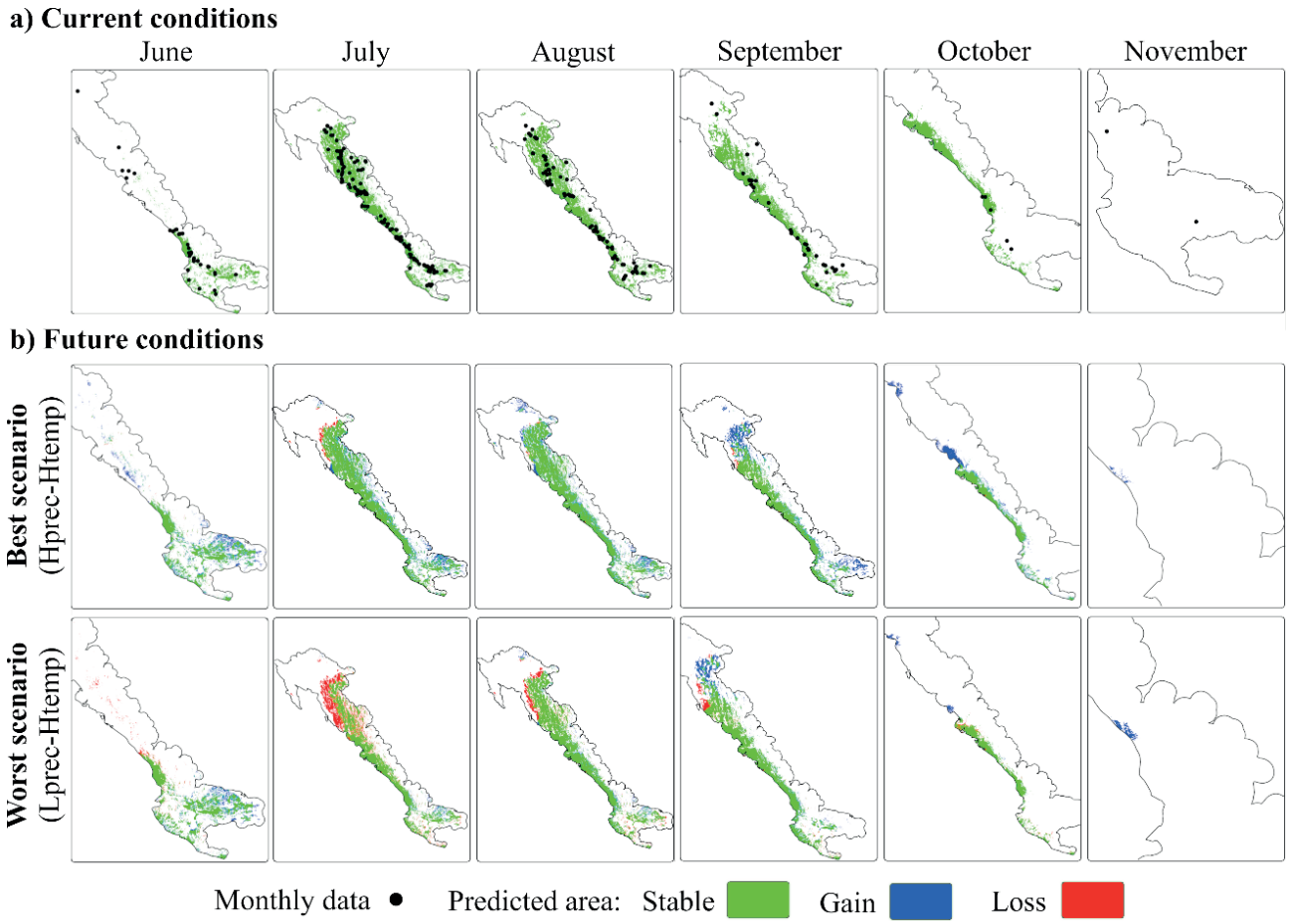

Fig. 3. Spatio-temporal variation of optimal conditions for *Smilisca fodiens* activity in the current (a) and future (b) climates. In the current condition, we found prediction (green shading) from June to October along the accessibility area (solid black line), and present data for each month were overlaid to assess geographic correspondence (black dots). In the future predictions, we found optimal conditions from June to November. Differences between the best scenario and the worst one was notably regarding gain (blue shading), stability (green shading) and loss (red shading) areas.

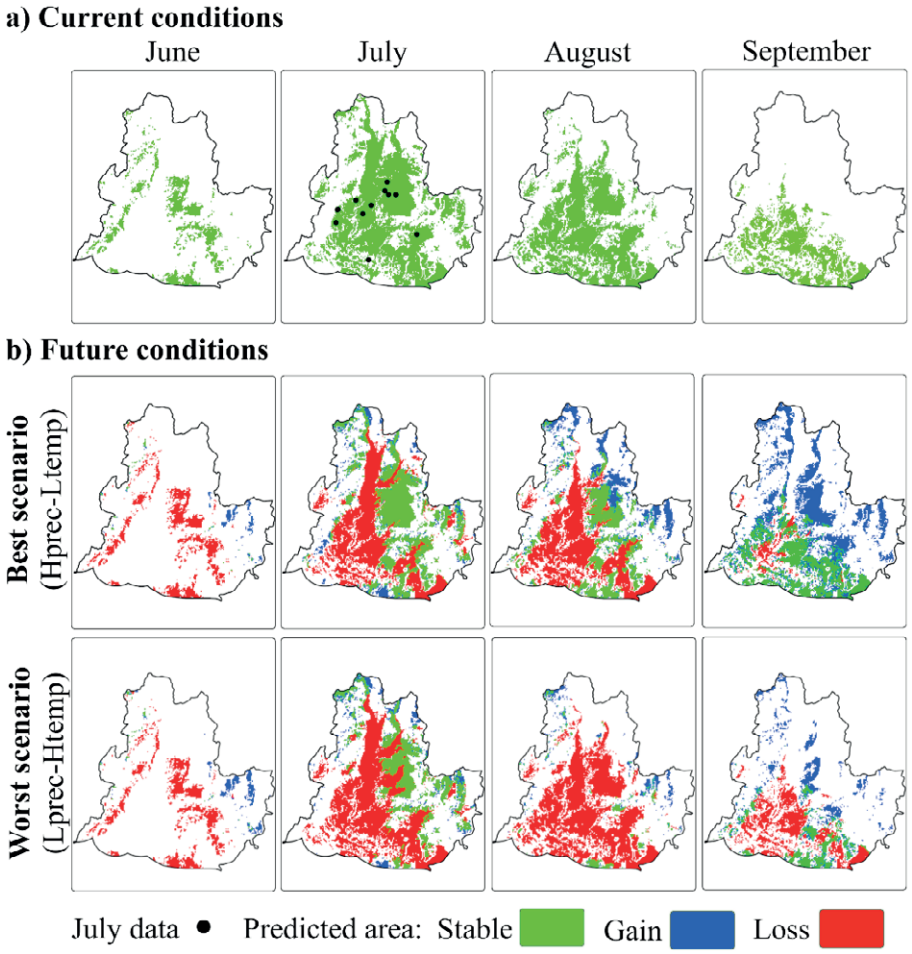

Fig. 4. Spatio-temporal variation of optimal conditions for *Smilisca dentata* activity in the current (a) and future (b) climates. In the current condition, we found prediction (green shading) from June to September along the accessibility area (solid black line), and present data for July (black dots) were overlaid to assess geographic correspondence with the July prediction. Differences between the best scenario and the worst one was notably regarding gain (blue shading), stability (green shading) and loss (red shading) areas. However, loss areas are considerable in all months for both scenarios.

dicted area was lower than that predicted under current conditions in almost all months, except for September (Fig. 4b). However, we found differences in the amount of predicted area concerning the four storylines analyzed (Fig. 5). In *S. fodiens*, Hprec-Htemp has the largest predicted area in almost all the months, while Lprec-Htemp predicts the smallest area even compared to current conditions (Fig. 5a). In addition, Hprec-Htemp predicts the highest amount of stable and gained area and the least amount of lost area in all months. The Lprec-Htemp scenario predicts the smallest amount of stable and gained area and the larger amount of lost area (Fig. 6a). For *S. dentata*, Hprec-Ltemp has the largest predicted area, in contrast to both Hprec-Htemp and Lprec-Htemp which agree in lower prediction in the future (Fig. 5b). Hprec-Ltemp predicts the largest amount of stable and gained area; however, a large amount of loss is predicted from June to August in all scenarios (Fig. 6b). According to the degree of agreement between the results of the GCMs for each species, we found two general future trends, one of which we hereafter refer to as the best and the other as the worst. The best future for *S. fodiens* is represented by Hprec-Htemp, which predicts a future with higher precipitation and temperature, and for *S. dentata* is represented by the Hprec-Ltemp, which is a future with higher precipitation and lower temperature. The worst-case scenario for both species was represented by the Lprec-Htemp, which predicts lower precipitation and higher temperature.

Analysis of geographic attributes shows that for *S. fodiens*, variation in longitude does not provide meaningful information (data not shown). The configuration

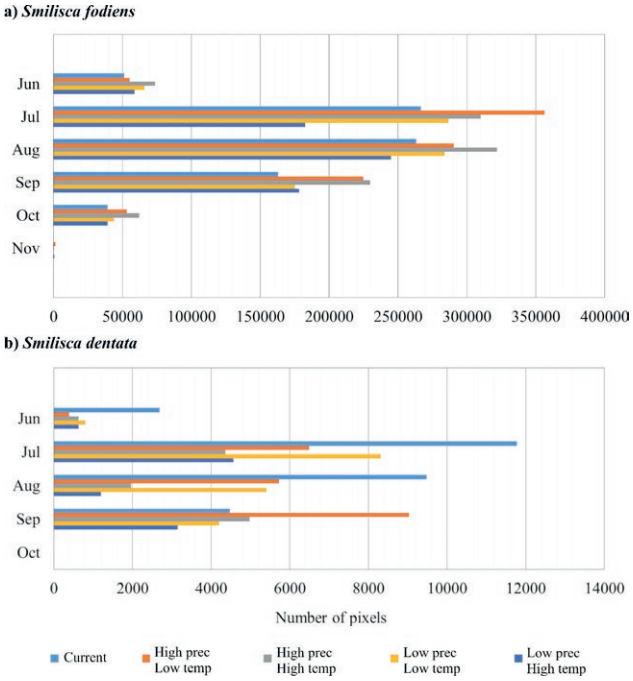

Fig. 5. Temporal variation of the predicted area in current and future conditions. The amount of area predicted in each month for *Smilisca fodiens* (a), and *S. dentata* (b) is plotted according to the number of pixels predicted with optimal conditions in current conditions (light blue bars) and in each of the four possible future scenarios for 2070 and 4.5 RCP: 1) High Prec – Low Temp (orange bars), 2) High Prec – High Temp (gray bars), 3) Low Prec – Low Temp (yellow bars) and, 4) Low Prec – High Temp (dark blue bars).

of the *M* range, given by the distribution of presence data, has a narrow longitudinal range, in contrast to the wide ranges in elevation and latitude. Regarding elevation, there is a variation from the slight slopes of the Mexican Pacific Coast ecoregion to the pronounced elevations of the Sierra Madre Occidental (Fig. 1). Therefore, we only present the results of the latitudinal (Fig. 7a) and elevational (Fig. 7b) analyses for this species. In the best-case scenario (Hprec-Htemp), the area gain of most months corresponds to the distribution of the July presence data in latitude but not in elevation. Except for October, the area gain of all the months is towards higher values of the median of the July presence data. In the worst-case scenario (Lprec-Htemp), the area gain in latitude corresponds only in August, and the elevation shows the same trend as in the best case. In the best-case scenario, the area predicted to be stable in the future corresponds in latitude to the July presence data only in September and October. In elevation, it corresponds only in July and August. In the worst-case scenario, we also found a latitudinal correspondence in July but the same trend in elevation as in the best-case scenario. Regarding the area lost in both scenarios, we found a lower correspondence with the latitudinal range of the July presence data, and only the median of the area lost in October is similar. In comparison, we found a higher correspondence of the range of lost area concerning the elevation values of the July presence data, but only in June, and in the worst-case scenario for September, we found similar medians.

The geographic analysis for *Smilisca dentata* was performed considering latitude (Fig. 8a), elevation (Fig. 8b), and longitude (Fig. 8c). In contrast to *S. fodiens*, the predictions for *S. dentata* extend along a longitudinal axis due to its habitat spanning the plains of the Central Plateau of Mexico, without significant topographic limitations such as the Pacific Ocean to the west and the Sierra Madre Occidental to the east in the case of *S. fodiens*. For the best-case scenario (Hprec-Ltemp), the gain areas correspond to the latitudinal range and the median of the July presence data in all the months with predicted distribution, except for August, in which the distribution of the gain area goes towards higher latitudes. Conversely, the gain area is much higher than the July presence data in all predicted months. Moreover, we do not find longitudinal correspondence between the area predicted as gain and the July presence data, except for the July transfer. This trend observed for the gain area is similar to that observed in the worst-case scenario (Lprec-Htemp). A difference is observed in June, where the gain areas occur at higher latitudes, moving away from the similarity with the July presence data and the loss of correspondence with the longitudinal range in all months. In the best-case scenario, the areas predicted to be stable in July and August correspond to the latitudinal range of the July presence data but, in any case, to the elevational range since, in most months, the stable areas tend to be at higher elevations. In longitude, the stable areas predicted in June and September coincide with the range described by the July presence data. The difference in the worst-case scenario is that the stable area predicted in July is the only one that coincides with the latitudinal range of the July presence data and that in September, the stable areas predicted coincide in elevation and longitude with the July presence data. Finally, in the best scenario, the area predicted as loss in all months has no latitudinal correspondence with July presence data concerning elevation; only in June, we observed correspondence, and contrary to from July to September, the correspondence of lost area was found in longitude. The same pattern was found in the worst-case scenario for latitude and longitude, but we found similar medians in all months concerning the July presence data for the elevation.

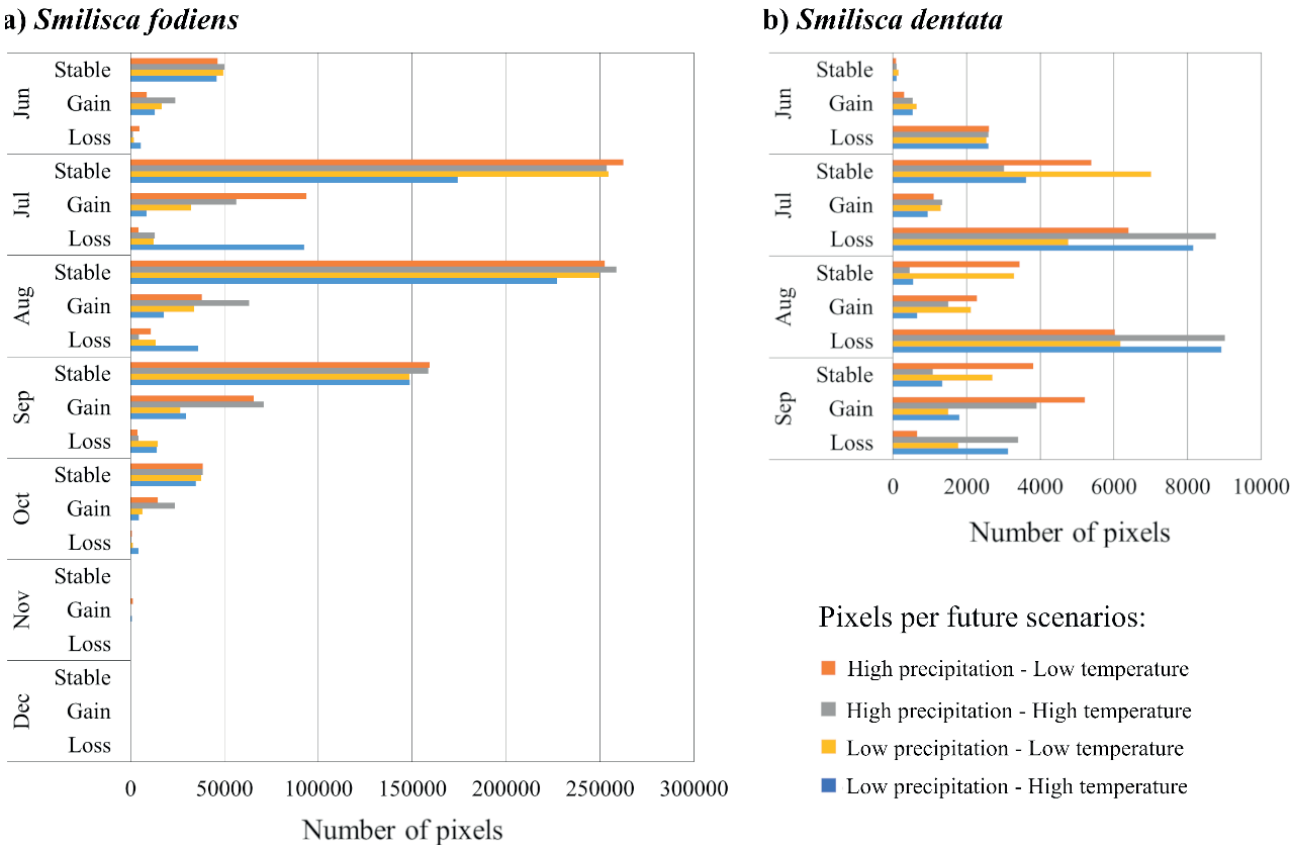

Fig. 6. Temporal variation of the predicted amount of area according to the degree of climate change impact. For *Smilisca fodiens* (a) and *S. dentata* (b) we identify three types of impacts concerning current predictions: the area that could be gained, either kept stable or contrary or worryingly lost in the future. The number of pixels for each type of area is plotted for each of the four possible future scenarios for 2070 and 4.5 RCP: 1) High Prec – Low Temp (orange bars), 2) High Prec – High Temp (gray bars), 3) Low Prec – Low Temp (yellow bars) and, 4) Low Prec – High Temp (dark blue bars).

DISCUSSION

The pattern of space-time variation of *Smilisca fodiens* under current conditions is similar to that found in Encarnación-Luévano et al. (2013). The spatial correspondence between predictions and the monthly activity data suggests a close relationship between climatic variation and temporal adjustment of activity outside burrows. For *S. dentata*, however, we could not identify a temporal pattern due to the lack of monthly presence data, although we did find a spatial variation between months. Although models generated with limited presence data may have low performance (Jimenez-Valverde, 2020), methodological adjustments and interpretation based on life history considerations can provide useful analyses for completing ecological hypotheses of rare and threatened species (Pearson et al., 2007; Breiner et al., 2015). However, expanding the temporary databases through fieldwork is crucial for enhancing correlative analyses of this kind of species.

The absence of prediction in the drier months of the year (i.e., February-April) toward the Sonoran Desert for *S. fodiens*, and in the Mexican Plateau for *S. dentata*, could be explained by the estivation period. However, in some of these regions, there are monthly historical records and evidence of activity on a fine scale; we call this "scale decoupling". Toward the center-south of the *S. fodiens* distribution, the monthly predictions for June, October, and November do not agree with the respective monthly presence data nor with the activity reported in the dry season in the region of Chamela, south of the species distribution (i.e., November to June; Soto-Sandoval et al., 2017). On the other hand, we found no predictions for *S. dentata* after September; however, active individuals were reported in October and November, although these were few and primarily juveniles (G.E. Quintero-Díaz, pers. comm.). The record of the activity of individuals throughout the year corresponds to a normal distribution in terms of abundance, with the opti-

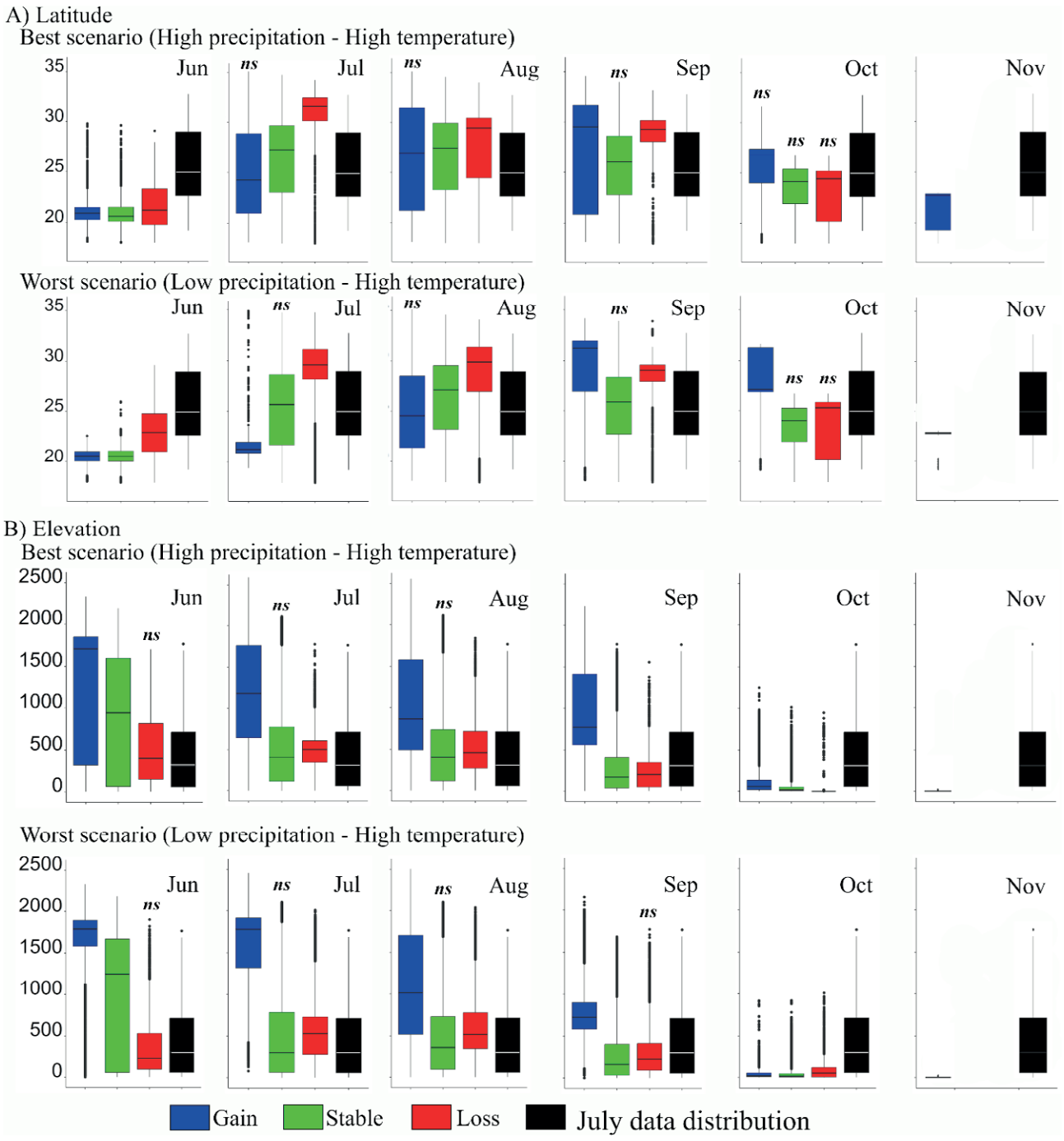

Fig. 7. Geographic correspondence of predicted areas such as gain, stability, and loss compared to the areas reached by *Smilisca fodiens* July presence data. We evaluate the latitudinal (a) and elevation (b) distributional change in both the best scenario (High Prec – High Temp) and the worst scenario (Low Prec – High Temp). We plot the variance of the data for each variable for each type of impact: gain (blue bars), stable (green bars), and loss (red bars). We indicate the impact type whose median is not significantly different from the median of the July presence data. Statistically significant differences were considered at $P \leq 0.05$.

mum coinciding with the intensive rainy period associated with reproduction. The presence of individuals outside this period is not rare and, on the contrary, is evidence of gradual inactivity due to the gradual loss of suitable conditions throughout the year. Field studies indicate that the most active individuals outside burrows occur in an

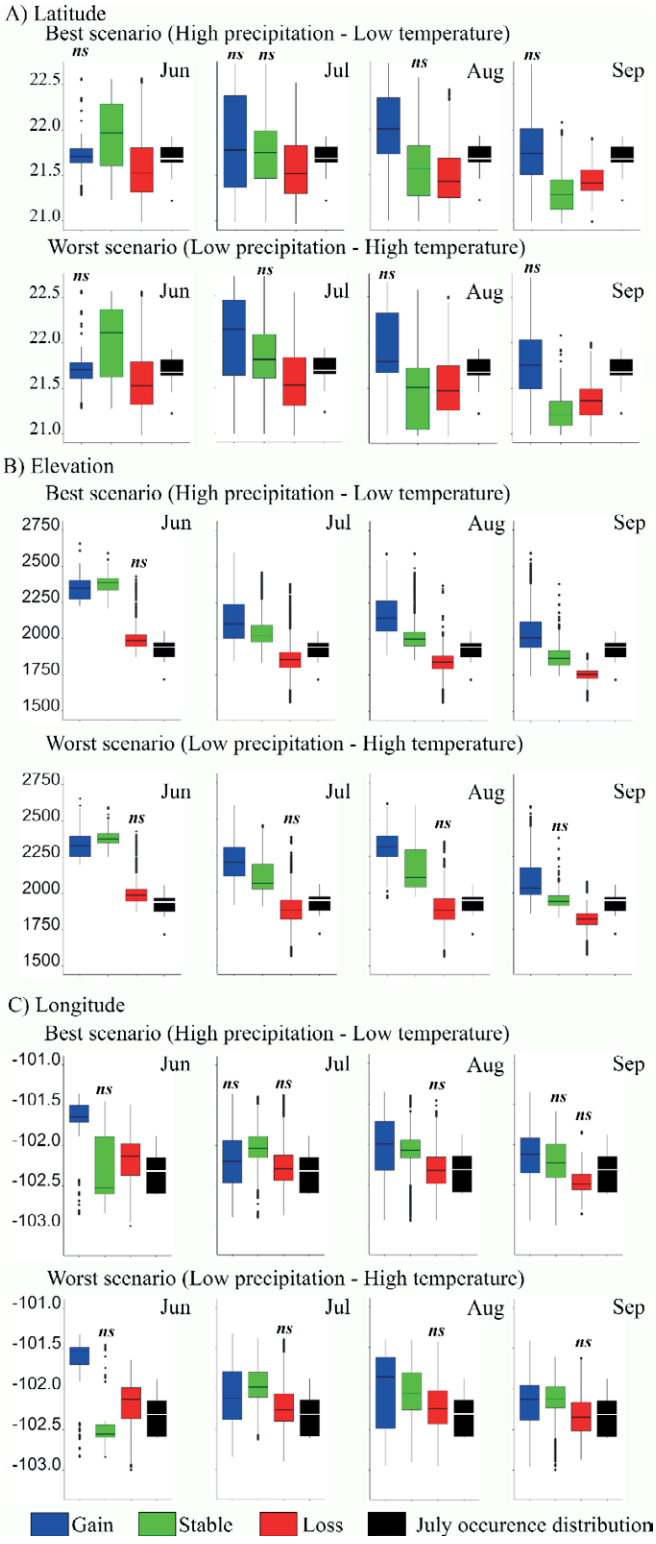

Fig. 8. Geographic correspondence of predicted areas such as gain, stability, and loss compared to the areas reached by *Smilisca dentata* July presence data. We evaluate the latitudinal (a), elevation (b), and (c) longitudinal distributional change in both the best scenario (High Prec – High Temp) and the worst scenario (Low Prec – High Temp). We plot the variance of the data for each variable for each type of impact: gain (blue bars), stable (green bars), and loss (red bars). We indicate the impact type whose median is not significantly different from the median of the July presence data. Statistically significant differences were considered at $P \leq 0.05$.

average temperature range of 20-23 °C; at higher values, the abundance decreases significantly (G.E. Quintero-Díaz, pers. comm.). The "scale decoupling" has also been observed in studies of hibernating species exhibiting spatiotemporal activity variation. For example, in black bears, some populations at the southern tip of the distribution occasionally exhibit atypical activity in winter (Gámez-Brunswick and Rojas-Soto, 2020).

In the transfers to future scenarios, we found that high precipitation values favor the best-case scenario for both species. Precipitation is the limiting variable for *S. fodiens*, because its low values determine the worst scenarios; conversely, for *S. dentata*, high-temperature values predict the worst scenarios for its activity. In the best-case scenario, *S. fodiens* could find optimal conditions for reproduction in a longer period than under current conditions due to stable or gain areas, especially in the northern and southern limits of its distribution. Furthermore, significant gain areas are observed from June towards the southern limit of its distribution. Given this, reproduction could be feasible because of the phenology of the species, where males present spermatogenesis from June to August and females are physiologically prepared for spawning from June to September (Goldberg, 2019). On the other hand, the worst-case scenario could pose a greater challenge for northern populations. This is due to the loss of favorable conditions in July, which could result in lower or no activity in these populations. It is important to note that this scenario may also alter their temporal activity pattern. The Pima and Vekoy Valley populations in Arizona have historically recorded a couple of reproductive events during this month, both associated with heavy rains (Sullivan et al., 1996). It also seems possible that low deciduous forest populations, particularly those in the southern part of the range, will be the least susceptible because reproductive conditions persist for a longer period, from June to September (Duellman, 2001).

Of the two species, *S. dentata* may face more challenging future conditions, even in the best-case scenarios. However, in the latter scenario, we identified a more favorable situation for a group of historical records located in the northeastern part of the known distribution and a less favorable situation for the remaining localities. In the northeast, suitable conditions could remain in July and appear in regions with potential habitat, natural grassland, in August and September (Quintero-Díaz and Vázquez-Díaz, 2009). The worst-case scenario would be devastating for all populations known for the species. Only in September we found small portions of stable and gained areas, but there is no evidence of the presence of this species in those areas.

We must take with caution the areas presented as gains but with no records of populations, especially above historical elevations for both species (*S. dentata*, 2050 m a.s.l., Quintero-Díaz and Vázquez-Díaz, 2009; *S. fodiens*, 1500 m a.s.l., Duellman, 2001). Reaching these elevation limits has substantial adaptive implications, e.g., morphological to move into these areas or competitive to settle there, despite species already established in the community. Displacement of migrant species in search of suitable conditions due to seasonal climatic changes has been reported (Martínez-Meyer et al., 2004; Nakazawa et al., 2004; Gámez-Brunswick and Rojas-Soto, 2020). However, migratory movements and colonization of new areas are limited in amphibians, mainly because of their highly moisture-dependent physiology and high fidelity to home sites and refugia (Smith and Green, 2005; altitudinal limits, Bachmann and Van Busckirk, 2021).

In the case of *S. dentata*, distribution is further restricted by its narrow habitat requirements and degree of vulnerability. This species inhabits temporary floodplains with natural grasslands and thorny scrub with soft, floodable soils that provide water for 4 - 6 months and burrows construction (Quintero-Díaz et al., 2008; Quintero-Díaz and Vázquez-Díaz, 2009). Unfortunately, this habitat is favored for human settlements and agricultural activities (de la Cerda, 2008). The high sensitivity of some populations to conversion zones has already been shown to be the greatest threat to the species (Quintero-Díaz and Vázquez-Díaz, 2009; IUCN SSC Amphibian Specialist Group 2020).

Our results also highlight the importance of temperature over reproductive activity. Population studies of temperate burrowing frogs find a greater correlation between the temperature and burrow emergence than with reproductive activity (e.g., *Bufo bufo*, Reading, 2003; *Anaxyrus fowleri*, Green et al., 2016). We found that the worst-case scenario for *S. dentata* is one of higher temperatures, consistent with the fine-scale data. Over a long period of fieldwork, it has been observed that the upper limit of the average temperature at which individuals can be found is 25 °C (G.E. Quintero-Díaz, pers. comm.). Individuals avoid the higher temperatures by being active at night (Quintero-Díaz and Vázquez-Díaz, 2009) or sporadically during the day on cloudy and rainy days (Encarnación-Luévano and Quintero-Díaz, In Press).

The northern populations of *S. fodiens* could be affected by the combination of high temperatures and low precipitation. Historically, temperature variability has been higher in the Sonoran Desert and northern portions of the Pacific Coast deciduous forest (Jaramillo et al., 2010). We believe behavioral adaptation may be closely linked to temperature in north populations of *S. fodiens*,

and in all populations of *S. dentata*. This burrowing habit allows them to cope with extreme climates (i.e., elevated temperatures) without compromising their range of phylogenetically conserved thermal tolerances (Encarnación-Luévano et al., 2021).

On the other hand, the burrowing behavior allows some individuals to descend to depths of more than a meter deep in search of constant environmental values (e.g., *Anaxyrus hemiophrys*, Breckenridge and Tester, 1961). However, behavioral adjustments may not be as rapid as climate change (Bodensteiner et al., 2021). Vulnerability to environmental change depends on the plasticity of each group or species (Chadwick et al., 2006), so the adaptive capacity to climate change of two species inhabiting the same arid region may not be the same (Esparza-Orozco et al., 2020). For example, climate change has been documented recently (≈1900), affecting the hydroperiod of ephemeral ponds and, thus, the reproductive success of amphibian species (Chandler et al., 2016). Early breeding has been observed in anurans due to rising temperatures (Reading, 2003; Todd et al., 2011). However, the reproductive period appears to depend more on geographic region and, thus, climatic stability (Green et al., 2016). It will be necessary to conduct studies to assess burrowing frogs' potential responses to future climate challenges.

Our study highlights the importance of the geographic and temporal patterns for seasonal species whose activity is determined by specific climate ranges. Vulnerability and decline of species with restricted niches are real (Clavel et al., 2011). The causes are multifactorial, but those directly or indirectly related to climate change are among the most important (Habibullah et al., 2021). Activity patterns of burrowing species are a useful measure of behavior under current climate conditions, but these patterns open the possibility of understanding the potential effects of future climate change. In particular, these groups have evolved in response to seasonal climates, making them more vulnerable to minor variations in the face of climate change.

ACKNOWLEDGMENTS

The authors express gratitude to the collections and institutions that provided presence data through the VertNet and GBIF portals. The authors also thank Danilo Borgatti and two anonymous reviewers for their valuable suggestions on the manuscript. It is declared that no animals were manipulated or disturbed during this work. The Universidad Autónoma de Aguascalientes and the Instituto de Ecología, A.C. provided institutional support, for which the authors are grateful. Additionally, the first author received a fellowship from CONACyT (No. 373460/246885).

REFERENCES

Bachmann, J.C., Van Buskirk, J. (2021): Adaptation to elevation but limited local adaptation in an amphibians. Evolution **75**: 956-969.

Barve, N., Barve, V., Jiménez-Valverde, A., Lira-Noriega, A., Maher, S.P., Peterson, A.T., Villalobos, F. (2011): The crucial role of the accessible area in ecological niche modeling and species distribution modeling. Ecol. Modell. **222**: 1810-1819.

Bellard, C., Bertelsmeier, C., Leadley, P., Thuiller, W., Courchamp, F. (2012): Impacts of climate change on the future of biodiversity. Ecol. Lett. **15**: 365-377.

Bodensteiner, B.L., Agudelo-Cantero, G.A., Arietta, A.Z.A., Gunderson, A.R., Muñoz, M.M., Refsnider, J.M., Gangloff, E.J. (2021): Thermal adaptation revisited: How conserved are thermal traits of reptiles and amphibians? J. Exp. Zool. **335**: 173-194.

Breckenridge, W.J., Tester, J.R. (1961): Growth, local movements and hibernation of the Manitoba toad, *Bufo hemiophrys*. Ecology **42**: 637-646.

Breiner, F.T., Guisan, A., Bergamini, A., Nobis, M.P. (2015): Overcoming limitations of modelling rare species by using ensembles of small models. Methods Ecol. Evol. **6**: 1210-1218.

Clavel, J., Julliard, R., Devictor, V. (2011): Worldwide decline of specialist species: toward a global functional homogenization? Front. Ecol. Environ. **9**: 222-228.

Chadwick, E.A., Slater, F.M., Ormerod, S.J. (2006): Inter- and intraspecific differences in climatically mediated phenological change in coexisting *Triturus* species. Global Chang. Biol. **12**: 1069-1078.

Chandler, H.C., Rypel, A.L., Jiao, Y., Haas, C.A., Gorman, T.A. (2016): Hindcasting historical breeding conditions for an endangered salamander in ephemeral wetlands of the southeastern USA: implications of climate change. PLoS ONE. **11**: e0150169.

Cobos, M.E., Peterson, A.T., Barve, N., Osorio-Olvera, L. (2019): kuenm: an R package for detailed development of ecological niche models using Maxent. PeerJ **7**: e6281.

Cohen, J., Jetz, W. (2023): Diverse strategies for tracking seasonal environmental niches at hemispheric scale. Global Ecol. Biogeog. **32**: 1549-1560.

Dawson, T.P., Jackson, S.T., House, I.J., Prentice, I.C., Mace, G.M. (2011): Beyond Forecasts: Conserving Biodiversity Under Climate Change. Science **332**: 53-58.

de la Cerda, L.M. (2008): Pastizal. In: La Biodiversidad en Aguascalientes: Estudio de Estado, pp. 92-97. Ávila, H., Melgarejo, E.D., Cruz, A., Eds, CONABIO, IMAE, UAA.

De Mendiburu, F. (2023): agricolae: Statistical procedures for agricultural research. R package version 1.2-6. https://CRAN.R-project.org/package=agricolae.

Duellman, W.E. (2001): The Hylid Frogs of Middle America. Society for the Study of Amphibians and Reptiles Press, Kansas.

Encarnación-Luévano, A., Quintero-Díaz, G.E. (In Press): Contribution to the ecology and natural history of the upland burrowing treefrog *Smilisca dentata*. J. Herpetol.

Encarnación-Luévano, A., Peterson, A.T., Rojas-Soto, O.R. (2021): Burrowing habit in *Smilisca* frogs as an adaptive response to ecological niche constraints in seasonally dry environments. Front. Biogeogr. **13**: e50517.

Encarnación-Luévano, A., Rojas-Soto, O.R., Sigala-Rodríguez, J.J. (2013): Activity response to climate seasonality in species with fossorial habits: a niche modeling approach using the Lowland Burrowing Treefrog (*Smilisca fodiens*). PLoS ONE. **8**: 1-7.

Esparza-Orozco, A., Lira-Noriega, A., Martínez-Montoya, J.F., Pineda-Martínez, L.F., Méndez-Gallegos, S.J. (2020): Influences of environmental heterogeneity on amphibian composition at breeding sites in a semiarid region of Mexico. J. Arid Enviro. **182**: 104259.

ESRI 2019. ArcGIS Desktop: Release 10.8. Redlands, CA: Environmental Systems Research Institute.

Fajardo, J., Corcoran, D., Roehrdanz, P.R., Hannah, L., Marquet, P.A. (2020): GCM compareR: A web application to assess differences and assist in the selection of general circulation models for climate change research. Methods Ecol. Evol. **11**: 656-663.

Farooqi, T.J., Irfan, M., Protela, R., Zhou, X., Shulin, P., Ali, A. (2022): Global progress in climate change and biodiversity conservation research. Glob. Ecol. Conserv. **38**: e02272.

Gámez-Brunswick, C., Rojas-Soto, O. (2020): The effect of seasonal variation in the activity patterns of the American Black Bear: an ecological niche modelling approach. Mammalia **84**: 315-322.

Goldberg, S.R. (2019): Notes on Reproduction of Lowland Burrowing Treefrogs, *Smilisca fodiens* (Anura: Hylidae), from Sinaloa and Sonora, Mexico. Bull. Chic. Herpetol. Soc. **54**: 83-84.

Green, T., Das, E., Green, D.M. (2016): Springtime Emergence of Overwintering Toads, *Anaxyrus fowleri*, in Relation to Environmental Factors. Copeia. **104**: 393-401.

Guevara, L., Gerstner, B.E., Kass, J.M., Anderson, R.P. (2017): Toward ecologically realistic predictions of species distributions: A cross-time example from tropical montane cloud forests. Glob. Chang. Biol. **24**: 1511-1522.

Habibullah, M.S., Din, B.H., Tan, S.H., Zahid, H. (2021): Impact of climate change on biodiversity loss: global evidence. Environ. Sci. Pollut. Res. **29**: 1073–1086.

Höök, M., Sivertsson, A., Aleklett, K. (2010): Validity of the Fossil Fuel Production Outlooks in the IPCC Emission Scenarios. Nat. Resour. Res. **19**: 63-81.

IPCC (2014): Climate Change 2014: Synthesis Report. Contribution of Working Groups I, II and III to the Fifth Assessment Report of the Intergovernmental Panel on Climate Change. Core Writing Team, Pachauri, R.K., Meyer, L.A. Eds, IPCC, Geneva, Switzerland.

Jaramillo, V.J., García-Oliva, F., Martínez-Yrízar, A. (2010): La selva seca y el disturbio antrópico en un contexto funcional. In: Diversidad, amenazas y áreas prioritarias para la conservación de las selvas secas del Pacífico de México, pp. 235-250. Ceballos, G., Martínez, L., García, A., Espinoza, E., Bezaury-Creel, Dirzo, R., Eds, Fondo de Cultura Económica and CONABIO.

Jimenez-Valverde, A. (2020): Sample size for the evaluation of presence-absence models. Ecol. Indic. **114**: 106289. https://doi.org/10.1016/j.ecolind.2020.106289

Karger, D.N., Conrad, O., Böhner, J., Kawohl, T., Kreft, H., Soria-Auza, R.W., Zimmermann, N.E., Linder, P., Kessler, M. (2017): Climatologies at high resolution for the Earth land surface areas. Sci. Data **4**: 170122.

Martínez-Meyer, E., Peterson, A.T., Navarro-Sigüenza, A. (2004): Evolution of seasonal ecological niches in the *Passerina* buntings (Aves: Cardinalidae). Proc. Royal Soc. B **271**: 1151-1157.

Nakazawa, Y., Peterson, A.T., Martínez-Meyer, E., Navarro-Sigüenza, A. (2004): Seasonal Niches of Nearctic-Neotropical Migratory Birds: Implications for the Evolution of Migration. The Auk. **121**: 610-618.

Navas, C.A., Gomes, F.R., Carvalho, J.E. (2008): Thermal relationships and exercise physiology in anuran amphibians: Integration and evolutionary implications. Comp. Biochem. Physiol. Part A Mol. Integr. Physiol. **151**: 344-362.

Olson, D.M., Dinerstein, E., Wikramanayake, E.D., Burgess, N.D., Powell, G.V.N., Underwood, E.C., D'amico, J.A., Itoua, I., Strand, H.E., Morrison, J.C., Loucks, C.J., Allnutt, T.F., Ricketts, T.H., Kura, Y., Lamoreux, J.F., Wettengel, W.W., Hedao, P., Kassem, K. (2001): Terrestrial ecoregions of the world: a new map of life on Earth. BioScience **51**: 933-938.

Owens, H.L., Campbell, L.P., Dornak, L.L., Saupe, E.E., Barve, N., Soberón, J., Ingenloff, K., Lira-Noriega, A., Hensz, C.M., Myers, C.E., Peterson, A.T. (2013): Constraints on interpretation of ecological niche models by limited environmental ranges on calibration areas. Ecol. Modell. **263**: 10-18.

Pacifici, M., Visconti, P., Butchart, S., Watson, J.E.M., Cassola, F.M., Rondinini, C. (2017): Species' traits influenced their response to recent climate change. Nat. Clim. Change **7**: 205-208.

Parra, J.L., Graham, C.C., Freile, J.F. (2004): Evaluating alternative data sets for ecological niche models of birds in the Andes. Ecography **27**: 350-360.

Pearson, R.G., Raxworthy, C.J., Nakamura, M., Peterson, A.T. (2007): Predicting species distributions from small numbers of occurrence records: a test case using cryptic geckos in Madagascar. J. Biogeogr. **34**: 102-117.

Peterson, A.T., Ortega-Huerta, M.A., Bartley, J., Sánchez-Cordero, V., Soberón, J., Buddemeier, R.H., Stockwell, D.R.B. (2002): Future projections for Mexican faunas under global climate change scenarios. Nature **416**: 626-629.

Peterson, A.T., Papeş, M., Soberón, J. (2008): Rethinking receiver operating characteristic analysis applications in ecological niche modeling. Ecol. Modell. **213**: 63-72.

Phillips, S.J., Anderson, R.P., Schapire, R.E. (2006): Maximum entropy modeling of species geographic distributions. Ecol. Modell. **190**: 231-259.

Quintero-Díaz, G.E., Vázquez-Díaz, J. (2009): Historia Natural de una Rana muy Mexicana. Municipio de Aguascalientes, SHM, Biodiversidad AC, SEMARNAT, Aguascalientes.

R Core Team. (2020): R: A language and environment for statistical computing. R Foundation for Statistical Computing, Vienna, Austria.

Reading, C.J. (2003): The effects of variation in climatic temperature (1980–2001) on breeding activity and tadpole stage duration in the common toad, *Bufo bufo*. Sci. Total Environ. **310**: 231-236.

Rojas-Soto, O., Baldo, D., Lescano, J., Encarnación-Luévano, A., Leynaud, G., Nori, J. (2021): Seasonal Dissociation in Fossorial Activity between the Llanos' Frog Populations as a Survival Strategy in Arid Subtropical Environments. J. Herpetol. **55**: 442-451.

Ruibal, R., Hillman, S. (1981); Cocoon structure and function in the burrowing hylid frog, *Pternohyla fodiens*. J. Herpetol. **15**: 403-40.

Scheffers, B.R., Edwards, D.P., Diesmos, A., Williams, S.E., Evans, T.A. (2014): Microhabitats reduce animal's exposure to climate extremes. Glob Chang Biol. **20**: 495-503.

Shcheglovitova, M., Anderson, R.P. (2013): Estimating optimal complexity for ecological niche models: A jackknife approach for species with small sample sizes. Ecol. Modell. **269**: 9-17.

Sierra-Morales, P., Rojas-Soto, O., Ríos-Muñoz, C.A., Ochoa-Ochoa, L.M., Flores-Rodríguez, P., Almazán-Núñez, R.C. (2021): Climate change projections suggest severe decreases in the geographic ranges of bird species restricted to Mexican humid mountain forests. Glob. Ecol. Conserv. **30**: e01794.

Smith, M.A., Green, D.M. (2005): Dispersal and the metapopulation paradigm in amphibian ecology and conservation: are all amphibian populations metapopulations? Ecography **28**: 110-128.

Soberon, J., Peterson, A.T. (2005): Interpretation of Models of Fundamental Ecological Niches and Species' Distributional Areas. Biodivers. Inform. **2**: 1-10.

Soto-Sandoval, Y., Suazo-Ortuño, I., Urbina-Cardona, N., Marroquín-Páramo, J., Alvarado-Díaz, J. (2017): Efecto de los estadios sucesionales del bosque tropical seco sobre el microhabitat usado por *Agalychnis dacnicolor* (Anura: Phyllomedusidae) y *Smilisca fodiens* (Anura: Hylidae). Rev. Biol. Trop. **65**: 777-798.

Sullivan, B.K., Bowker, R.W., Malmos, K.B., Gergus, E.W.A. (1996): Arizona distribution of three Sonoran Desert anurans: *Bufo retiformis*, *Gastrophryne olivacea*, and *Pternohyla fodiens*. Great Basin Nat. **56**: 38-47.

Thomas, C.D., Cameron, A., Green, R.E., Bakkenes, M., Beaumont, L.J., Collingham, Y.C., Erasmus, B.F.N., Siqueira, M.F., Grainger, A., Hannah, L., Hughes, L., Huntley, B., van Jaarsveld, A.S., Midgley, G.F., Miles, L., Ortega-Huerta, M.A., Peterson, A.T., Phillips, O.L., Williams, S.E. (2004): Extinction risk from climate change. Nature **427**: 145-148.

Todd, B.D., Scott, D.E., Pechmann, J.H., Gibbons, J.W. (2011): Climate change correlates with rapid delays and advancements in reproductive timing in an amphibian community. Proc. Royal Soc. B. **278**: 2191-2197.

van-Vuuren, D.P., den-Elzen, M.G.J., Lucas, P.L., Eickhout, B., Strengers, B.J., van Ruijven, B., Wonink, S., van Houdt, R. (2007): Stabilizing greenhouse gas concentrations at low levels: an assessment of reduction strategies and costs. Clim. Change **81**: 119-159.

Weatherhead, P.J., Sperry, J.H., Carfagno, G.L.F., Blouin-Demers, G. (2012): Latitudinal variation in thermal ecology of North American ratsnakes and its implications for the effect of climate warming on snakes. J. Therm. Biol. **37**: 273-281.

Wickham, H. (2016): ggplot2: Elegant graphics or data analysis. Springer-Verlag, New York.

Acta Herpetologica 19(2): 155-159, 2024
DOI: 10.36253/a_h-16840

Invited Review

Uncertain future and uncertain projections: assessing extinction risks in European salamanders from projected chytrid fungus invasion using IUCN Criterion E

Stefano Canessa[1,2], Dino Biancolini[3], Mattia Iannella[4], Ilaria Bernabò[5], Daniele Salvi[4], Leonardo Vignoli[6], Enrico Lunghi[4], Andrea Costa[7], Edoardo Razzetti[8], Gentile Francesco Ficetola[1], Antonio Romano[3,*]

[1] *Dipartimento di Scienze e Politiche Ambientali, Università degli Studi di Milano, Via Celoria 10, 20133 Milano, Italy*
[2] *Institute for Ecology and Evolution, University of Bern, Baltzerstrasse 6, CH-3012 Bern, Switzerland*
[3] *Istituto per la Bioeconomia (IBE), Consiglio Nazionale delle Ricerche (CNR), Via dei Taurini 19, I- 00185, Roma, Italy*
[4] *Dipartimento di Medicina Clinica, Sanità Pubblica, Scienze della Vita e dell'Ambiente (MeSVA), Università degli Studi dell'Aquila, Via Vetoio snc, 67100, L'Aquila, Italy*
[5] *Dipartimento di Biologia, Ecologia e Scienze della Terra (DiBEST), Università della Calabria, Via P. Bucci 4/B, I-87036, Rende (CS), Italy*
[6] *Dipartimento di Scienze, Università degli Studi Roma Tre, Viale Guglielmo Marconi 446, 00146 Roma, Italy*
[7] *Dipartimento di Scienze della Terra, dell'Ambiente e della Vita (DISTAV), Università degli Studi di Genova, Corso Europa 26, 16132, Genova, Italy*
[8] *Museo di Storia Naturale, Università degli Studi di Pavia, Piazza Botta 9/10, 27100 Pavia, Italy*
**Corresponding author.* Email: antonio.romano@cnr.it; antonioromano71@gmail.com

Submitted on: 2024, 20th November; revised on: 2024, 23rd November; accepted on: 2024, 26th November
Editor: Marco Mangiacotti

Abstract. Amphibians are among the most threatened vertebrates globally, and their conservation status continues to decline. In the updated Global Amphibian Assessment (GAA2), the use of IUCN Criterion E, which projects extinction risks through quantitative models, highlighted southern Europe as a hotspot for salamander extinction risk due to the risk of invasion by the fungal pathogen *Batrachochytrium salamandrivorans* (*Bsal*). In particular, for five Italian salamander species, risk categories were elevated significantly based on Criterion E, from Vulnerable or lower to Endangered or Critically Endangered. This increased reliance on Criterion E raises concerns regarding its treatment of uncertainty, as these projections depend heavily on assumptions about *Bsal* spread, environmental suitability, and host dynamics. Limited exploration of alternative scenarios and reliance on extreme parameter values may result in inflated extinction risk estimates. We emphasize the need for improved documentation of uncertainty and integration of diverse expert opinions in extinction risk assessments, to balance proactive conservation planning with robust scientific methodology.

Keywords. Chytridiomycosis, pathogen modeling, conservation priorities, *Batrachochytrium salamandrivorans,* environmental suitability, salamander disease.

SOUTHERN EUROPE: A HOTSPOT OF SALAMANDER STATUS DETERIORATION?

Amphibians are among the most threatened animals, and a recent updated assessment (Global Amphibian Assessment 2 [GAA2]; Luedtke et al., 2023) reports that their conservation status is worsening globally. However, this new evaluation also shows a shift in the criteria used for species assessments. The first global amphibian assessment (GAA1; Stuart et al., 2004) was exclusively based

ISSN 1827-9635 (print)
ISSN 1827-9643 (online)

on observed and inferred data on species declines, range, and abundance (IUCN Red List criteria A-D). Criterion E (projected extinction risk, for example from population viability analysis) has traditionally been less used because it requires high-quality data and is of more complex application (Collen et al., 2016). Consequently, no species had been listed under this criterion in the GAA1 (Stuart et al., 2004).

The GAA2 used Criterion E to determine the extinction risk of European salamanders, particularly in light of the threat posed by chytridiomycosis, a disease caused by the fungus *Batrachochytrium salamandrivorans* (*Bsal*). *Bsal* has been introduced and it is invasive in Europe and has been linked to the severe population declines of fire salamanders (*Salamandra salamandra*) in the Netherlands and Germany (Spitzen-van der Sluijs et al., 2016). Using a pathogen spread model developed by Akçakaya et al. (2023), and assuming that any salamander could be infected by *Bsal*, the GAA2 found that species from the Italian peninsula could face a significant or complete distributional overlap with the pathogen's spread area in the future. Consequently, for five of these species (Fig. 1), the application of Criterion E led to a substantial uplisting to higher extinction risk categories compared to previous assessments. In particular, *Speleomantes italicus*, *S. strinatii*, and *Salamandrina perspicillata*, with a projected

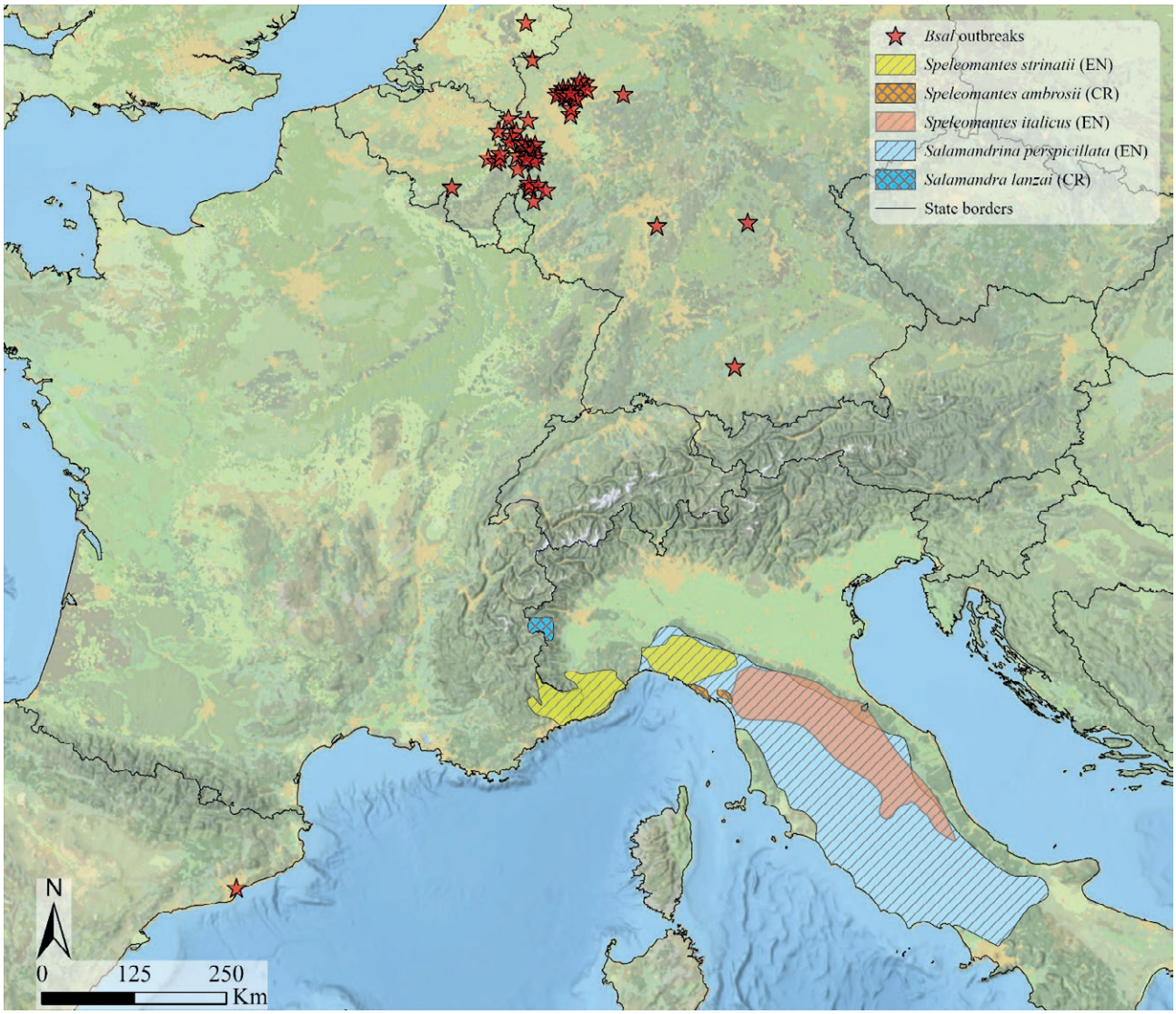

Fig. 1. IUCN ranges of Urodela species (IUCN, 2024) that changed conservation status (hatched pattern: reclassified as Endangered; double-hatched pattern: reclassified as Critically Endangered) and the distribution of *Bsal* outbreaks, as indicated by data from bsaleurope.com (accessed November 2024).

extinction probability of over 20% within the next five generations, have moved from the lowest risk category (Least Concern) to a high-risk category (Endangered). Similarly, *Speleomantes ambrosii* and *Salamandra lanzai*, with a projected population decline of more than 50% within the next three generations, were reclassified from Near Threatened and Vulnerable, respectively, to Critically Endangered. These new assessments of GAA2 conflict with the results of the recent IUCN assessment of Italian vertebrates (Rondinini et al., 2022) and with evidence suggesting stable trends for some of these species (e.g., Ficetola et al., 2018, 2024).

As a consequence of the GAA2 reclassification, Italy appears as one of the hottest spots of amphibian status deterioration globally; this evaluation is strongly linked to projected impacts by pathogens. Furthermore, for most amphibians threatened by *Bsal* (237 out of 240 species), the impacts of the pathogen are exclusively projected for the future (Luedtke et al., 2023). This increased reliance on Criterion E requires particular attention to assumptions and uncertainty, particularly if it contradicts evidence from other sources. We are concerned that, for these European salamander species, the treatment of uncertainty appears incomplete despite its substantial influence on projected extinction risks.

THE IMPORTANCE OF DOCUMENTING UNCERTAINTY IN ASSESSMENTS BASED ON CRITERION E

Extinction risk models project alternative trends of current phenomena, which can then be used to inform mitigation strategies against climate change, biological invasions, pathogen spread, and human development (IPBES, 2023). The IUCN Red List Criterion E seeks to harness this potential. However, alternative projection scenarios can radically differ depending on assumptions, methods, data types and quality (IPBES, 2023). Because projections require more assumptions than analysis of empirical data, they also suffer from greater linguistic, epistemic and stochastic uncertainty (Regan et al., 2002). Criterion E is thus fundamentally different from other Red List criteria, as recognized implicitly by its limited application to date (Cazalis et al., 2022) and more explicitly by the Red List Guidelines (IUCN, 2022), which clearly state that "uncertainty in the data or quantitative model must be documented". This means, for example, using ranges and distributions to represent uncertain parameters, and alternative scenarios or model structures to represent different assumptions, documenting the effect of uncertainty on projected extinction risks and justifying choices.

ISSUES IN THE APPLICATION OF CRITERION E TO EUROPEAN SALAMANDERS

In the GAA2, southern Europe emerges as a global hotspot for extinction risk, and Italy in particular, with five species of salamanders (Fig. 1) showing significant status deterioration based on quantitative projections of *Bsal* spread (Luedtke et al., 2023). When projecting the impacts of such a largely unknown threat in its early stages of invasion, optimistic and pessimistic scenarios should, at the very least, assess different patterns of pathogen spread, different levels of environmental suitability, and different host dynamics. For a recent invader like *Bsal*, these parameters are both highly influential and severely uncertain (Akçakaya et al., 2023). The GAA2 states that "uncertainty in the data [was] documented as a range of values" (Luedtke et al., 2023), but supplementary information and published IUCN entries do not reflect such evaluation of alternative scenarios for critical determining factors. Several key parameters are set at their extreme values, often relying on personal communications without formal expert elicitation and quantification of uncertainty.

For example, in the model used for the criterion E projections, environmental suitability for *Bsal* is implicitly assumed to be at its maximum possible value (100%) over the whole area reachable through its natural dispersal, whereas past research suggests that current and future environmental suitability for *Bsal* can vary significantly but is never perfect (Sun et al., 2023; Xie et al., 2016). *Bsal* dispersal is set as a chordal distance, ignoring host and pathogen ecology (Spitzen-van der Sluijs et al., 2018), plausible human-mediated dispersal (Martel et al., 2020), and barriers to hosts and the pathogen besides the Mediterranean Sea and mountains above 2500 m asl (Akçakaya et al., 2023). However, estimates of extinction risk are highly susceptible to even minimal changes in those parameters. Assuming a linear spread and disregarding environmental factors that might limit *Bsal* spread (thus assuming perfect environmental suitability across different types of European environments), the most vulnerable species are paradoxically located in areas where studies incorporating environmental suitability indicate very low levels of current and projected *Bsal* suitability (Sun et al., 2023; Katz et al., 2018; Beukema et al., 2021).

CONCLUSIONS

In the GAA2, in the case of European salamanders, criterion E was applied to risks by emerging invasive pathogens. However, in principle, this approach to the criterion E could also apply to other threats, such

as interactions with invasive species, climate change, and land-use change. The widespread use of modelling might lead to a more frequent use of this criterion, and accounting for uncertainty is crucial for any of these projected risks (Williams et al., 2021). In the face of rapid and dynamic global change, quantitative projections of imminent but not yet realized threats must play an increasing role in listing decisions.

For amphibians, the recognition in the GAA2 of the substantial threat posed by emerging diseases, even where they have not yet struck, is a step in the right direction. However, this increased application of model-based projections should be accompanied by a step up in adopting established best practices in the treatment of uncertainty (Sutherland and Burgman, 2015; Ladle, 2009). Unclear and overestimated projections of extinction risks can inflate conservation language, diverting attention from ongoing, ascertained threats to potential but uncertain ones, and deteriorating the crucial trust needed for promoting conservation actions (Ladle, 2009). Listing decisions undeniably influence the allocation of limited conservation resources for threatened species, critically affecting their future. Providing clear information about uncertainty, and integrating feedback from multiple local and global experts, should be a guiding principle of extinction risk assessments.

REFERENCES

Akçakaya, H.R., Neam, K., Hobin, L., Loetters, S., Martel, A., Pasmans, F. (2023): Assessing the extinction risks of amphibians impacted by infectious diseases. Biol. Conserv. **284**: 110205.

Beukema, W., Erens, J., Schulz, V., Stegen, G., Spitzen-van der Sluijs, A., Stark, T., Laudelout, A., Kinet, T., Kirschey, T., Poulain, M., Miaud, C., Steinfartz, S., Martel, A., Pasmans, F. (2021): Landscape epidemiology of *Batrachochytrium salamandrivorans*: reconciling data limitations and conservation urgency. Ecol. Appl. **31**: e02342.

Cazalis, V., Di Marco, M., Butchart, S. H. M., Akçakaya, H. R., González-Suárez, M., Meyer, C., Clausnitzer, V., Böhm, M., Zizka, A., Cardoso, P., Schipper, A. M., Bachman, S. P., Young, B. E., Hoffmann, M., Benítez-López, A., Lucas, P. M., Pettorelli, N., Patoine, G., Pacifici, M., Jörger-Hickfang, T., Brooks, T.M., Rondinini, C., Hill, S., Visconti, P., Santini, L. (2022): Bridging the research-implementation gap in IUCN Red List assessments. Trends Ecol. Evol. **37**: 359-370 (2022).

Collen, B., Dulvy, N.K., Gaston, K.J., Gärdenfors, U., Keith, D.A., Punt, A.E., Regan, H.M., Böhm, M., Hedges, S., Seddon, M., Butchart, S.H., Hilton-Taylor, C., Hoffmann, M., Bachman, S.P., Akçakaya, H.R. (2016): larifying misconceptions of extinction risk assessment with the IUCN Red List. Biol. Lett. **12:** 20150843.

Ficetola, G.F., Manenti, R., Barzaghi, B., Romagnoli, S., Lo Parrino, E., Melotto, A., Marta, S., Giachello, S., Balestra, V., Lana, E., Maiorano, L., Pennati, R., Lunghi, E., Falaschi, M. (2024): Integrating historical and recent data to measure long-term trends of endangered subterranean species. Biol. Conserv. **296**: 110695.

Ficetola, G.F., Barzaghi, B., Melotto, A., Muraro, M., Lunghi, E., Canedoli, C., Lo Parrino, E., Nanni, V., Silva-Rocha, I., Urso, A., Carretero, M.A., Salvi, D., Scali, S., Pennati, R., Andreone, F., Manenti, R. (2018): N-mixture models reliably estimate the abundance of small vertebrates. Sci. Rep. **8**: 10357.

Katz, T.S., Zellmer, A.J. (2018): Comparison of model selection technique performance in predicting the spread of newly invasive species: a case study with *Batrachochytrium salamandrivoran*s. Biol. Invasions **20:** 2107-2119.

IPBES (2023): Thematic Assessment Report on Invasive Alien Species and their Control of the Intergovernmental Science-Policy Platform on Biodiversity and Ecosystem Services (H. E. Roy, A. Pauchard, P. Stoett, T. Renard Truong, Eds.). IPBES Secretariat.

IUCN (2022): Standards and Petitions Committee. Guidelines for Using the IUCN Red List Categories and Criteria. Version 15.1. https://www.iucnredlist.org/documents/RedListGuidelines.pdf

IUCN (2024): The IUCN Red List of Threatened Species. Version 2024-1.

Ladle, R.J. (2009): Forecasting extinctions: uncertainties and limitations. Diversity **1**: 133-150.

Luedtke, J.A., Chanson, J., Neam, K., Hobin, L., Maciel, A. O., Catenazzi, A., et al. (2023): Ongoing declines for the world's amphibians in the face of emerging threats. Nature **622**: 308-314.

Martel, A. Vila-Escale, M., Fernández-Guiberteau, D., Martinez-Silvestre, A., Canessa, S., Van Praet, S., Pannon, P., Chiers, K., Ferran, A., Kelly, M., Picart, M., Piulats, D., Li, Z., Pagone, V., Pérez-Sorribes, L., Molina, C., Tarragó-Guarro, A., Velarde-Nieto, R., Carbonell., F., Obon, E., Martínez-Martínez, D., Guinart, D., Casanovas, R., Carranza, S., Pasmans, F. (2020): Integral chain management of wildlife diseases. Conserv. Lett. **13**: e12707.

Regan, H., Colyvan, M., Burgman, M. (2002): A taxonomy and treatment of uncertainty for ecology and conservation biology. Ecol. Appl. **12**: 618-628.

Rondinini, C., Battistoni, A., Teofili, C. (2022): Lista Rossa IUCN dei vertebrati italiani. Comitato Italiano

IUCN e Ministero dell'Ambiente e della Sicurezza Energetica, Roma.

Spitzen-van der Sluijs, A., Martel, A., Asselberghs, J., Bales, E. K., Beukema, W., Bletz, M. C., Dalbeck, L., Goverse, E., Kerres, A., Kinet, T. (2016): Expanding distribution of lethal amphibian fungus *Batrachochytrium salamandrivorans* in Europe. Emerging Infect. Dis. **22**: 1286.

Spitzen-van der Sluijs, A., Stegen, G., Bogaerts, S., Canessa, S., Steinfartz, S., Jansenn, N., Bosmann, W., Pasmans, F., Martel, A. (2018): Post-epizootic salamander persistence in a disease-free refugium suggests poor dispersal ability of *Batrachochytrium salamandrivorans*. Sci. Rep. **8**: 3800.

Stuart, S.N., Chanson, J.S., Cox, N.A., Young, B.E., Rodrigues, A.S.L., Fishman, D.L., Walle, R.W. (2004): Status and trends of amphibian declines and extinctions worldwide. Science **306**: 1783-1786.

Sun, D., Ellopola, G., Herath, J., Meegaskumbura, M. (2023): Ecological barriers for an amphibian pathogen: a narrow ecological niche for *Batrachochytrium salamandrivorans* in an Asian chytrid hotspot. J. Fungi **9**: 911.

Sutherland, W.J., Burgman, M.A. (2015): Policy advice: Use experts wisely. Nature **526**: 317-318.

Williams, D.R., Clark, M., Buchanan, G.M., Ficetola, G.F., Rondinini, C., Tilman, D. (2021): Proactive conservation to prevent habitat losses to agricultural expansion. Nat. Sustain. **4**: 314-322.

Xie, G.Y., Olson, D.H., Blaustein, A.R. (2016): Projecting the global distribution of the emerging amphibian fungal pathogen, *Batrachochytrium dendrobatidis*, based on IPCC climate futures. PLoS One **11**: e0160746.

Acta Herpetologica 19(2): 161-165, 2024
DOI: 10.36253/a_h-15090

Leukocyte formula of the Walser's Viper (*Vipera walser*)

Giacomo Vanzo[1,*], Lorenzo Laddaga[2], Samuele Ghielmi[3], Federico Storniolo[1], Marco Mangiacotti[1], Marco A.L. Zuffi[4], Stefano Scali[5], Roberto Sacchi[1]

[1] *Dipartimento di Scienze della Terra e dell'Ambiente, Università degli Studi di Pavia, Via Torquato Taramelli 24, Pavia, 27100, Italy*
[2] *Società di Scienze Naturali del Verbano-Cusio-Ossola, Museo di Scienze Naturali, Collegio Mellerio Rosmini, Via Antonio Rosmini 24, Domodossola, 28845, Italy*
[3] *MUSE - Museo delle Scienze, Trento, Corso del Lavoro e della Scienza 3, Trento, 38122, Italy*
[4] *Museo di Storia Naturale, Università di Pisa, Via Roma 79, Calci, 56011, Italy*
[5] *Museo di Storia Naturale di Milano, Corso Venezia 55, Milano, 20121, Italy*
**Corresponding author.* Email: giacomo.vanzo01@universitadipavia.it

Submitted on: 2023, 4th September; revised on: 2024, 7th April; accepted on: 2024, 20th July
Editor: Emilio Sperone

Abstract. *Vipera walser* is a recently assessed species of North-Western Italian Alps, that has been regarded as an isolated population of *V. berus* until 2016, when it has been identified as a separate taxonomical unit according to molecular markers. Due to its restricted and fragmented range and the potential threat of climate change in mountain systems, it complies with the IUCN criteria to be classified as EN. In order to investigate, in part, the health status of this taxon, we have performed blood smears to describe whether a haematological parameter such as leukocytes is consistent with those of more widespread viperids of the Italian peninsula. Overall, we sampled 20 Walser's Vipers across the species range and characterised leukocyte formula. We found that lymphocytes were the most common (~70% of total leukocytes). Eosinophils and heterophils were less abundant, while neutrophils and monocytes are the least represented. Our data is in accordance with that of other European viperids.

Keywords. *Vipera walser,* leukocyte differential count.

Vipera walser Ghielmi, Menegon, Marsden, Laddaga & Ursenbacher 2016 is a relict viper endemic to Alpine areas of North-Eastern Piedmont (Ghielmi et al., 2016). This viper lives exclusively in high altitude valleys up to about 2500 metres, in ecologically particular contexts, characterised by some of the highest rainfall in the entire Alpine region and an average annual temperature below 10 °C (Mercalli et al., 2008; Osservatorio Di Oropa - Meteo, 2022).

V. walser has an extremely limited geographical range, with a distribution area (Extent of occurrence - EOO) estimated at <1000 km^2 (Ghielmi et al., 2016). Therefore, it should be classified as "Endangered" (EN) according to the criteria of the IUCN Red List (2014) B1a/B2a, but the species conservation status has not been assessed yet. Given that the range of this species is strongly fragmented and that the area actually occupied (Area of occupancy - AOO) is less than 500 km^2, *V. walser* turns out to be one of the most threatened vipers in the world (Ghielmi et al., 2016). However, several studies are currently underway to clarify its taxonomic status, as recently its validity as a species has been questioned (Speybroeck et al., 2020; Doniol-Valcroze et al., 2021; Vanzo et al. 2024).

The population is already fragmented in two main subpopulations and, presumably, the complex topography of ridges and valleys might further increase the isolation among populations, as it was found in *V. berus* (Ursenbacher et al., 2009). Furthermore, such fragmentation implies an additional intrinsic threat factor, i.e., limited

ISSN 1827-9635 (print)
ISSN 1827-9643 (online)

www.fupress.com/ah

genetic variability compared to that of more widespread European vipers such as the adder and the asp viper (Ursenbacher et al., 2006; Ursenbacher, Conelli, et al., 2006; Ferchaud et al., 2011; Ghielmi et al., 2016). *V. walser* is considered a relict species that occurs in a very restricted range, so it can be regarded as an evolutionary dead end (Allendorf et al., 2012). *V. walser* is potentially threatened by decreasing habitat suitability due to both climate change (Ghielmi et al., 2016), and the abandonment of areas involved in agropastoral activities leading to natural reforestation (Carlson et al., 2014; Garbarino et al., 2014).

The presence of potentially pathological or stressful condition can significantly impact local and restricted populations, especially in endangered species (Schumacher, 2006; Buttke et al., 2015; Thomas et al., 2019). The leukocyte formula can be an important tool to assess the presence of inflammation and infection and can be used as an index of general stress and immune status of the animal (Blaxhall, 1972). In particular, in reptiles, heterophilia (increase in heterophils) and lymphocytopenia (decrease in lymphocytes) are the outcome of stress conditions; therefore, the relative proportion of heterophils over lymphocytes (i.e., H/L ratio) is often used as a composite measure of stress response (Davis et al., 2008; Stacy et al., 2011). Consequently, being able to provide baseline values of haematological parameters from wild populations is essential to evaluate possible threats and in species conservation (Stacy et al., 2011; Sacchi et al., 2020).

In this scenario, we have assessed for the first time the leukocyte formula of *V. walser*, in order to provide benchmarks that may be useful for assessing the health status of individuals of this species. Sampling took place via field surveys performed between May and October 2021: 20 adult individuals (13♀ and 7♂) of *V. walser* were captured across the entire distribution range of the species (as in Ghielmi et al., 2016). Fresh blood was sampled through tail clipping using surgical scissors (Duguy, 1970; Brown and Shine, 2018, 2022). This way to draw blood was not specifically designed for leukocyte analyses, but was a by-product of the methodology used for high quality DNA collection, which is the topic of another research project on the target species. Afterwards, the wounds were thoroughly disinfected with iodine tincture and eventually the individuals were released in their capture site. From each blood draw, a single-layer cell film was produced by depositing a small drop of blood at one end of the glass slide and placing a second glass slide close to the drop, slanted by 30-40 degrees, allowing the drop to adhere to the entire margin of the slide for capillarity (Nardini and Girolamo, 2017). The latter glass was slid gently and quickly along the former to create a blood smear that was air-dried. Subsequently, smears were col-

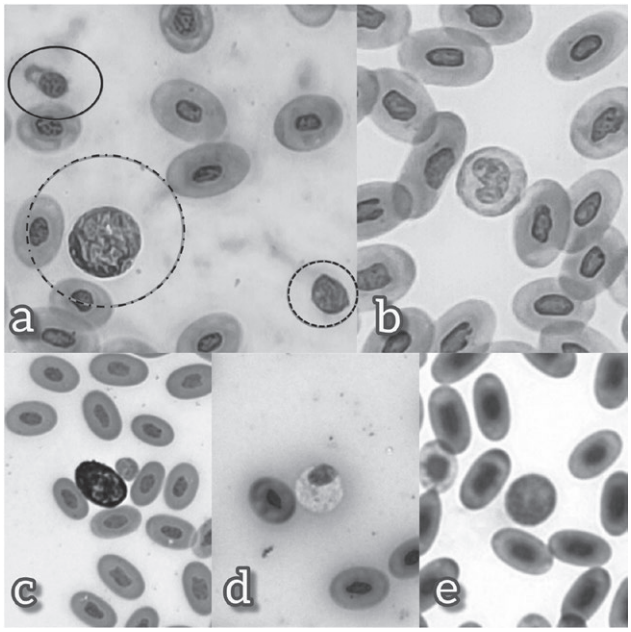

Fig. 1. Different leukocyte cell types detected in a sampled blood smear along the visual transects. Respectively, in each panel are shown: a) large heterophile (dot-dashed circle), a lymphocyte (dashed circle) and a blood platelet (solid circle); b) monocyte; c) basophile; d) heterophile; e) eosinophile.

Table 1. Table of the leukocyte formula of the 13 females and 7 males of *V. walser* sampled for this study. For each leukocyte cell type, mean ± SD and range are shown.

% of cell type	Females		Males		Total	
	Mean ± SD	Range	Mean ± SD	Range	Mean ± SD	Range
Heterophils	6.9 ± 3.1	2.0 – 12.9	10.2 ± 6.6	2.9 – 19.3	8.0 ± 4.8	2.0 – 19.3
Eosinophils	10.4 ± 3.5	1.8 – 6.9	14.0 ± 8.5	3.9 – 27.9	11.7 ± 5.8	3.9 – 27.9
Basophils	4.3 ± 3.4	0.0 – 14-0	6.1 ± 5.7	1.3 – 18.0	4.9 ± 4.3	0.0 – 18.0
Monocytes	1.9 ± 2.6	0.0 – 8.5	0.8 ± 1.0	0.0 – 2.6	1.5 ± 2.2	0.0 – 8.5
Lymphocytes	74.8 ± 6.0	65.3 – 88.2	67.9 ± 14.1	46.6 – 85.4	72.4 ± 9.9	46.6 – 88.2
Neutrophils	1.7 ± 2.5	0.0 – 9.4	1.0 ± 1.5	0.0 – 3.6	1.4 ± 2.2	0.0 – 9.4

Table 2. Comparative table of the White Blood Cells cell type percentages among data available in literature and our study. WBC cell types are shown as follows: Lymphocytes - L, Heterophils - H, Eosinophils - E, Basophils - B, Monocytes - M, Neutrophils - N. For each cell type, data are reported as percentage mean ± SD when available, otherwise percentage range is provided. Data reported for Monocytes in italics refers to works where they were classified as azurophils.

Family	Species	cell type %						Reference
		L	H	E	B	M	N	
Viperidae	*Vipera walser*	72.4 ± 9.9	8.0 ± 4.8	11.7 ± 5.8	4.9 ± 4.3	1.5 ± 2.2	1.4 ± 2.2	this work
Viperidae	*Vipera ammodytes*	52.3 ± 8.7	12.6 ± 3.2	22.6 ± 4	5.3 ± 4.9	7	/	Baycan et al., 2022
Viperidae	*Vipera ammodytes*	♂♂ 19.61 - 65.17	4.52 - 48.02	4.98 - 32.35	0 - 4.83	*6.9 - 50.79*	/	Lisičić et al. 2013
		♀♀ 35.32 - 67.14	7.46 - 50.24	1.48 - 21.7	0 - 4.48	*11.44 - 42.21*		
Viperidae	*Bothrops ammodytoides*	52.2 ± 6.9	12.2 ± 1.3	16.3 ± 1.8	1 ± 0.3	8.2 ± 0.9	/	Troiano et al., 1999
Colubridae	*Oxyrhopus guibei*	39.1 ± 11.4	15.1 ± 10.8	/	8 ± 5.7	*37.8 ± 10.8*	/	Ozzetti et al., 2015
Colubridae	*Xenodon neuwiedii*	36.9 ± 10.5	42.9 ± 10.3	/	7.9 ± 5.3	*42.9 ± 10.3*	/	Ozzetti et al. 2015
Boidae	*Corallus hortulanus*	25 ± 8.18	37 ± 14.87	/	0.8 ± 1.21	1.4 ± 1.8	/	Quadrini et al. 2018
Pythonidae	*Python bivittatus*	18.22 ± 12.56	42 ± 12.52	1 ± 1.94	0.22 ± 0.44	0.33 ± 0.71	/	Quadrini et al. 2018
Boidae	*Boa constrictor*,							
Viperidae	*Bothrops jararaca*, *Crotalus durissus*	58.6 - 78.2	6.6 - 17.1	/	/	*15 - 24.8*	/	Carvalho et al. 2016

oured using the May-Grünwald/Giemsa stain and stabilised through Entellan® (Vu et al., 2021). Two-five blood smears were prepared for each snake, and the best one was visually scanned by performing zig-zag scans across the slide. Leukocytes were classified as heterophiles, eosinophils, basophiles, neutrophils, lymphocytes, and monocytes (Fig. 1). These procedures were carried out using 40x magnification on an Optika B-383PLi microscope, distinguishing and counting on average 154 ± 8.9 leukocytes per sample.

Lymphocytes were the most common leukocytes (over 70% of total leukocytes). Eosinophils and heterophils were the second and third most abundant components. Neutrophils and monocytes are the least represented (Table 1). To test for differences in relative abundance of cell types between sexes, a non-parametric Mann-Whitney test was performed. No statistically significant difference was detected between sexes for all cell types ($W < 59$, $P > 0.29$).

Our investigation on *V. walser* is a first attempt to provide a benchmark of the leukocyte formula of wild populations in this species. Our data is consistent with available literature for other snakes from Europe (Duguy, 1970; Lisičić et al., 2013; Baycan et al., 2022) and South America (Troiano et al., 1997; Troiano et al., 1999; Grego et al., 2006, Carvalho et al., 2016), including Viperidae, and three major snake families (Colubridae, Pythonidae, and Boidae; Table 2). Notably, Lymphocytes are generally the most abundant white blood cell type and, consistently, heterophils and monocytes are generally the second- and third-most abundant ones, respectively. However, it is necessary to point out that across literature authors tend to identify and quantify different cell types according to necessity and interest; for instance, azurophils are sometimes identified as immature monocytes, according to cytochemical similarities (Lisičić et al., 2013), and used in their place (Ozzetti et al., 2015; Carvalho et al., 2016). In this matter, authors are not in accordance with one another and therefore interpreting and comparing leukograms can be sometimes complicated due to the terminology applied for cell type classification.

The implementation of heterophil and lymphocyte counts in past research has been correlated to stress so that higher H/L ratios are generally associated to higher stress levels (Davis et al. 2008). According to the published data we retrieved, a major variability in this measure was found as it can vary from low ratios (~0.11 in Carvalho et al., 2016 and our work) to very high values (~2.3 in Quadrini et al., 2018). Therefore, lacking marked clinical effects that correlate with higher values, we suggest using cautiously ratios of such kind to provide information about the health status of wild or captive popu-

lations of snakes. Consequently, we highlight the importance of the implementation of shared protocol and methodologies to undertake broad scale haematological studies of snake populations and to assess their relation to health and stress conditions.

In conclusion, with this work we provide, for the first time, information on some haematological parameters of the Walser's Viper, an endemic and endangered species of the Italian Alps, that might be of interest for future conservation measures. However, this work does not fully address this matter as it requires further investigations on health condition measures such as Body Condition Indices as well as comparative studies that take into account how sister species cope with the same threats in similar environmental conditions.

ACKNOWLEDGEMENTS

We would like to thank Parco Naturale dell'Alta Val Sesia e dell'Alta Val Strona, and Società di Scienze Naturali del Verbano-Cusio-Ossola for providing access to sampling areas and their support for the field work. Additionally, we thank Viviana Minolfi for her participation to data collection. Snake capture and manipulation was carried out in accordance with national and European regulations; the permits provided by the Ministero dell'Ambiente e della Tutela del Territorio e del Mare (MATTM) prot. n. 0141665 of 2021. Blood sampling was performed as a by-product because this methodology was not specifically designed for such purpose, instead it was used for high quality DNA collection which is the topic of another research project on the target species.

REFERENCES

Allendorf, F.W., Luikart, G.H., Aitken, S.N. (2012): Conservation and the genetics of populations. John Wiley & Sons, Hoboken.

Baycan, B., Boran, B., Gül, Ç., Tosunoğlu, M. (2022): Clinical Hematology of the Nose-Horned Viper, *Vipera ammodytes* (Linnaeus 1758). Reptil. Amphib. **29**: 461-469.

Blaxhall, P.C. (1972): The haematological assessment of the health of freshwater fish: a review of selected literature. J. Fish Biol. **4**: 593-604.

Buttke, D.E., Decker, D.J., Wild, M.A. (2015): The role of one health in wildlife conservation: a challenge and opportunity. J. Wildl. Dis. **51**: 1-8.

Carlson, B.Z., Renaud, J., Biron, P.E., Choler, P. (2014): Long-term modeling of the forest-grassland ecotone in the French Alps: implications for land management and conservation. Ecol Appl. **24**: 1213-1225.

Carvalho, M.P.N., Queiroz-Hazarbassanov N.G.T., Massoco, C.O., Rossi, S., Sant'Anna, S.S., Catão-Dias, J.L., Grego, K.F. (2016): Flow cytometric characterization of peripheral blood leukocyte populations of 3 neotropical snake species: *Boa constrictor*, *Bothrops jararaca*, and *Crotalus durissus*. Vet. Clin. Pathol. **45**: 271-280.

Davis, A.K., Maney, D.L., Maerz, J.C. (2008). The use of leukocyte profiles to measure stress in vertebrates: a review for ecologists. Funct. Ecol. **22**: 760-772.

Doniol-Valcroze, P., Ursenbacher, S., Mebert, K., Ghielmi, S., Laddaga, L., Sourrouille, P., Kariş, M., Crochet, P. (2021): Conflicting relationships of *Vipera walser* inferred from nuclear genes sequences and mitochondrial DNA. J. Syst. Evol. Res. **59**: 2307-2320.

Duguy, R. (1970): Numbers of blood cells and their variation. In: Biology of the Reptilia, pp. 93-109. Gans, C., Parsons, T.S., Eds, Academic Press, London.

Ferchaud, A.L., Lyet, A., Cheylan, M., Arnal, V., Baron, J.P., Montgelard, C., Ursenbacher, S. (2011): High genetic differentiation among French populations of the Orsini's viper (*Vipera ursinii ursinii*) based on mitochondrial and microsatellite data: implications for conservation management. J. Hered. **102**: 67-78.

Garbarino, M., Sibona, E., Lingua, E., Motta, R. (2014): Decline of traditional landscape in a protected area of the southwestern Alps: The fate of enclosed pasture patches in the land mosaic shift. J. Mt. Sci. **11**: 544-554.

Ghielmi, S., Menegon, M., Marsden, S.J., Laddaga, L., Ursenbacher, S. (2016): A new vertebrate for Europe: the discovery of a range-restricted relict viper in the western Italian Alps. J. Zool. Syst. Evol. Res. **54**: 161-173.

Grego, K.F., Alves, J.A.S., Rameh De Albuquerque L.C., Fernandes, W. (2006): Referencias hematologicas para a jararaca de rabo branco (*Bothrops leucurus*) recom capturadas da natureza. Arq Bras Med. Vet. Zootec. **58**: 1240-1243.

Hawkey, C.M., Dennett, T.B. (1989): Comparative veterinary haematology. Ipswich, WS Cowell.

LeBlanc C.J., Heatley, J.J., Mack, E.B. (2000): A review of the morphology of lizard leukocytes with a discussion of the clinical differentiation of bearded dragon, *Pogona vitticeps*, leukocytes. J. Herpetol. Med. Surg. **10**: 27-30.

Lisičić, D., Đikić, D., Benković, V., Knežević, A.H., Oršolić, N., Tadić, Z. (2013): Biochemical and hematological profiles of a wild population of the nose-horned viper *Vipera ammodytes* (Serpentes: Viperi-

dae) during autumn, with a morphological assessment of blood cells. Zool. Stud. **52**: 1-9.

Mercalli, L., Cat Berro, D., Acordon, V., Di Napoli, G. (2008): Cambiamenti climatici sulla montagna piemontese. Rapporto tecnico realizzato da Società meteorologica Subalpina per conto di Regione Piemonte. Società Meteorologica Subalpina Castello Borello, Bussoleno (TO), Italy.

Nardini, G., Di Girolamo, N. (2017): Reptile clinical pathology. Veterinaria (Cremona) **31**: 197-205.

Osservatorio di Oropa - Meteo (2022). http://www.osservatoriodioropa.it/meteoropa/meteoropa.htm

Ozzetti, P.A., Cavlac, C.L., Sano-Martins, S. (2015): Hematological reference values of the snakes *Oxyrhopus guibei* and *Xenodon neuwiedii* (Serpentes: Dipsadidae). Comp. Clin. Path. **24**: 101-108.

Quadrini, A.E., Garcia, V.C., Freire, B.C., Martins, M.F.M. (2018): Haematological reference of snakes: Amazon tree boa (*Corallus hortulanus*, Linnaeus, 1758) and Burmenese Python (*Python bivittatus*, Kuhl, 1820) in captive. Arq Bras Med. Vet. Zootec. **70**: 1172-1178.

Sacchi, R., Mangiacotti, M., Scali, S., Coladonato, A.J., Pitoni, S., Falaschi, M., Zuffi, M.A.L. (2020): Statistical methodology for the evaluation of leukocyte data in wild reptile populations: A case study with the common wall lizard (*Podarcis muralis*). PLoS One **15**: e237992.

Schumacher, J. (2006): Selected infectious diseases of wild reptiles and amphibians. J. Exot. Pet Med. **15**: 18-24.

Speybroeck, J., Beukema, W., Dufresnes, C., Fritz, U., Jablonski, D., Lymberakis, P., Martínez-Solano I., Razzetti, E., Vamberger, M., Vences, M., Vörös, J., Crochet, P. (2020): Species list of the European herpetofauna – 2020 update by the Taxonomic Committee of the Societas Europaea Herpetologica. Amphibia-Reptilia **41**: 139-189.

Stacy, I.N., Alleman, A.R., Sayler, A. (2011): Diagnostic Hematology of Reptiles. Clin. Lab. Med. **31**: 87-108.

Thomas, V., Wang, Y., Van Rooij, P., Verbrugghe, E., Baláž, V., Bosch, J., Cunningham, A.A., Fisher, M.C., Garner, T.W., Gilbert, M.J., Grasselli, E., Kinet, T., Laudelout, A., Lötters, S., Loyau, A., Miaud, C., Salvidio, S., Schmeller, D.S., Schmidt, B.R., Spitzen-van der Sluijs, A., Steinfartz, S., Veith, M., Vences, M., Wagner, N., Canessa, S., Martel, A., Pasmans, F. (2019): Mitigating *Batrachochytrium salamandrivorans* in Europe. Amphibia-Reptilia **40**: 265-290.

Troiano, J.C., Vidal, J.C., Gould, E.F., Malinskas, G., Gould, J., Scaglione, M., Scaglione, L., Heker, J.J., Simoncini, C., Dinápoli, H. (1999): Haematological and blood chemical values from *Bothrops ammodytoides* (Ophidia-Crotalidae) in captivity. Comp. Haematol. Int. **9**: 31-35.

Troiano, J.C., Vidal, J.C., Gould, J., Gould, E. (1997): Haematological reference intervals of the south american rattlesnake (*Crotalus durissus terrificus*, Laurenti, 1768) in captivity. Comp. Haematol. Int. **7**: 109-112.

Ursenbacher, S., Carlsson, M., Helfer, V., Tegelström, H., Fumagalli, L. (2006): Phylogeography and Pleistocene refugia of the adder (*Vipera berus*) as inferred from mitochondrial DNA sequence data. Mol. Ecol. **15**: 3425-3437.

Ursenbacher, S., Conelli, A., Golay, P., Monney, J. C., Zuffi, M. A. L., Thiery, G., Durand, T., Fumagalli, L. (2006). Phylogeography of the asp viper (*Vipera aspis*) inferred from mitochondrial DNA sequence data: evidence for multiple Mediterranean refugial areas. Mol. Phyl. Evol. **38**: 546-552.

Ursenbacher, S., Monney, J.C., Fumagalli, L. (2009): Limited genetic diversity and high differentiation among the remnant adder (*Vipera berus*) populations in the Swiss and French Jura Mountains. Conserv. Genet. **10**: 303-315.

Vanzo, G., Storniolo, F., Laddaga, L., Ghielmi, S., Mangiacotti, M., Zuffi, M.A.L, Scali, S., Sacchi R. (2024). Does morphology support the taxonomic status of the Walser's viper (*Vipera walser*)? Insight from head shape and hemipenes. *Amphibia-Reptilia* accepted.

Vu, Q.H., Van, H.T., Tran, V.T., Huynh, T.D.P., Nguyen, V.C., Le, D.T. (2021): Development of a robust blood smear preparation procedure for external quality assessment. Pract. Lab. Med **27**: e00253.

Acta Herpetologica 19(2): 167-171, 2024
DOI: 10.36253/a_h-16188

Phylogenetic placement of the Mount Bamboutos endemic skink, *Trachylepis mekuana* (Chirio and Ineich, 2001)

Michele M. Kameni N.[1], Walter P. Tapondjou N.[2], Werner Conradie[3,4,*]

[1] *Laboratory of Zoology, University of Yaoundé I, Cameroon*
[2] *Florida Museum of Natural History, University of Florida, Gainesville, Florida, USA*
[3] *Port Elizabeth Museum (Bayworld), 23 Beach road, Humewood 6013, Gqeberha, South Africa*
[4] *Department of Nature Conservation Management, George Campus, Nelson Mandela University, George, South Africa*
**Corresponding author.* Email werner@bayworld.co.za

Submitted on: 2024, 23rd May; revised on: 2024, 14th October; accepted on: 2024, 20th October
Editor: Raoni Rebouças

Abstract. African skinks of the genus *Trachylepis* is one of the most diverse genera of lizards in Africa. Although, many species have not been validated phylogenetically in recent years. In this study we evaluate the phylogenetic status of the Cameroon Volcanic Line endemic montane skink, *Trachylepis mekuana*. We recover this species as part of the larger *Trachylepis varia* group, with sister relationship to the morphological similar skinks from Eastern Africa *Trachylepis megalura* and central Africa *Trachylepis raymondlaurenti*. Low sequence divergence (<1.6% *16S*) have been observed among the three species. Based on some morphological and colouration differences, as well as mostly allopatric distribution we regard them as good species.

Keywords. Endemic, volcanic, scincidae, montane, allopatric.

Trachylepis is one of the most diverse Scincidae genera in Africa, with a taxonomically convoluted history and many unresolved species complexes. A recently published review of this genus in Angola has raised the number of species in the genus to ~94 species (Ceríaco et al., 2024).

In 2015, an unusual plainly coloured *Trachylepis* skink with an exceptionally long tail was found in Cangandala National Park, Angola (Ceríaco et al., 2016, 2018), which was subsequently described as a new species, *T. raymondlaurenti* (Marques et al., 2019). The new species was reported to be differentiated from its closest congener *T. megalura* by 4% *16S* sequence divergence, the fact that the supranasals are always separated, and a uniform greyish dorsal colouration versus fine longitudinal black or white dorsolateral stripes dorsally. However, in a later study on the *Trachylepis* of Angola (Ceríaco et al., 2024), the authors reported a lower (2.12%) *16S* uncorrected p-distance between these two species, but a large *RAG1* uncorrected p-distance of 3.42%.

In a broad-scale phylogenetic study of the *Trachylepis* genus, Weinell et al. (2019) recovered the two above-mentioned species (*T. raymondlaurenti* ~labelled as *T. megulara* and *T. megalura*) as part of the larger *T. varia* group. Within this group *T. varia* has undergone a substantial revision, in which previous works recovered a widespread species complex (*T. varia* complex) comprising seven well differentiated lineages (Weinell and Bauer, 2018). Consequently, some of these have subsequently be allocated to older names (*T. laevigata*, *T. damarana*, *T. albopunctata*), while others remain undescribed due to lacking material. Nevertheless, authors of the above studies have not made further mention to the close sister relationship between *T. megalura* and the rest of the *T. varia* group.

Of special interest is that when *T. raymondlaurenti* was described, the authors did not make any compari-

ISSN 1827-9635 (print)
ISSN 1827-9643 (online)

www.fupress.com/ah

son to *T. mekuana* from Mount Bamboutos in Cameroon, which was documented to be morphologically closely related to *T. megalura* (Chiro and Ineich, 2003). *Trachylepis mekuana* shares morphological similarities to *T. raymondlaurenti* in that the supranasals are mostly separated, yet it differs in having a bolder dorsal colouration versus uniform greyish in the latter. In an independent study looking at the phylogenetic status of the Lygosominae, *16S* sequences of *T. mekuana* (as *Mubuya* sp.) were included in their analyses (Honda et al., 2003). Another study looking at the Central and West Africa *Trachylepis* published *ND2* sequences of *T. mekuana* (Allen et al. 2019). None of these sequences were incorporated into the broad scale study of Weinell et al. (2019) or in the recent Angolan *Trachylepis* revision (Ceríaco et al., 2024). Consequently, the close morphological similarities of *T. mekuana* with *T. megalura* and *T. raymondlaurenti*, combined with the above-mentioned discrepancies in genetic results, have motivated a deeper re-analysis of the group using all the available genetic data of these three species to shed light on the taxonomic and phylogenetic position of this group.

To this aim, previously published sequences of *16S*, *ND2*, *RAG1* and *KIF24* genes (Table S1; Honda et al. 2003; Marques et al. 2019; Allen et al. 2019; Weinell et al. 2019) were obtained from GenBank, including four newly generated *16S* sequences of *T. mekuana*, and aligned in MEGA v.7.0.27 (Tamura et al., 2013), using the ClustalW v.1.6 alignment method (Thompson et al., 1994) with default parameters. The final dataset comprised 51 samples (Table S1), including *T. laevis* as the outgroup taxon. Separate alignments were created for each gene, and a concatenated dataset, was created using SequenceMatrix v.1.8.2 (Vaidya et al., 2011). The best-fitting models and partition schemes were determined using ModelFinder implemented in IQ-TREE (Chernomor et al., 2016; Minh et al., 2021). The following settings were used: *-p* partition file (each partition with its own evolution rate), a greedy strategy and the FreeRate heterogeneity model excluded (only invariable site and Gamma rate heterogeneity considered) (Chernomor et al., 2016; Kalyaanamoorthy et al., 2017). The following models and partition schemes were used: GTR+F+I (*16S*), GTR+F+I+G4 (*ND2*), and HKY+F+I (*RAG1* + *KIF24I*). A maximum likelihood (ML) phylogeny was generated in IQ-TREE, using a random starting tree and the best-fitting model schemes selected for each dataset as selected above. The ultrafast bootstrap approximation (UFBoot) method (Hoang et al., 2017) was implemented using 1000 replicates and minimum correlation coefficient of 0.99. For accuracy, the analysis was run twice to ensure that independent ML searches recovered the same topologies. The ML phylogeny was rooted with *Trachylepis laevis* and visualised using FigTree v.1.4.4 (Rambaut, 2018). Nodes with bootstrap support (BS) ≥ 95% were regarded as well supported. Finally, an uncorrected pairwise distance (p-distance) analysis was conducted in MEGA X (Kumar et al., 2018) for the *16S* and *ND2* gene. The hyper-variable region of the *16S* gene was retained. Sequences were grouped according to species, and pairwise distance analyses were conducted using uniform rates, pairwise deletion and 500 bootstrap replicates.

The phylogenetic reconstructions recovered a similar topology within the *T. varia* group compared to previous studies (Weinell et al., 2019; Ceríaco et al., 2024), showing a well-supported sister relationship between the *T. megalura* group and the rest of the *T. varia* complex (Figs. 1 and S1). The only difference is the inclusion of *T. mekuana* in this study. *Trachylepis mekuana* was recovered as sister to *T. raymondlaurenti*, although not well-supported. In turn, these two species were recovered as a well-supported sister clade to *T. megalura.* The uncorrected *16S* p-distance obtained between these three species varies between 0.9 – 1.6% *16S*. This is well below the interspecific threshold observed between the other species of the *T. varia* complex (4.2 – 9.6 %, average 6.1 ± 1.1% *16S* average uncorrected p-distance; Table 1). Similarly, the uncorrected *ND2* p-distance sequence divergence between *T. mekuana* and *T. raymondlaurenti* was 9.4% (Table 2), also well below the interspecific threshold observed between the other species of the *T. varia* complex (13.5 – 20.4%, average 16.5 ± 1.6% *ND2* average uncorrected p-distance).

Morphologically, these three species are reported to differ only in their dorsal colouration (striped dorsal pattern, with a number of fine longitudinal black or white stripes and a distinct white dorsolateral stripe in *T. megalura*; *T. mekuana* is similar in colouration to *T. megalura* but the dorsal stripes are more defined; uniform greyish-brown with no stripes in *T. raymondlaurenti*), and head scalation (supranasals always in contact in *T. megalura* versus never in contact in *T. raymondlaurenti* and *T. mekuana* [except paratype female in narrow contact]). In addition, the three species occur mostly allopatrically, except at the Upemba National Park area in southern Democratic Republic of the Congo, where both *T. raymondlaurenti* and *T. megalura* occur sympatrically (Marques et al., 2019). In the Port Elizabeth Museum, a *T. megalura* specimen from north of Shabeli, Ethiopia (PEM R08590) shares morphological characters with *T. mekuana* (supranasals separated and similar dorsal colour pattern). This agrees with the conclusions of Chirio and Ineich (2003), who refer to specimens from Koffole, Ethiopia that share morphological similarities with *T. mekua-*

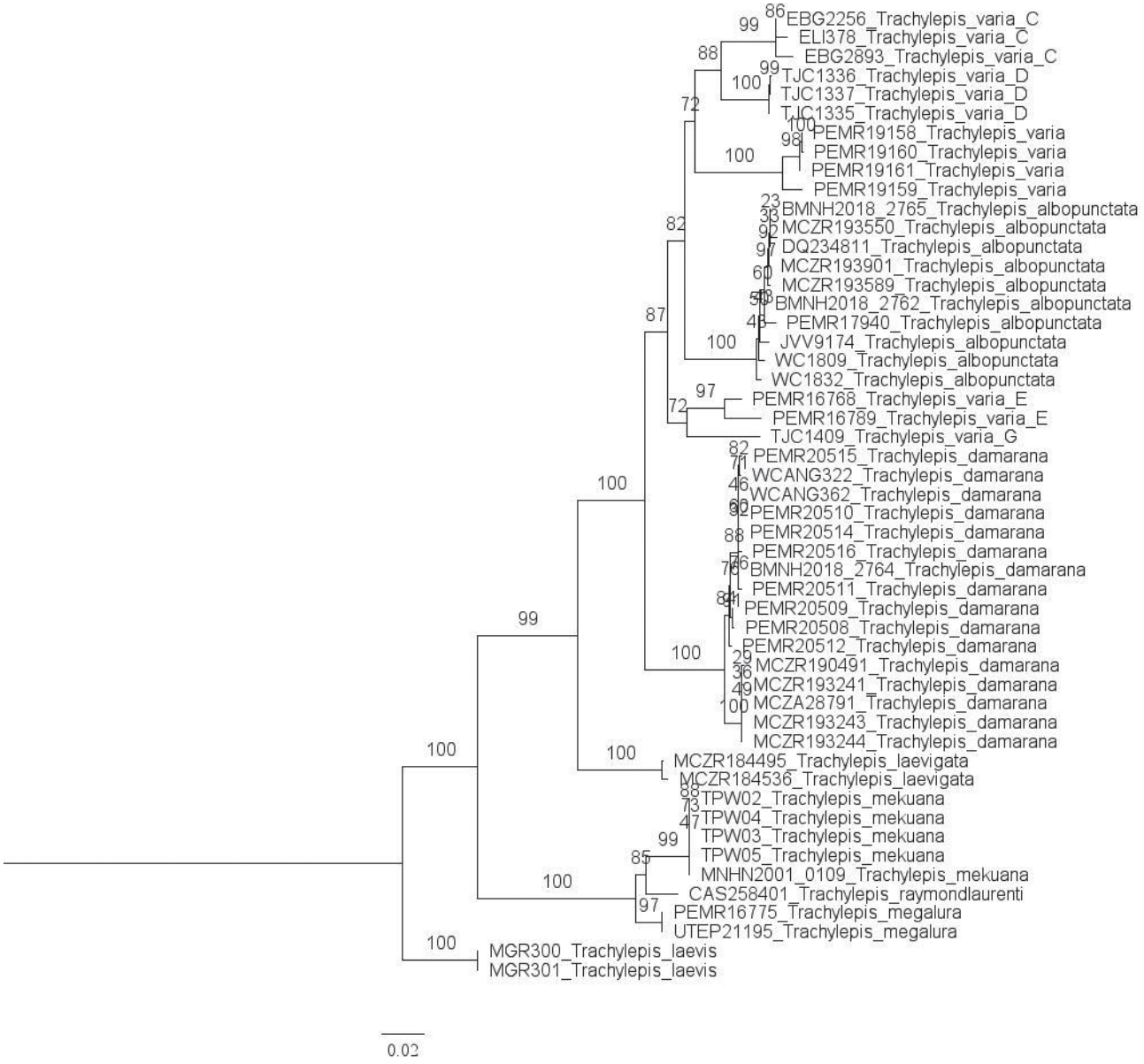

Fig. 1. Maximum Likelihood (ML) concatenated phylogeny (*16S*, *ND2*, *RAG1*, *KIF24*), showing relationships between the *Trachylepis varia* group and the placement of *Trachylepis mekuana*.

na. Other specimens of interest here include the undescribed *Trachylepis* sp. observed by Kameni et al. (2022) on Mt. Bamboutos, occurring at lower elevation than *T. mekuana*. The two individuals observed present the habitus and uniform colouration of *T. raymondlaurenti* and occur sympatrically with *T. mekuana*. These population warrants further investigation.

Although the sequence divergence between the species in the *T. megalura* group are on the low side, the minor morphological and colouration differences in conjunction with the mostly allopatric distribution provides multiple lines of evidence to retain all three species as valid. Wider sampling, especially of the Ethiopian population, may help shedding further light on this group and potentially discover additional cryptic species in this group. Of further interest is the close relationship between reptile species from the high lying areas of Cameroon and East African. Other species showing similar patterning as *T. mekuana* and *T. megalura* is: *Lepthosiaphos koutoui* versus *L. kilimensis* and *Trachylepis nganghae* versus undescribed *Trachylepsis* species from Uganda (Ineich and Chirio, 2004). These species pairs

Table 1. Mean sequence divergences (uncorrected p-distances) within the *Trachylepis varia* complex (group names based on Weinell and Bauer 2018) for *16S* gene, given as percentages. The numbers in the diagonal grey boxes represent the mean intraspecific sequence divergences, numbers below the diagonal grey boxes represent the mean interspecific sequence divergences, while numbers above the diagonal grey boxes represent standard errors of the interspecific sequence divergences. Important values have been framed. n/c – was not possible to estimate sequence divergences.

	16S	1	2	3	4	5	6	7	8	9	10	11
1	*T. varia* C	0.7	*0.9*	*0.9*	*1.0*	*0.9*	*1.0*	*1.0*	*1.2*	*1.4*	*1.4*	*1.3*
2	*T. varia* D	4.1	0.0	*1.0*	*1.1*	*1.0*	*1.3*	*1.2*	*1.3*	*1.3*	*1.4*	*1.3*
3	*T. varia* sensu stricto	4.9	5.6	0.0	*1.0*	*0.8*	*1.0*	*1.0*	*1.2*	*1.3*	*1.4*	*1.3*
4	*T. albopunctata*	5.6	6.2	4.9	0.6	*0.9*	*1.1*	*0.9*	*1.3*	*1.3*	*1.4*	*1.2*
5	*T. varia* E	4.7	5.1	4.4	4.8	1.5	*1.0*	*0.9*	*1.2*	*1.3*	*1.3*	*1.2*
6	*T. varia* G	5.2	7.7	4.7	5.5	5.5	n/c	*1.1*	*1.3*	*1.4*	*1.5*	*1.4*
7	*T. damarana*	5.9	7.0	5.5	4.6	4.7	6.0	1.0	*1.2*	*1.4*	*1.4*	*1.3*
8	*T. laevigata*	8.4	8.3	8.0	8.5	7.5	8.6	8.3	0.2	*1.3*	*1.3*	*1.3*
9	*T. raymondlaurenti*	9.9	9.5	9.2	9.1	8.7	10.1	10.0	8.2	n/c	*0.4*	*0.6*
10	*T. mekuana*	10.4	10.0	9.7	9.6	9.2	10.6	10.4	8.3	0.9	n/c	*0.6*
11	*T. megalura*	9.4	9.1	8.9	8.8	8.0	9.8	9.6	7.7	1.5	1.6	0.0

Table 2. Mean sequence divergences (uncorrected p-distances) within the *Trachylepis varia* complex (group names based on Weinell and Bauer 2018) for *ND2* gene, given as percentages. The numbers in the diagonal grey boxes represent the mean intraspecific sequence divergences, numbers below the diagonal grey boxes represent the mean interspecific sequence divergences, while numbers above the diagonal grey boxes represent standard errors of the interspecific sequence divergences. Important values have been framed. n/c – was not possible to estimate sequence divergences.

	ND2	1	2	3	4	5	6	7	8
1	*T. varia* D	0.2	*1.4*	*1.2*	*2.0*	*1.4*	*1.4*	*1.6*	*1.6*
2	*T. varia* sensu stricto	15.0	2.6	*1.4*	*1.8*	*1.4*	*1.5*	*1.7*	*1.7*
3	*T. albopunctata*	13.5	16.1	5.6	*1.8*	*1.2*	*1.4*	*1.5*	*1.5*
4	*T. varia* G	14.9	16.4	15.5	n/c	*2.0*	*2.0*	*2.2*	*2.3*
5	*T. damarana*	16.3	18.2	14.8	16.2	1.6	*1.4*	*1.6*	*1.6*
6	*T. laevigata*	17.9	20.4	18.6	17.9	16.3	0.6	*1.6*	*1.5*
7	*T. raymondlaurenti*	22.0	21.4	23.3	19.9	22.3	22.0	n/c	1.1
8	*T. mekuana*	22.4	22.2	22.5	22.9	22.3	21.2	9.4	0.0

are separated by a large geographical gab with no records in-between due to a lack of suitable montane habitat and potential sampling effort.

In conclusion, this study phylogenetic placed *T. mekuana* in the *T. megalura* subgroup and eluded to the low sequence divergence among species in this group.

ACKNOWLEDGMENTS

We thank the Rufford small grant, University of Kansas Biodiversity institute Panorama grant, and Idea Wild materials grant for supporting this project. We are grateful to Kaitlin Allen for assistance generating the additional sequences for this study.

SUPPLEMENTARY MATERIAL

Supplementary material associated with this article can be found at <http://www-9.unipv.it/webshi/appendix/index.html> manuscript number 16188

REFERENCES

Allen, K.E., Tapondjou, W.P., Welton, L.J., Bauer, A.M. (2017): A new species of *Trachylepis* (Squamata: Scincidae) from Central Africa and a key to the *Trachylepis* of West and Central Africa. Zootaxa **4268**: 255-269.

Ceríaco, L.M.P., Marques, M.P, Bandeira S. (2016): Anfiẽbios e Reẽpteis do Parque Nacional da Cangandala. Cafilesa -Soluções Gráficas, Lda. Lisboas.

Ceríaco, L.M.P., Marques, M.P., Bandeira, S., Blackburn, D.C., Bauer, A.M. (2018): Herpetological Survey of Cangandala National Park, with a Synoptic List of the Amphibians and Reptiles of Malanje Province, Central Angola. Herpetol. Rev. **49**: 408-431.

Ceríaco, L.M.P., Marques, M.P., Parrinha, D., Tiutenko, A., Weinell, J.L., Butler, B.O., Bauer, A.M. (2024): The *Trachylepis* (Squamata: Scincidae) of Angola: an integrative taxonomic review with the description of seven new species. Bull. Am. Mus. Nat. Hist. **465**: 1-153.

Chernomor, O., Von Haeseler, A., Minh, B.Q. (2016): Terrace aware data structure for phylogenomic inference from supermatrices. Syst. Biol. **65**: 997-1008.

Chirio, L., Ineich, I. (2000): Description d'un nouveau scincidé endémique des montagnes du Cameroun (Lacertilia: *Mabuya mekuana*). Bull. Soc. Herp. Fr. **125**: 185-196.

Hoang. D.T., Chernomor, O., Von Haeseler, A., Minh, B.Q., Vinh, L.S. (2018): UFBoot2: Improving the ultrafast bootstrap approximation. Mol. Biol. Evol. **35**: 518-522.

Honda, M., Ota, H., Köhler, G., Ineich, I., Chirio, L., Chen, S.L., Hikida, T. (2003): Phylogeny of the lizard subfamily Lygosominae (Reptilia: Scincidae), with special reference to the origin of the new world taxa. Genes Genet. Syst. **78**: 71-80.

Ineich, I., Chirio. L. (2004): L'Archipel Afro-montagne et les affinités de son herpetofaune: description d'une espèce nouvelle indiquant des relations phylétiques entre le Camerun et l'Afrique de l'est (Lacertilia, Scincidae, genre *Trachyleps*. Bull. Soc. Herp. Fr. **129**: 317-331.

Kalyaanamoorthy, S., Minh, B.Q., Wong, T.K.F., Von Haeseler, A., Jermiin, LS. (2017): ModelFinder: Fast model selection for accurate phylogenetic estimates. Nat. Methods **14**: 587-589.

Kameni, M.M., Gonwouo, L.N., Tapondjou, W.P., Tchassem, A.M., Doherty-Bone, T., Allen, K.E., Fomena, A. (2022): Status and habitat preferences of montane endemic skinks, genera *Lacertaspis*, *Leptosiaphos*, and *Trachylepis*, in the central Cameroon Volcanic Line. Herpetol. Notes **15**: 271-281.

Kumar, S., Stecher, G., Li, M., Knyaz, C., Tamura, K. (2018): MEGA X: Molecular Evolutionary Genetics Analysis across Computing Platforms. Mol. Biol. Evol. **35**: 1547-1549.

Marques, M.P., Ceríaco, L.M.P., Bandeira, S., Pauwels, O.S.G., Bauer, A.M. (2019): Description of a new long-tailed skink (Scincidae: *Trachylepis*) from Angola and the Democratic Republic of the Congo. Zootaxa **4568**: 51-68.

Minh, B.Q., Lanfear, R., Trifinopoulos, J., Schrempf, D., Schmidt. H.A. (2021): IQ-TREE version 2.1.2: Tutorials and Manual Phylogenomic software by maximum likelihood. Available at: http://www.iqtree.org/doc/iqtree-doc.pdf [*Accessed on 21 March 2022*]

Rambaut, A. (2018): FigTree. Tree Figure Drawing Tool Version 1.4.4 Available at http://tree.bio.ed.ac.uk/software/figtree/ [*Accessed on 21 March 2022*]

Tamura, K., Stecher, G., Peterson, D., Filipski, A., Kumar, S. (2013): MEGA6: molecular evolutionary genetics analysis version 6.0. Mol. Biol. Evol. **30**: 2725-2729.

Uetz, P., Freed P., Aguilar, R., Reyes, F., Kudera,. J, Hošek, J. (2023): The Reptile Database. Available at http://www.reptile-database.org [*Accessed on 25 February 2024*]

Vaidya, G., Lohman, D.J., Meier, R. (2011): SequenceMatrix: concatenation software for the fast assembly of multigene datasets with character set and codon information. Cladistics **27**: 171-180.

Weinell, J.L, Bauer, A.M. (2018): Systematics and phylogeography of the widely distributed African skink *Trachylepis varia* species complex. Mol. Phylogenet. Evol. **120**: 103-117.

Weinell, J.L., Branch, W.R., Colston, T.J., Jackman, T.R., Kuhn, A., Conradie, W., Bauer, A.M. (2019): A species-level phylogeny of *Trachylepis* (Scincidae: Mabuyinae) provides insight into their reproductive mode evolution. Mol. Phylogenet. Evol. **136**: 183-195.

Finito di stampare da
Logo s.r.l. – Borgoricco (PD) – Italia

Cover: *Vipera ammodytes*, subadult male, photographed on 24 May 2014 in north-western Bulgaria (photo by Angel Dyugmedzhiev).

Università degli Studi di Firenze
Firenze University Press
via Cittadella 7, 50144 Firenze, Italy
http://www.fupress.com/
E-mail: journals@fupress.com

Periodicità: semestrale
ISSN 1827-9643 (online)
ISSN 1827-9635 (print)
Registrata al n. 5450 del 3.11.2005
del Tribunale di Firenze

ACTA HERPETOLOGICA

CONTENTS

December **2024** Vol. **19** – N. **2**